

### Abstract

It is shown that auroral hiss emissions observed in high latitudes can be categorized into two types on the basis of the power spectrum and its temporal variation. They are called the narrow-band continuous hiss and the wide-band impulsive hiss. The continuous hiss has a narrow frequency range with a center frequency of about 10 kHz and a band width of a few kHz and is characterized by a long time duration (longer than a few tens of minutes). The impulsive hiss, on the other hand, has a wide frequency range with a spectral peak frequency of about 10 kHz and a band width of a few tens of kHz and is of a short time duration (usually shorter than 10 minutes).

On the basis of observations at the two Stations, Syowa and Mizuho and the ISIS 2 satellite, the continuous hiss emissions are found usually to occur associated with the steady auroral arc located near the poleward horizon of Syowa Station, and the impulsive hiss emissions, on the other hand, are found to occur accompanying the initial brightening of active aurora (corona, rayed-band, westward traveling surge) that appeared near the zenith. These relationships between two types of hiss and the global auroral activity are confirmed by the comparison between the global auroral data observed on the DMSP satellite and the ground data of hiss.

A systematic local time variation of the arrival direction of the continuous hiss emissions is also found. It is shown that the arrival direction in early evening (18h–19h) is the east and it changes from east to west around 20h–21h. This local time variation of the arrival direction will be discussed in relation to the statistical distribution of the source region of the continuous hiss emissions. The arrival direction of the waves was next examined and it shows that the continuous hiss arrives from several hundreds of km equatorward of the related aurora, while the impulsive hiss sometimes arrives from the region nearer the auroral location. It also becomes clear that the distance between the exit (the arrival direction) of hiss and the auroral location depend on the magnetic dip angle of the station by comparing the results obtained at Churchill and Syowa Station. Namely the arrival direction nearly tends to coincide with the auroral active region at Church-

ill with a large dip angle (Dip  $\sim 83^\circ$ ) and the wave exit is likely located hundreds of km equatorward of the aurora at Syowa Station with a small dip angle (Dip  $\sim 65^\circ$ ). Simultaneous observations of VLF emissions observed on ISIS 2 and on the ground support the conclusion that the continuous hiss does not propagate along the magnetic field line from the satellite altitude ( $h \sim 1400$  km) to the ground but along a non-ducted path.

The ray path of the VLF waves was calculated in comparison with the observational results mentioned above. It was found that the distance between the region where the wave normal angles lie within the transmission cone at the ionospheric level ( $h \sim 200$  km) and the foot point of the field line along which the duct terminates at 3000 km in altitude, is about 300–400 km at Syowa Station. These results explain the fact that the arrival direction of continuous hiss is several hundreds of km equatorward of the related aurora, and further that the duct of auroral hiss terminates at about 3000 km in altitude. By contrast, the arrival direction of the impulsive hiss is found sometimes much nearer to the auroral activity. Likewise, the impulsive hiss seems to propagate along the field line lower than 3000 km in altitude on account of the strong field-aligned irregularities or the large-scale horizontal gradient of ionization.

Assuming that particles and waves are coupled in the Cerenkov condition and waves are generated with an electron beam with energy of a few keV or less, and further assuming that the enhancement factor along the field line is smaller than 0.5, the generation region of auroral hiss observed on the ground is estimated. It is shown that auroral hiss emissions generated around the altitude where the wave frequency is near to the local gyro or plasma frequency can propagate to the ground. Thus, it is concluded that the continuous hiss with a frequency range from 2 to 20 kHz would be generated around the altitude from  $1.5 \times 10^4$  to  $3.0 \times 10^4$  km and the impulsive hiss with a frequency range from 2 to 100 kHz would be generated around the altitude from  $5 \times 10^3$  to  $3 \times 10^4$  km. The generation region concluded here is consistent with that of other studies of auroral hiss and auroral kilometric radiation.

## 1. Introduction

### 1.1. Waves in magnetosphere

Naturally occurring electromagnetic and electrostatic waves at very low frequency and low frequency generated in the magnetosphere are called VLF and LF emissions. Some can penetrate the ionosphere and are recorded on the ground, while others are only observed in rockets and satellites. These phenomena give interesting and important information on the plasma process (wave-particle interaction) of the magnetosphere and they can also be useful as a diagnostic tool for the study of the magnetospheric structure. Recently various kinds of emissions were observed in the magnetosphere on the satellite and their spatial distribution of the deduced generation regions are shown in Fig. 1. The waves observed in the magnetosphere may be roughly categorized into three types. (1) Bow-shock turbulence (RODRIGUEZ and

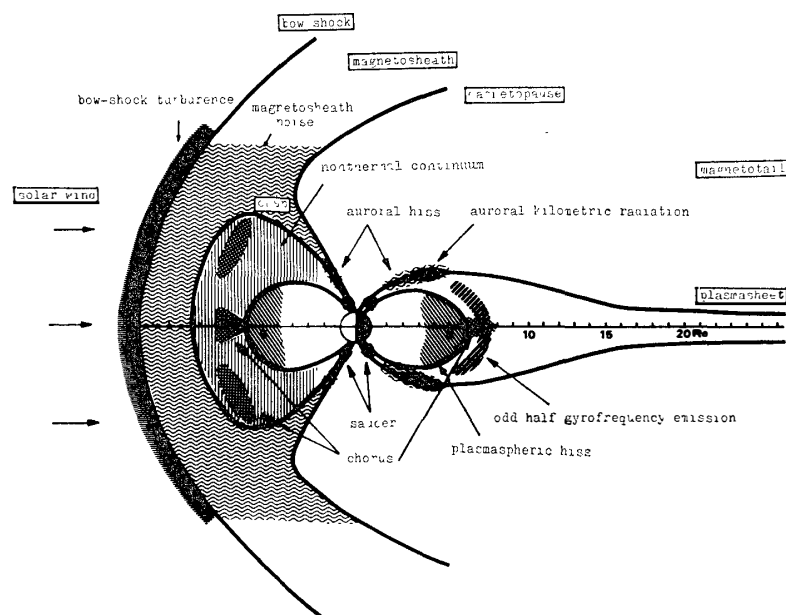


*Fig. 1. Regions of plasma wave occurrence located in a noon-midnight meridian cross-section of the Earth's magnetosphere.*

GURNETT, 1975), magnetosheath noise (SMITH *et al.*, 1969) and day-side auroral hiss (LAASPERE and HOFFMAN, 1976) belong to the emissions which are directly generated by solar wind particles. (2) Chorus (BURTIS and HELLIWELL, 1969; DUNCKEL and HELLIWELL, 1969; ANDERSON and GURNETT, 1973; TSURUTANI and SMITH, 1974; BURTON and HOLZER, 1974; HOLZER *et al.*, 1974; BURTIS and HELLIWELL, 1975; TSURUTANI and SMITH, 1977), plasmaspheric hiss (THORNE, 1973) and non-thermal continuum (FRANKEL, 1973; GURNETT, 1975) are categorized as other kinds of emissions which are generated by the particles located around the closed field line of the magnetosphere. (3) Auroral hiss (GURNETT, 1966; BARRINGTON *et al.*, 1971; HUGHES *et al.*, 1971; MOSIER and GURNETT, 1972), saucer (GURNETT and FRANK, 1972; JAMES, 1976), auroral kilometric radiation (GURNETT, 1974) and odd half gyrofrequency emissions (KENNEL *et al.*, 1970, FREDRICKS and SCARF, 1973) belong to the other types of emissions which are generated by the particles located around the open field line of the magnetosphere.

The characteristics of these emissions were shown in the  $\omega$ - $k$  diagram in Fig. 2 (STRINGER, 1963). Bow-shock turbulence is observed in the frequency range from 10 Hz to 200 kHz. These emissions belong to both the electrostatic and whistler-mode wave and are generated by the upstream solar wind particles from bow-shock. Magnetosheath noises are observed around a few hundred Hz

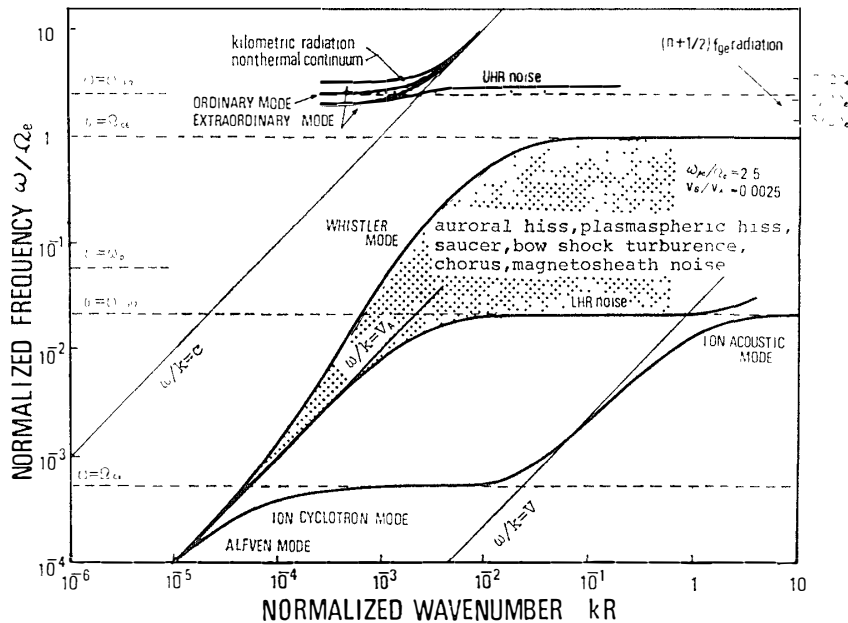


Fig. 2. Plasma waves dispersion curves for a low  $\beta$  plasma with  $\Omega_e < \omega_{pe}$ . Auroral hiss, plasmaspheric hiss, saucer, chorus, bow-shock turbulence and magnetosheath noise belong to whistler mode waves. Kilometric radiation and non-thermal continuum belong to ordinary or extraordinary electromagnetic waves (after YAMAMOTO, 1976).

and belong to the whistler mode wave. These emissions are observed in the cusp region as lion's roar (SMITH *et al.*, 1969) and occasionally propagates to the ground (HAYASHI and KOKUBUN, 1971). Day-side auroral hiss is observed in the frequency range from a few kHz to a few tens of kHz and is similar to the midnight auroral hiss. This emission is generated by soft electrons in the magnetosheath precipitating in the cusp region. Plasmaspheric hiss is seen in the frequency less than 1 kHz, and is a typical phenomenon in the plasmasphere. According to KENNEL and PETSCHKE (1966), electrons with energy higher than a few tens of keV steadily precipitate into the plasmasphere and generate this emission. A part of the plasmaspheric hiss propagates to the ground and is observed as low-latitude hiss (HAYAKAWA *et al.*, 1975). Chorus emissions are observed around the frequency from a few hundred Hz to a few kHz. Although chorus emissions are dominantly observed in the dayside (03–15h), similar emissions are also observed in the midnight in the development of a substorm (TSURUTANI and SMITH, 1974). The characteristics of chorus emissions detected on the satellite are similar to those observed on the ground in the auroral zone (HAYASHI *et al.*, 1968; KOKUBUN *et al.*, 1969; SATO *et al.*, 1974). Non-thermal continuum is a faint radio emission and seems to be excited by the relativistic electrons ( $>100$  keV). The frequency of this wave is higher than the local plasma frequency. If the wave frequency is lower than the plasma frequency in the solar wind, the emission is trapped in the magnetosphere. Odd half gyrofrequency emission is a very strong electrostatic wave (1–10 mV/m). This emission seems to be related to the acceleration of auroral particles but its characteristics are not clear in detail. Saucer emission is observed in a frequency range from a few hundred Hz to a few tens of kHz. It is usually observed on the lower latitude side of the hiss occurrence region. It seems to be produced by upflowing positive ion flux at energies of less than about 50 eV (JAMES, 1976). Auroral kilometric radiation is the intense radio emission escaping from the earth's auroral regions at frequencies above the local electron plasma frequency (a few tens of kHz–500 kHz). This emission seems to be generated by auroral particles along the auroral field line relatively close to the earth, a radial distance from about 2 to 5  $R_E$  polar regions is associated with visible aurora. Out of these emissions in the magnetosphere, the auroral hiss observed in the midnight region is the main topic of this paper and we will review the examinations of auroral hiss phenomena obtained by many investigators in following sections.

## 1.2. Auroral hiss observations

The first direct observation of VLF emission associated with aurora was made in 1932 in New Hampshire (magnetic latitude  $57^\circ\text{N}$ ) by BURTON and BOARDMAN (1933) while they were listening to atmospherics. Hiss usually appears as band limited thermal noise and, it is identified aurally by a hissing sound. In the following two decades the interest in VLF phenomena was small and the

next observation of VLF emission associated with the aurora was not made until 1957. ELLIS (1957, 1960, 1961) observed the hiss emission at 4.6 kHz band and auroral luminosity at red line (6300 Å). He showed that the fluctuations of hiss intensity are at times correlated with the luminosity of aurora. DOWDEN (1959) examined the hiss intensity in detail at Tasmania and found that the moderate intensities of hiss at 9 kHz and 230 kHz are about  $10^{-15}$  W/m<sup>2</sup> Hz and  $10^{-19}$  W/m<sup>2</sup> Hz respectively. Statistical correlation between visual aurora and hiss has been established by MARTIN *et al.* (1960), JØRGENSEN and UNGSTRUP (1962), MOROZUMI (1962, 1965) and MOROZUMI and HELLIWELL (1966). Hiss associated with visual aurora usually appears around 4 kHz but the low frequency limit may fall below 1 kHz. The upper frequency limit of the observed hiss often exceeds a few hundreds of kHz. MARTIN *et al.* (1960) stated that the center frequency of the hiss band is usually around 8 kHz and that intensity and band width vary with ionospheric absorption and may vary with the intensity of aurora. During strong absorption the intensity of the hiss drops to an undetectable level even in the presence of intense and active aurora. Their observations were made at Byrd Station, Antarctica (geomagnetic latitude 70.5°S). Simultaneous observations of 8 kHz hiss and visual aurora were also carried out at Godhavn, Greenland (geomagnetic latitude 79.9°N) well inside the northern auroral zone (UNGSTRUP, 1959, 1966; UNGSTRUP and JACKROTT, 1963; JØRGENSEN and UNGSTRUP, 1962). A clear correlation between the occurrence of the two phenomena was found and furthermore the intensity variations of the hiss and the aurora were similar. MOROZUMI (1962) studied the auroral occurrence at the South Pole (geomagnetic latitude 78°S) in relation to VLF emission. The auroral occurrence exhibited two diurnal peaks, one near midnight UT and one near noon UT. The midnight peak was related to VLF hiss and the auroras were of the band type. During the noon peak the auroras were of the rayed type with ionospheric absorption and no hiss. There was a chorus maximum at noon UT but no statistical correlation was found between aurora and chorus. MOROZUMI (1965) also showed that there is a typical sequence of events during the midnight local time. The first phase is the pre-breakup phase, the hiss being the most prominent feature. The second phase is breakup with a sudden onset of strong auroral activity. During this phase large amplitude variations of hiss occur. In the third or after breakup phase, the auroral hiss disappears and the chorus type emission occurs. HARANG *et al.* (1965), HARANG and LARSEN (1965), HARANG and HAUGE (1965) and HARANG (1969) studied hiss at Tromsø, Norway (geomagnetic latitude 67.1°N) and found hiss is related to weak auroral absorption events less than 1 dB at 30 MHz. During strong absorption events, there was a negative correlation between intensity of hiss and absorption. ROSENBERG (1968), HIRASAWA and NAGATA (1972) and KOKUBUN *et al.* (1972) showed that burst-like hiss enhancements with a duration of a few minutes are closely related to an increase in luminosity of aurora with

similar duration. OGUTI (1974, 1975) examined a precise relationship between a auroral activity and an enhancement of hiss emissions using real time auroral records on a video tape and simultaneous records of VLF waves on the sound track of the same video tape. He reported that specific small scale auroral activities were found to be associated with specific burst-like hiss enhancements with durations of 0.1–1 s. The enhancements of local auroral activity and of hiss emissions are concluded to be simultaneous within a time accuracy of 200 ms at worst, and within a few tens of ms at best.

JØRGENSEN (1966) studied the general pattern and locations of the 8 kHz auroral hiss zone on the basis of the observations from three Greenland stations (Nord, Godhavn and Narssarsuaq). A contour map of the percentage of hiss occurrence is shown in Fig. 3a. It is clear that hiss activity is greatest about an hour before magnetic midnight at approximately 70° latitude and that the hiss activity region is located around 80° in latitude in the afternoon. GURNETT (1966), BARRINGTON *et al.* (1971) and HUGHES *et al.* (1971) examined the spatial distribution of auroral hiss observed on satellites. Fig. 3b shows the occurrence

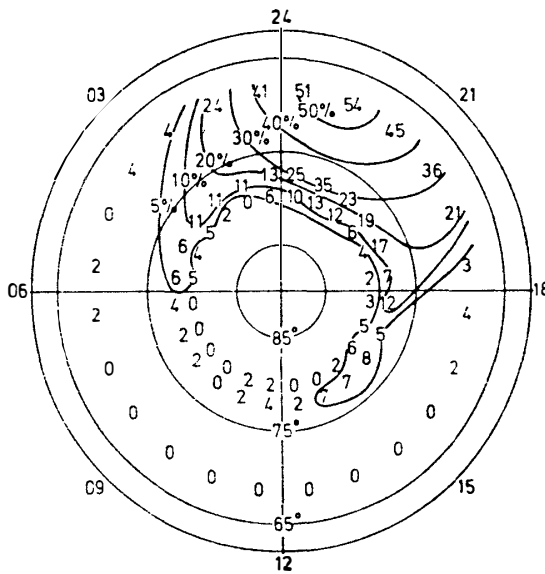


Fig. 3a. Contour map of the 8 kHz hiss zone based on observations from the three stations in Greenland during November and December 1964. The contours surround regions in which hiss bursts with spectral densities above  $1 \times 10^{-15} \text{ W/m}^2 \text{ Hz}$  occur in a given percentage of the hourly intervals (after JØRGENSEN, 1966).

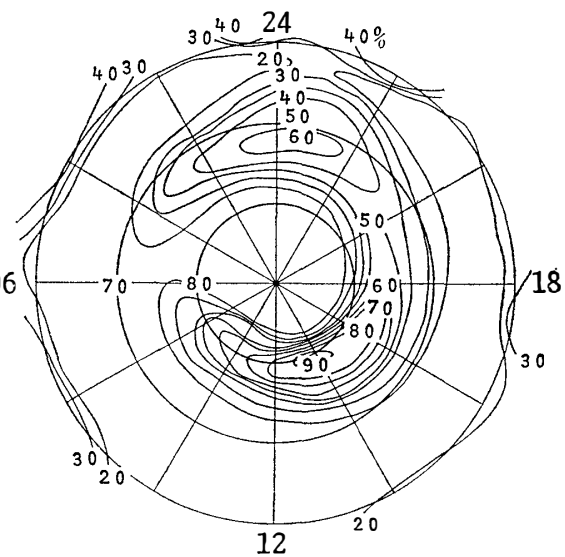


Fig. 3b. The frequency of occurrence distribution of auroral hiss at 9.6 kHz as a function of invariant latitude and magnetic local time. Only events with magnetic field intensities greater than  $10^{-12} \text{ gamma}^2 \text{ Hz}^{-1}$  were counted (after HUGHES *et al.*, 1971).

frequency of auroral hiss observed on Ariel 3 by HUGHES *et al.* (1971). The maximum occurrence of auroral hiss closely follows the auroral oval varying from about  $80^\circ$  invariant latitude on the day side of the earth to about  $72^\circ$  invariant latitude on the nightside of the earth. The statistical distributions of auroral hiss observed on the ground and on the satellite are very similar. JØRGENSEN (1968) examined the spectral density of a moderate hiss burst observed in detail at Byrd Station. Results showed that the peak intensity is seen around 10 kHz as in Fig. 4a. However the spectrum may drastically change in relation to the auroral luminosity and ionospheric condition. The spectrum of auroral hiss observed on a polar-orbiting satellite have been reported by GURNETT (1966),

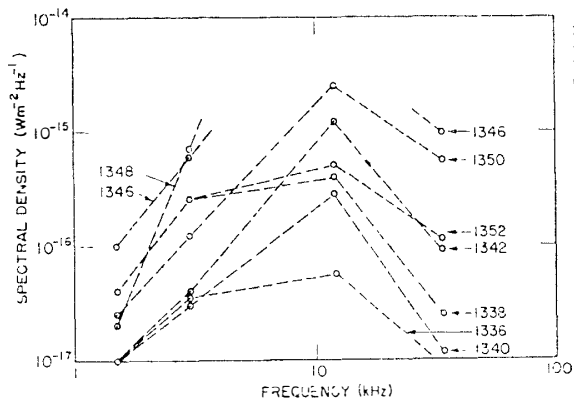


Fig. 4a. Moderate auroral hiss spectral density observed at Byrd Station in 1966. Spectral density is a function of the frequency and the universal time (after JØRGENSEN, 1968).

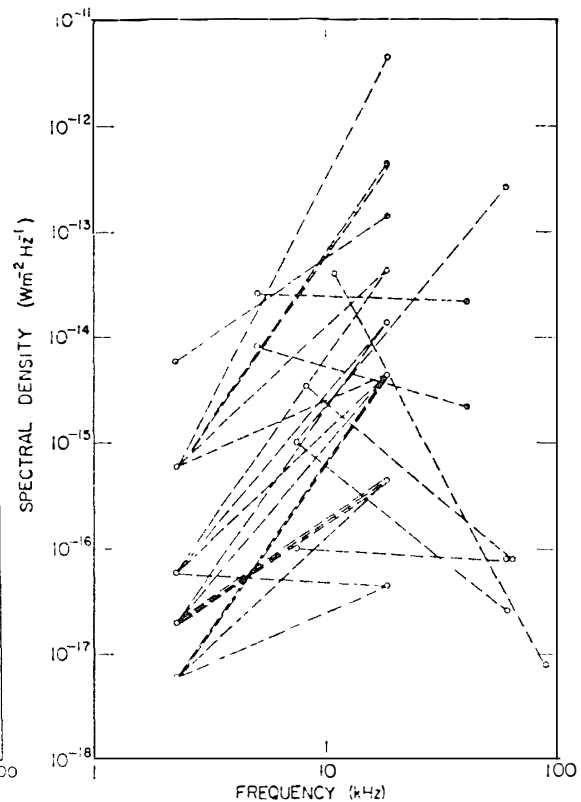


Fig. 4b. Auroral hiss observed on OGO 2, November 12-23, 1965. Each dashed line corresponds to one pass of the satellite through a noise region, and end points of a line represent the spectral densities measured at two frequencies simultaneously (after JØRGENSEN, 1968)

JØRGENSEN (1968), BARRINGTON *et al.* (1971) and MOSIER and GURNETT (1972). Fig. 4b shows the auroral hiss spectra observed on the OGO 2 satellite by JØRGENSEN (1968). The spectra observed on the satellite have a peak near 10 kHz, similar to hiss observed on the ground. The maximum spectral density was  $4.4 \times 10^{-12}$  W/m<sup>2</sup> Hz, the typical average spectral density being  $10^{-14}$ – $10^{-15}$  W/m<sup>2</sup> Hz. BARRINGTON *et al.* (1971) and MOSIER and GURNETT (1972) examined the spectral density of auroral hiss in detail and reported that the intensity of hiss occasionally was higher than  $10^{-11}$  W/m<sup>2</sup> Hz, around a few kHz. The spectral density of auroral hiss observed on the satellite also seems to change remarkably with space and time.

GURNETT (1966) showed that auroral hiss is closely correlated with intense fluxes of precipitating electrons with energy less than 10 keV. Subsequent studies have firmly established that auroral hiss is generated along the auroral field lines by intense fluxes of electrons precipitating into the ionosphere with energies in the range from a few hundreds of eV to several keV (HOFFMAN, 1969; HARTZ, 1970; GURNETT and FRANK, 1972; HOFFMAN and LAASPERE, 1972). GURNETT and FRANK (1972) examined the spectrum of the auroral electron precipitation related to auroral hiss.

Fig. 5 shows the auroral hiss emissions that occur in direct association with an intense inverted-V electron precipitation discussed by FRANK and ACKERSON (1972). They also indicated that there is a threshold low energy electron flux ( $10^4$ – $10^5$  electron/cm<sup>2</sup>·s·sr·keV at 100 eV) below which hiss is not observed. A VLF saucer emission is evident near the low-latitude boundary of the electron precipitation region. Both the auroral hiss and the saucer emissions are characterized by a V-shaped frequency-time structure. The characteristic frequency-time variation is actually understood as a spatial effect caused by the frequency-dependent limiting ray direction of the whistler mode wave at large wave normal angles (MOSIER and GURNETT, 1969; JAMES, 1976). The essential distinction between the auroral hiss and saucer emissions is found in the direction of propagation, which is downward for the auroral hiss and upward for the saucer (MOSIER and GURNETT, 1969; MOSIER, 1971). Fig. 5 also illustrates the occurrence of ELF noise bands in the same region as the inverted-V electron precipitation occurs. The propagation mode of this emission is not yet known either in the whistler mode or in the ion cyclotron mode.

HOFFMAN and LAASPERE (1972) also compared the auroral hiss with the simultaneous data of auroral particles. They showed that the occurrence of VLF hiss, especially the day side auroral hiss, correlates well with electron precipitation with 0.7 keV energy but, in general, it relates very poorly with the activity in the higher energy channels. The simultaneous occurrence of 1 keV electron precipitation and broad band auroral hiss is shown in Fig. 6a. The maximum electron fluxes encountered reached nearly  $10^{10}$  (electron/cm<sup>2</sup>·s·sr·keV) and were

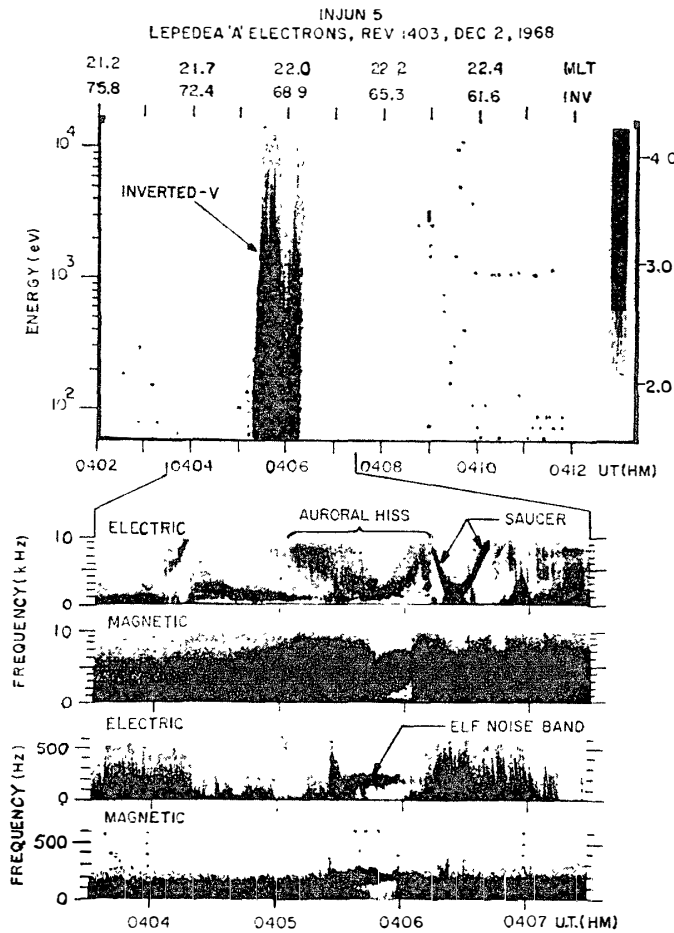


Fig. 5. High resolution frequency-time spectrograms of electric and magnetic fields detected by the Injun 5 spacecraft at an altitude of about 2500 km showing the occurrence of auroral hiss, saucer emissions and an ELF noise band in close association with an inverted-V electron precipitation event (after GURNETT and FRANK, 1972).

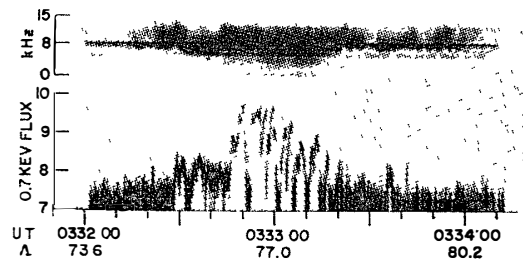


Fig. 6a. An event illustrating positive correlation between precipitating 0.7 keV electrons and VLF hiss observed simultaneously. The numbers on the ordinate of electron data give the logarithms of electron flux in  $\text{electron}/\text{cm}^2 \cdot \text{s} \cdot \text{sr} \cdot \text{keV}$ . The data were acquired on April 22, 1968, at about 1430 MLT (after HOFFMAN and LAASPERE, 1972).

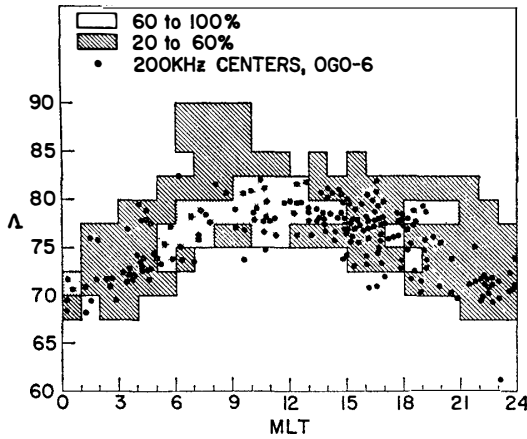


Fig. 6b. A superposition of the centers of the auroral hiss zone at 200 kHz as observed on OGO 6 (dark circles) (LAASPERE *et al.*, 1971) on the probability of occurrence of 0.7 keV structured precipitation on OGO 4 (HOFFMAN and BERKO, 1971). Only events for which  $K_p < 2$  were included in both studies.

centered within the region of auroral hiss. The general relationships between the region of soft electron precipitation observed on OGO 4 (HOFFMAN and BERKO, 1971) and the locations of the auroral hiss zone at 200 kHz as observed on OGO 6 (LAASPERE *et al.*, 1971; LAASPERE and JOHNSON, 1973) are superimposed in Fig. 6b (HOFFMAN and LAASPERE, 1972). It shows that the centers of auroral hiss at 200 kHz fall remarkably well within the region of this type of electron precipitation, even during the midnight hours. From detailed inspections of the records based on OGO 4 data, LAASPERE and HOFFMAN (1976) reported that electrons of energies below about 0.7 keV are the predominant source of the nightside as well as the dayside hiss.

### 1.3. Generation mechanism of auroral hiss

Ever since ELLIS (1957) first pointed out the possibility that incoherent Cerenkov radiation could be the source mechanism of VLF hiss in high latitude, considerable effort has gone into investigating the possibility that hiss is generated by incoherent Cerenkov or Cyclotron radiation from the precipitating electrons (EIDMAM, 1958; DOWDEN, 1960; LIEMOHN, 1965; MCKENZIE, 1967; MANSFIELD, 1967; TRULSEN and FEJER, 1970). However, ELLIS (1957), LIEMOHN (1965) and others concluded that the total energy produced by an incoherent Cerenkov radiation process was several orders of magnitude too low to explain the observed power densities. It was clear that there may exist several reasons for the discrepancies between theory and observations in earlier attempts to explain emissions by Cerenkov radiation. For example, no data on the thermal electron concentration above the F2 layer maximum were available when ELLIS did his work in 1957. LIEMOHN (1965) estimated the total power produced by energetic electrons in a tube of lines of force. The total power from an incoherent process was calculated by the expression  $P_{\text{total}} = P_e \cdot N_e \cdot V$ , where  $P_e$  is the average emitted power per electron ( $10^{-30}$ – $10^{-28}$  W/Hz electron),  $N_e$  is the density of the energetic electrons and  $V$  is the volume of the tube. He showed that the observed power exceed

the calculated power by seven orders of magnitude. This difference is much too large for the following three reasons. (1) The observed power with which the calculated power was compared was claimed to be  $10^{-10}$  W/m<sup>2</sup> Hz. But in a recent paper BARRINGTON *et al.* (1971) reported the moderate spectral density to be about  $10^{-12}$  W/m<sup>2</sup> Hz. (2) Although the emissions were observed at latitudes where the magnetic shell parameter  $L$  (McILWAIN, 1961) is about 7 and higher (HUGHES *et al.*, 1971), the tube of lines of force, the volume which was used in the total power calculation, was located by LIEMOHN at  $L=3$ . (3) The density of the energetic particles was taken to be  $0.1$  cm<sup>-3</sup>, but densities of electrons with energies between 1 and 10 keV observed in the auroral zone found to be almost 1 order of magnitude higher (EVANS, 1968; ARNOLDY and CHOY, 1973; ARNOLDY *et al.*, 1974). Using comparatively new experimental information, JØRGENSEN (1968) made a quantitative calculation of the Cerenkov emission according to the expression derived by MANSFIELD (1967) [Whose results are in agreement with those of LIEMOHN (1965)]. The power produced by Cerenkov radiation from a single particle expressed in W/Hz was given by the following equation.

$$dp/df = \left| \sum_{j=1}^2 q^2 2\pi f [\beta_{\perp}^2 T_{11} J_1^2(L_0) + \beta_{\parallel}^2 T_{33} J_0^2(L_0) - 2\beta_{\perp} \beta_{\parallel} T_{13} J_1(L_0) J_0(L_0)] / \right. \\ \left. 2\varepsilon_0 V_{\parallel} (B_n^2 - 4C_n \varepsilon_1)^{1/2} \right|_{\mu=\mu_j}. \quad (1)$$

Notations are given in Appendix A. Assuming an appropriate model for region in space and beam of precipitating electrons, he calculated the total power generated in the region. It was found that a calculated peak power as produced by an incoherent radiation was about  $10^{-14}$  W/m<sup>2</sup> Hz at 10 kHz. It was shown that there was a difference is about two orders of magnitude between the observed spectral density ( $\sim 10^{-12}$  W/m<sup>2</sup> Hz) and the maximum calculated spectral density ( $\sim 10^{-14}$  W/m<sup>2</sup> Hz). He concluded that this difference was not serious for the calculated spectrum is produced by electron with energies above 1 keV only. Knowledge of auroral electrons with energies below 1 keV was poor at that time. Recently a better correlation has been shown between auroral hiss occurrence and precipitation of electrons with energy less than 1 keV rather than higher energy by the simultaneous satellite observations of auroral hiss and of electron precipitations (GURNETT and FRANK, 1972; HOFFMAN and LAASPERE, 1972).

Using this new background information, LIM and LAASPERE (1972) reexamined the possibility that incoherent Cerenkov radiation is the source of auroral hiss, considering in particular, the contribution from electrons with energy less than 1 keV. However, their result yields the power of the spectral peak of the order of  $10^{-13}$  W/m<sup>2</sup> Hz with the frequency at 70 kHz. This calculated power is still about two orders of magnitude less than a recent observation on Injun 5 ( $\sim 10^{-11}$  W/m<sup>2</sup> Hz MOSIER and GURNETT, 1972). Furthermore, JAMES (1973) has pointed out that hiss emissions have a strong correlation with precipitating soft electrons

and that their propagation direction is near the electrostatic resonance cone of the whistler mode. From the computation of Cerenkov radiation accounting for the ray path spreading, he concluded that the incoherent theory for the auroral hiss generation mechanism is inappropriate. RAO *et al.* (1973) showed that the intense field-aligned irregularities ( $\Delta n/n > 3$ ) are necessary in order for the field-line guiding of auroral hiss to be completely effective. TAYLOR and SHAWAN (1974) studied again in detail the incoherent Cerenkov mechanism for auroral hiss by using a refined model. They argued also that the emitted wave normal is near the resonance angle, so that the waves are nearly electrostatic. The complete guided wave propagation yields a peak intensity of  $7 \times 10^{-13}$  W/m<sup>2</sup> Hz at 10 kHz, while the more accurate model taking into account ray path spreading as well as collisional absorption yields a reduced peak intensity of  $5 \times 10^{-14}$  W/m<sup>2</sup> Hz. Their results also indicated that the incoherent Cerenkov mechanism cannot produce the observed noise level.

ENGLISH and HUGHES (1974) and NODA and TAMAO (1976) showed that the shape of the spectrum obtained from the incoherent mechanism is mostly determined by a given model of plasma density distribution. It is pointed out that a peak spectral power for the guided Cerenkov emission occurs near the local electron plasma frequency at a point along the field line where the plasma frequency coincides with the local electron cyclotron frequency ( $f_{\text{peak}} = f_{pe} \sim f_{He}$ ). This result gives us a reasonable explanation for the difference in the calculated hiss spectra between (1) JØRGENSEN and (2) LIM and LAASPERE. MAEDA (1975) showed that the maximum intensity of auroral hiss at the ground is of the order of  $10^{-14}$  W/m<sup>2</sup> Hz around 20 kHz and is ascribable to the incoherent Cerenkov radiation from soft auroral electrons with intensity of the order of  $10^8$  el./cm<sup>2</sup> · s · sr · eV at 100 eV. However, he also suggested that there are some types of VLF hiss in the magnetosphere which cannot be explained solely by incoherent Cerenkov radiation from electrons but require at least partially coherent, amplified Cerenkov sources or emissions caused by plasma instabilities.

GALLET and HELLIWELL (1959) first, and then DOWDEN (1962) suggested that VLF hiss is produced by amplification of parallel propagating whistlers by the traveling wave tube instability. SWIFT and KAN (1975) suggested that VLF hiss is produced by beam amplification of electrostatic whistlers. They calculated the group velocity and growth rate for whistlers and argued that the beam mechanism will produce VLF hiss around the regions of low background electron density at frequencies near the electron plasma frequency. Because they did not solve the wave kinetic equation, they could not describe the VLF hiss power flux spectrum and accurately determine the convective growth or recognize the importance of geometric factors and the ratio of the electron plasma frequency to gyrofrequency. Recently, MAGGS (1976, 1978) and YAMAMOTO (1979) showed that the observed power fluxes of VLF hiss can be accounted for by convective beam

amplification of incoherent Cerenkov whistler radiation by the beam of precipitating auroral electrons. The beam amplification mechanism was investigated by using the lowest order WKB wave kinetic equation and linear growth rates. The power flux at an observer in the auroral arc is given by MAGGS (1978) as

$$\frac{d^2}{dk_{\parallel}d\omega}P(\omega, k_{\parallel}) = \int_{\text{obs}}^{\infty} E \cdot F \exp [2M(\omega, k_{\parallel}, s')] ds', \quad (2)$$

where

$\omega$ : whistler frequency

$k_{\parallel}$ : whistler parallel wave number at the observation point

$M$ : the amplification factor  $\int_{\text{obs}}^s (\gamma/V_g) ds'$

$\gamma$ : temporal linear growth rate

$V_g$ : group velocity

$E$ : power flux per unit frequency of incoherent whistler mode radiation

$F$ : geometric term resulting from the divergence of ray path.

Following the calculation of the linear growth rate calculated by YAMAMOTO (1979), the growth rate for the drift Maxwellian velocity distribution can be written as

$$\frac{\gamma}{\omega} = \frac{1-Z}{2} (A^2 - R^2/Z) D_L [N(A^2 - R^2/Z) + GAC_1 + \sin^2 \theta C_2]^{-1} \quad (3)$$

where

$$D_L = -2\pi \frac{n_b}{n_o} \frac{\omega}{k_z} \frac{\Pi^2}{k^2} \int 2\pi t dt J_0^2(\lambda t) \left(1 - \frac{u}{v'_z}\right) \times \frac{1}{n_b} F_-(at, \omega/k_z, s) \quad (4)$$

and the notations  $R$ ,  $Z$ ,  $A$ ,  $G$ ,  $C_1$  and  $C_2$  are given in Appendix B.

The power flux is mostly determined by the ray path length and spatial growth rate ( $\gamma/V_g$ ) with frequency. MAGGS (1978) and YAMAMOTO (1979) show that the growth rate ( $\gamma/\omega$ ) without the variation of beam velocity distribution is proportional to the ratio of beam density ( $n_b$ ) to cold electron density ( $n_o$ ),  $n_b/n_o$  (see eqs. (3) and (4)). Then the peak growth rate for the same relative frequency  $\omega/\Omega_e$  (or  $\omega/\pi_e$ ) decreases with a decrease in altitude due to the rapid increase in  $n_o$ . The important point to be noted is that the growth rate depends on the shape of the drift Maxwellian velocity distribution, especially the drift speed  $u$  and the thermal velocity  $a$ . According to YAMAMOTO (1979), the growth rate above increases as the ( $u/a$ ) ratio increases. He concluded that a large value of ( $\gamma/\omega$ ) is retained even at low altitudes ( $n_b/n_o$  is small) when the  $u/a$  ratio (for a fixed  $n_b$ ) is large.

The theory of the coherent Cerenkov radiation seems hopeful for explaining the auroral hiss phenomena. However, the saturation level of hiss near the plasma frequency cannot be correctly estimated within a linear theory. Non-linear

theory is necessary to explain the intensity of emission near the plasma frequency (also near the gyrofrequency). Furthermore, the magnitude of power flux calculated by this theory depends on the precipitating electron differential energy spectrum and the scale size of the ray path along which the wave is amplified. Since these factors are not sufficiently known yet, determination of the precipitating electron differential energy spectrum and the amplification region of auroral hiss on the observation basis, and comparison of the expected with the calculated hiss spectrum is essentially important.

#### 1.4. Observations in this study

Coordinated VLF observation were carried out at the two ground Stations, Syowa and Mizuho, and on board ISIS 1 and 2 satellites from June to December in 1976. The geographical location of Syowa Station ( $-69.03^\circ$ ,  $39.60^\circ$ ) and Mizuho Station ( $-70.70^\circ$ ,  $44.33^\circ$ ) are shown in Fig. 7; geomagnetic coordinates of the two stations are  $-70.38^\circ$ ,  $79.39^\circ$  and  $-72.32^\circ$ ,  $80.62^\circ$  respectively. Mizuho Station is about 260 km poleward of Syowa Station along the geomagnetic meridian. Both stations are situated in the auroral zone and are suitable for studying the auroral activities, related phenomena and their latitude dependence as well. The equipment for observations of aurora, magnetic variations and VLF emission at Syowa and Mizuho Stations are listed in Table 1 (NAGATA *et al.*, 1976a). The data of VLF emissions used here were obtained at both Stations for the period from June to October in 1976 during which, except in September, the VLF instruments at both stations were operated normally. We examined also the arrival direction of VLF waves at Syowa Station from April to October in 1976. In addition, some VLF emission data obtained at Syowa Station in 1969, 1970, 1974, 1975 and 1977 were also analyzed to examine the statistical tendencies of auroral hiss emissions. The all-sky camera auroral photographs and the data of the auroral luminosity by use of the meridian scanning photometer were compared with the VLF activities and arrival directions. An auroral photograph was taken every 10 s and it was used to study the location, pattern and slow movement of aurora. The auroral luminosities of 5577 Å green line recorded by a scanning photometer were also used to examine the absolute luminosity of aurora. An auroral TV camera was operated to record the fast motion of aurora. However, the TV data are not presented here, except for some references on the fast activity of aurora. Some auroral photographs taken by DMSP satellite were also examined in order to compare the ground VLF emissions with the global auroral pattern.

Almost the same observation system for measuring VLF emissions was adopted at both Syowa and Mizuho Stations. The block diagram of the VLF observation systems at these Stations are shown in Fig. 8. Three loop antennae (A, B, C) were used for receiving VLF emissions at Syowa Station and a loop antenna D

Table 1. Equipment of Syowa and Mizuho Stations. The all-sky camera, photometer and direction finder were installed only at Syowa Station (after NAGATA et al., 1976a).

Syowa Station			
Item	Equipment	Recorder	Remarks
Aurora	All-sky camera	35 mm camera	6 frames/min
	Meridian scanning photometer ( $H_{\beta}$ , 5577 Å)	3 ch. pen oscillograph Digital data recorder	Chart speed, 30 cm/min Sampling freq., 1 Hz
	High sensitive TV camera	Video tape recorder	60 frames/s
Magnetism	Fluxgate magnetometer	3 ch. pen oscillograph Digital data recorder	Chart speed, 15 cm/hour Sampling freq., 0.1 Hz
	Induction magnetometer	5 ch. scratch film recorder Analog data recorder	Chart speed, 15 cm/hour Magnetic tape speed, 3 mm/s Frequency range, 0.001–3 Hz
VLF emissions	Wide-band receiver	Analog data recorder	Magnetic tape speed, 4.75 cm/s Frequency range, 0.2–20 kHz
	Narrow-band intensity recorder	6 ch. pen oscillograph	(0.75, 1, 2, 4, 8 kHz etc.) Chart speed, 30 cm/hour
	Direction finder	6 ch. pen oscillograph Video tape recorder	Chart speed, 15 cm/hour 60 frames/s
Mizuho Station			
Item	Equipment	Recorder	Remarks
Aurora	High sensitive TV camera	Video tape recorder	60 frames/s
Magnetism	Fluxgate magnetometer	3 ch. pen oscillograph Digital data recorder	Chart speed, 15 cm/hour Sampling freq., 0.1 Hz
	Induction magnetometer	5 ch. scratch film recorder Analog data recorder	Chart speed, 15 cm/hour Magnetic tape speed, 3 mm/s Frequency range, 0.001–3 Hz
VLF emissions	Wide-band receiver	Analog data recorder	Magnetic tape speed, 4.75 cm/s Frequency range, 0.2–20 kHz
	Narrow-band intensity recorder	6 ch. pen oscillograph	(0.75, 1, 2, 8 kHz) Chart speed, 30 cm/hour

Fig. 7. Location of Syowa and Mizuho Stations. The dotted region represents sea. Mizuho Station ( $-70.70^\circ, 44.33^\circ$ ) is about 260 km poleward of Syowa Station ( $-69.03^\circ, 39.60^\circ$ ) along the geomagnetic meridian.

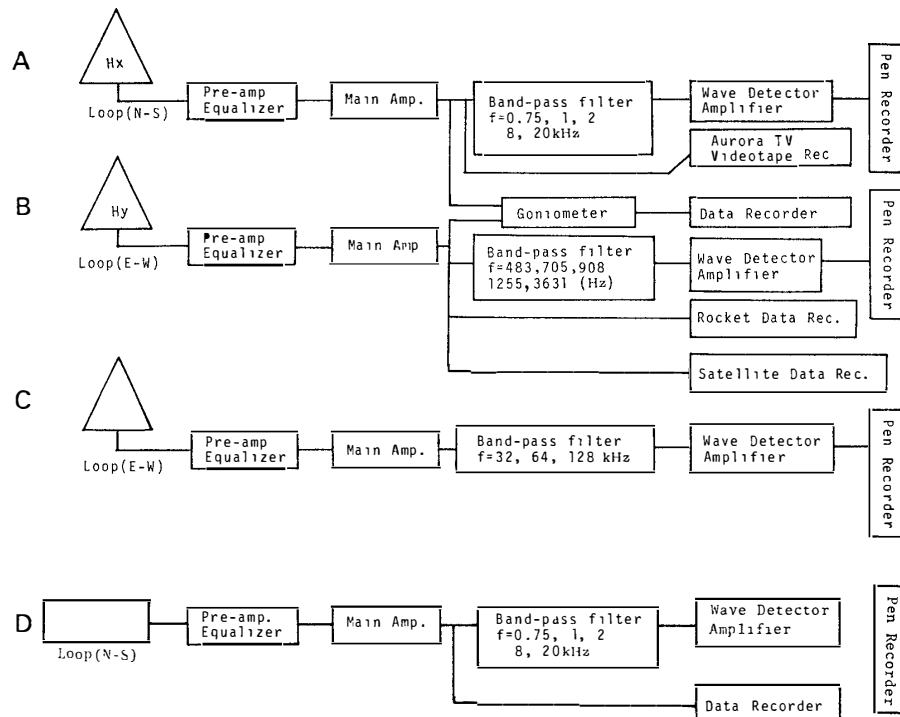
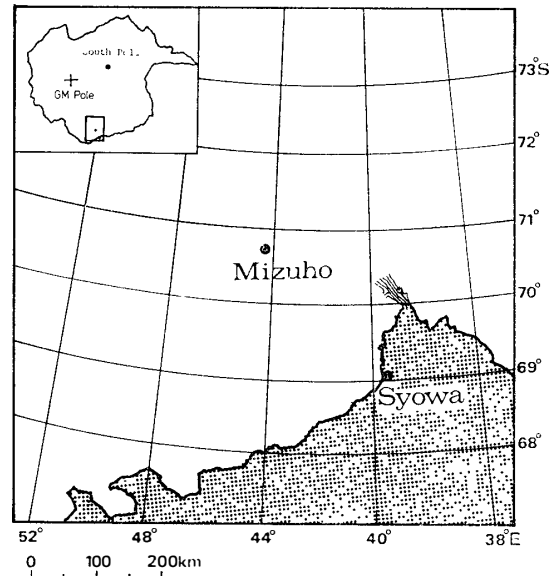


Fig. 8. Block diagram of the VLF observation systems at Syowa (A, B, C) and Mizuho Stations (D).

was used at Mizuho Station. Two loop antennae (A, B) were used for receiving the low frequency bands of VLF emissions ( $f < 20\text{ kHz}$ ). They were also used for determining the arrival directions of VLF emissions. The height and the width

of a triangle loop antenna (A and B) is 10 m and 20 m respectively with an effective area of 100 m<sup>2</sup>. These antennae lie in the geomagnetic E–W and N–S planes respectively. Another loop antenna C was used to receive the high frequency bands of auroral hiss emissions ( $f < 128$  kHz). The dimension of the C antenna is 20 m in height and 40 m at the base with an effective area of 400 m<sup>2</sup>. The antenna plane lies in the geographical N–S direction. Antenna D at Mizuho is a square loop and its dimension is 2 m in height and 20 m in width with an effective area of 40 m<sup>2</sup>. Both of antennae A and D were set in a vertical plane whose normals orient are in the geomagnetic east–west direction. A specially designed circuit for equalizing the frequency characteristics of antennae was assembled in the pre-amplifier in order to make possible a quantitative comparison of the intensity in VLF emission between the two stations. The frequency-amplitude characteristics of both receivers (including equalizer and pre-amplifier) are shown in Fig. 9. Both receivers can detect waves with intensities above  $10^{-16}$  W/m<sup>2</sup> Hz in the

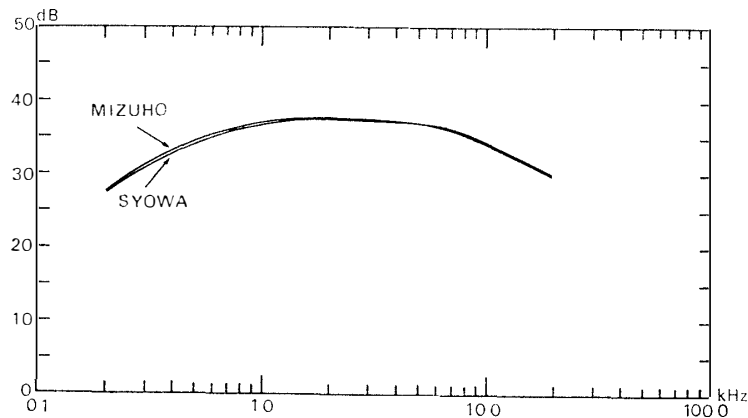


Fig. 9. The frequency-amplitude characteristics of VLF receivers at Syowa and Mizuho Stations.

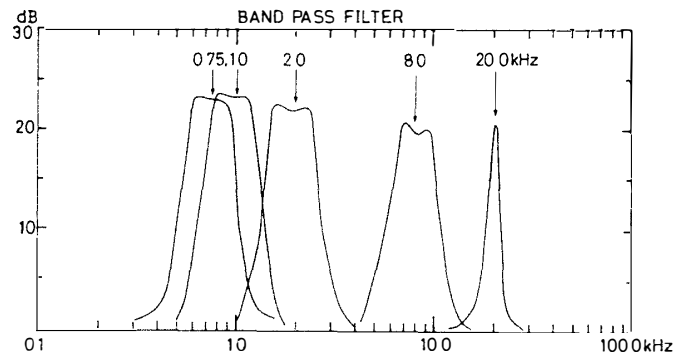


Fig. 10. The characteristics of the narrow band-path filters at both stations. The center frequency of the narrow band-path filters are 750 Hz, 1 kHz, 2 kHz, 8 kHz and 20 kHz respectively.

frequency range from 300 Hz to 20 kHz. VLF emissions were recorded by several magnetic tape recorders (video tape recorder, audio tape recorder) and the band limited intensities were recorded by pen writing recorders. The characteristics of the narrow band-pass filters at both stations are shown in Fig. 10. The center-frequency of the narrow band-pass filters are 750 Hz, 1 kHz, 2 kHz, 8 kHz and 20 kHz and their band-widths of them are 300 Hz, 400 Hz, 800 Hz, 3.2 kHz and 1.6 kHz respectively. The intensities of other narrow-band VLF signals were also recorded at Syowa Station. The center-frequencies are 483 Hz, 750 Hz, 900 Hz, 1255 Hz, 3631 Hz, 32 kHz, 64 kHz and 128 kHz with band-widths of 40 Hz, 40 Hz, 40 Hz, 40 Hz, 40 Hz, 3.2 kHz, 6.4 kHz and 12.8 kHz respectively. The most difficult problem during our observations was how to achieve the grounding of the electronic circuits. Mizuho Station especially is located on thick continental ice (the thickness is about 2000 m) and hence it was difficult to properly ground the circuits. The low frequency range of VLF emissions (lower than 2 kHz) was seriously disturbed by the dynamo noise because of the poor grounding of the power system at Mizuho Station for the first half of the observation period. A radial counterpoise (radius=30 m, number of radial lines are 24) extending under the snow surface near the foot of the antenna reduced the noise level fairly well, and a high S/N level of VLF emissions was obtained for the last half of the observation period.

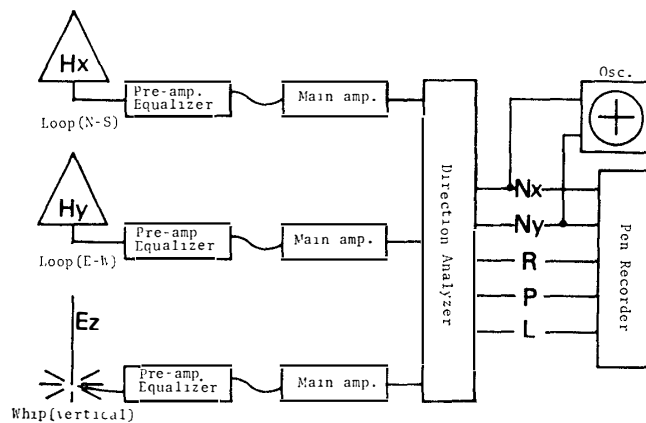


Fig. 11. The block diagram of the direction finding system at Syowa Station.

A system for detecting the arrival directions of the waves was operated at Syowa Station in 1976. This method, which can be applied to the elliptically polarized VLF electromagnetic waves, has been developed by TSURUDA and HAYASHI (1975). Fig. 11 shows the block diagram of this system at Syowa Station. The magnetic components of VLF emissions were received by the two loop antennae (A, B) and the electric component by one whip antenna 6 m high. Both the magnetic and electric signals were fed to the direction analyzer

and the results were recorded on a pen writing recorder and occasionally on a video tape. The principle of the analysis and system of the direction analyzer used here are described in Appendix C.

The tracking and the reception of the VLF records from the ISIS 1 and 2 satellites were also carried out at Syowa Station in 1976. The detailed descriptions about the tracking system are reported by NAGATA *et al.* (1976b). The orbit parameters and objectives of observation of ISIS 1 and 2 are listed in Table 2. The total orbital number of ISIS 1 and 2 which we examined here were 184 during the period from April 1976 to January 1977.

Table 2. The orbit parameters and objectives of observations of ISIS 1 and 2.

National name	Apo. (km)	Peri. (km)	Inc.	Period (min)	Objectives	Sponsor
ISIS 1	3514	574	88.42°	128.21	Topside sounding VLF etc.	Canada (CRC) -USA (NASA)
ISIS 2	1429	1367	88.16°	113.6	"	"

### 1.5. Contributions of the present research

Although many investigators have studied the characteristics of auroral hiss phenomena, especially its relationships with auroral activities, the change in the auroral hiss spectrum related to various types of aurora is not clear yet. In this paper, we will first examine the spectrum of auroral hiss simultaneously observed at Syowa and Mizuho Stations in Antarctica in Chapter 2. It will show that auroral hiss emissions can be categorized into two types; narrow-band continuous hiss and wide-band impulsive hiss. In Chapter 3, the characteristics of auroral type, luminosity and location related to these two types hiss will be examined. It will show that the continuous hiss emission are associated with the brightening of the auroral arc located a few hundreds km ( $\sim 300$  km) poleward of Syowa Station and the impulsive hiss emissions usually appear accompanied by active bright aurora near the zenith. The relationships between the arrival directions of these two types of hiss and the location of aurora will be examined in Chapter 4. It will be seen that the continuous hiss generally arrives from several hundreds km equatorward of the related aurora, while the impulsive hiss sometimes arrives from the region nearer the auroral location. In Chapter 5, VLF emissions observed on the satellite (ISIS 2) and on the ground (Syowa Station) will be compared, and it will be shown that the continuous hiss observed on the ground propagates along the non-ducted path from the satellite altitude to the ground.

The relationship between the auroral hiss and the global auroral activity and the occurrence of auroral hiss in the development of the magnetospheric substorm will be examined in Chapter 6. A reference will be made to the fact

that both of the impulsive and the continuous hiss are observed during the expansion phase of a substorm. It will also show that hiss emissions usually are not observed at Syowa Station when the aurora is located beyond about 700 km poleward of Syowa Station.

We will discuss the propagation path of auroral hiss and the differences in these two types of hiss from the view point of the generation mechanism and we will also estimate the generation region of hiss in Chapter 8. The generation region of continuous hiss will be estimated at about  $1.5 \times 10^4 \sim 3 \times 10^4$  km in altitude and that of impulsive hiss will be estimated at about  $5 \times 10^3 \sim 3 \times 10^4$  km in altitude.

## 2. Morphology of Auroral Hiss Emissions

The characteristics of auroral hiss observed at high latitudes have been investigated extensively by many workers, including MARTIN *et al.* (1960), HARANG and LARSEN (1965), MOROZUMI (1965) and JØRGENSEN (1966, 1968). The seasonal and daily occurrences of hiss emission were examined by HARANG and HAUGE (1965), KOKUBUN *et al.* (1972) and TANAKA *et al.* (1976). MOROZUMI (1965) has classified the auroral hiss into two types taking into account its association with auroral display and geomagnetic variations. One is characterized by the association of arc-like auroras and positive magnetic variations of 50–100  $\gamma$ . Another type is associated with a sudden increase in brightness of aurora followed by a sharp negative bay. In his work, however, the spectral differences of the two types were not fully examined. The purpose of this chapter is to examine the characteristics of auroral hiss based on data obtained at Syowa and Mizuho Stations in Antarctica.

### 2.1. Characteristics of auroral hiss

The auroral hiss is most active before the magnetic midnight and appears frequently in winter and equinox seasons. In summer, hiss emissions are rarely observed on the ground. The diurnal variation of the occurrence frequencies of hiss emissions at 4, 8, 32, 64 and 128 kHz bands is shown in Fig. 12a. In this figure percentage occurrences during the period from May to August in 1969 are plotted. Auroral hiss events are selected by the criterion that the intensity was stronger than the receiver threshold level ( $1.5 \times 10^{-15}$  W/m<sup>2</sup> Hz at 4 kHz,  $1.0 \times 10^{-15}$  W/m<sup>2</sup> Hz at 8 kHz,  $1.0 \times 10^{-16}$  W/m<sup>2</sup> Hz at 32 kHz,  $3 \times 10^{-17}$  W/m<sup>2</sup> Hz at 64 kHz and  $3 \times 10^{-18}$  W/m<sup>2</sup> Hz at 128 kHz). It is found that auroral hiss is dominantly observed at the pre-midnight of magnetic local time. These results are in good agreement with earlier works by HARANG and LARSEN (1965), JØRGENSEN (1968) and HARANG (1968). In addition, satellite observations demonstrate another maximum in hiss intensity around 1400 UT in the afternoon (GURNETT, 1966; McEWEN and BARRINGTON, 1976; BULLOUGH *et al.*, 1969; LAASPERE *et al.*, 1971; HUGHES *et al.*, 1971; KAISER, 1972). The disappearance

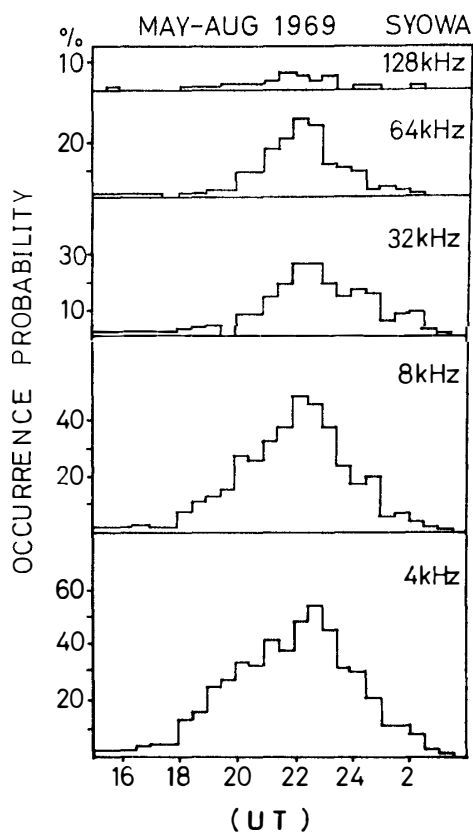


Fig. 12a. The diurnal variation of the occurrence frequencies of auroral hiss at the 4, 8, 32, 64 and 128 kHz bands observed at Syowa Station from May to August 1969.

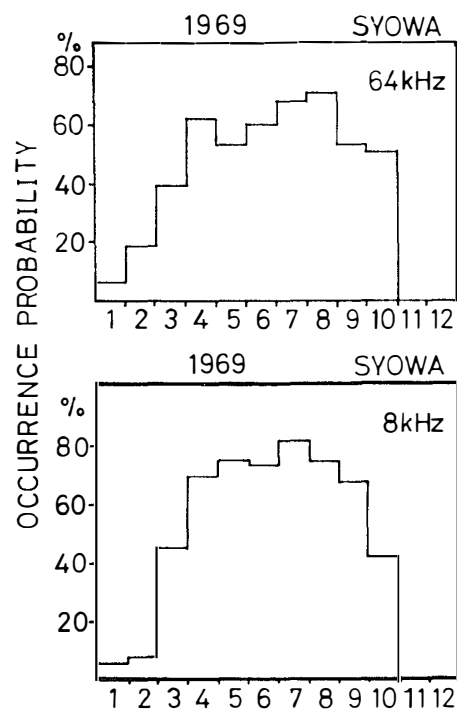


Fig. 12b. Seasonal variation of the occurrence frequencies of auroral hiss at the 8 and 64 kHz bands observed at Syowa Station in 1969.

of afternoon hiss on the ground is probably due to the enhanced ionospheric absorption of VLF waves. The seasonal variations of the occurrence frequency of auroral hiss at 8 kHz and 64 kHz bands are shown in Fig. 12b. We selected the auroral hiss events whose intensities are stronger than  $\sim 10^{-15}$  W/m<sup>2</sup> Hz at 8 kHz and  $\sim 3 \times 10^{-16}$  W/m<sup>2</sup> Hz at 64 kHz. As seen in this figure, hiss emissions with frequencies of both 8 kHz and 64 kHz are mainly observed from April to September, while they are rarely observed in January, February, November and December. We also examined the diurnal and seasonal dependences of the occurrence of hiss at the 4 kHz band. Fig. 13a shows that the auroral hiss frequency band tends to be observed at earlier magnetic local times ( $\sim 1700$  UT) during equinoctial seasons (March, April, September and October). On the other hand, auroral hiss in winter tends to appear at later magnetic local times ( $\sim 1800$  UT) and is intermittently observed till about 0200 UT. Fig. 13b also shows the occurrence of LF emission at the 64 kHz band. The similar feature

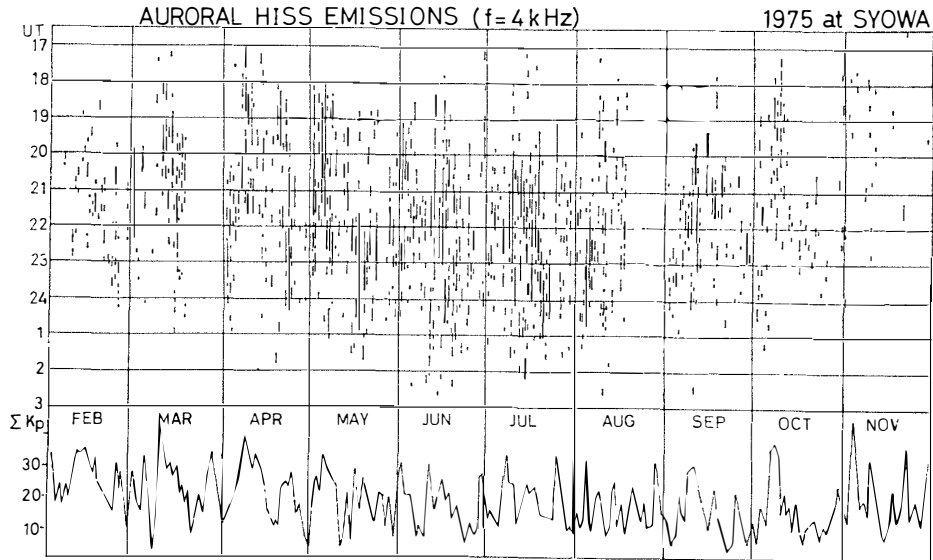


Fig. 13a. Diurnal and seasonal variations of the occurrence rate of auroral hiss at the 4 kHz band. Each dot represents a hiss event. Only events with spectral densities above  $1.5 \times 10^{-15} \text{ W/m}^2 \text{ Hz}$  were selected. Bottom panel shows the seasonal variation of  $\Sigma K_p$  index.

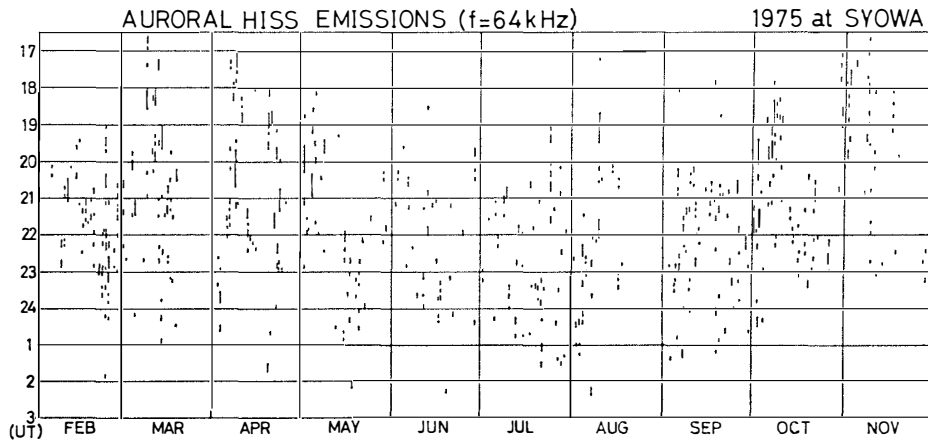


Fig. 13b. Diurnal and seasonal variations of the occurrence rate of auroral hiss at the 64 kHz band. Only events with spectral densities above  $2 \times 10^{-17} \text{ W/m}^2 \text{ Hz}$  were selected.

is more evident in this band. The relationships between  $\Sigma K_p$  and the occurrence of auroral hiss are also shown in Fig. 13a. When  $\Sigma K_p$  is larger than  $\sim 30$ , auroral hiss emission appears at earlier magnetic local time ( $\sim 1700$  UT). Those emissions are not specific to the hiss emissions observed in 1970, 1975, 1977 but are general characteristics being applicable to the emission observed in other years. Fig. 14 represents all auroral hiss events with intensities higher than the threshold level at the 8 kHz band, based on the records of Syowa and Mizuho Stations. The

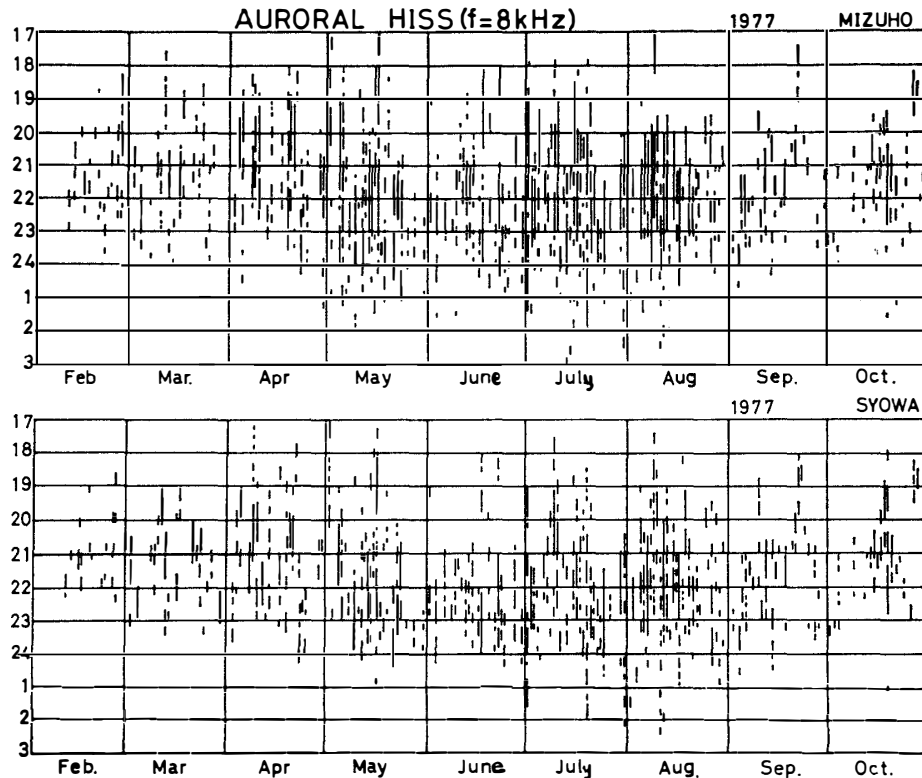


Fig. 14. Diurnal and seasonal variations of the occurrence rate of auroral hiss at the 8 kHz band observed at Syowa and Mizuho Stations. The events with spectral densities above  $1.0 \times 10^{-15} \text{ W/m}^2 \text{ Hz}$  were selected at Syowa Station and above  $0.5 \times 10^{-15} \text{ W/m}^2 \text{ Hz}$  at Mizuho Station.

hiss tends to appear at earlier magnetic local times in equinoxes in a similar fashion at the two stations. A similar  $K_p$  dependence is also seen at the two stations. Therefore, there is no systematic difference of occurrence of hiss between Syowa and Mizuho Stations, although the difference of the geomagnetic latitude is about  $3^\circ$ . It is seen in this figure that the auroral hiss emissions occur more frequently at Mizuho Station than Syowa Station. However, this is not real, but is due to the fact that we selected hiss emissions stronger than  $0.5 \times 10^{-15} \text{ W/m}^2 \text{ Hz}$  at Mizuho Station and hiss emissions stronger than  $1.0 \times 10^{-15} \text{ W/m}^2$  at Syowa Station. We examined the association of auroral hiss with the world-wide geomagnetic activity in more detail. Fig. 15a shows the occurrence probability of auroral hiss at the 8 kHz band versus universal time (universal time  $\sim$  magnetic local time at Syowa Station), categorized by the magnitudes of the  $K_p$  index. The figure shows that the occurrence interval of auroral hiss extends slightly to both earlier and later local times as the  $K_p$  index becomes larger. Fig. 15b shows the occurrence probability of auroral hiss at the 64 kHz band, similar to Fig. 15a. It is evident that the occurrence time of auroral hiss apparently shifts to the earlier local time

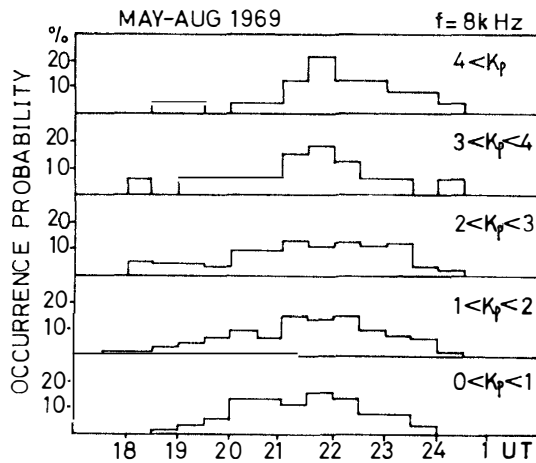


Fig. 15a. Local time dependence of the occurrence probability of auroral hiss at the 8 kHz band as a function of magnetic activity,  $K_p$ .

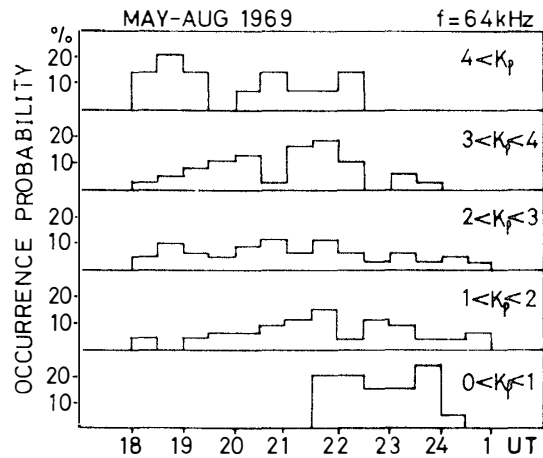


Fig. 15b. Local time dependence of the occurrence probability of auroral hiss at the 64 kHz band as a function of magnetic activity,  $K_p$ .

as the  $K_p$  index becomes larger. Clearly the appearance time of hiss emissions at 64 kHz depends more on the magnitude of the  $K_p$  index than the 8 kHz band. When the geomagnetic activity increases, the auroral oval expands to the lower latitude. In such a case, the region where the auroral hiss occurs can expand also to the lower latitudes. Since the auroral oval is slanted with respect to the geomagnetic latitude, we can expect that the occurrence region of the auroral hiss may shift towards an earlier magnetic local time.  $\Sigma K_p$  in equinoctial seasons is generally larger than it is in winter. Therefore the shift of the auroral hiss occurrences to the earlier magnetic local time in equinoxes is also expected. KAMIDE and WINNINGHAM (1977) reported that the location of the auroral oval changes from winter to summer. The lower latitude boundary of the auroral oval in winter is a few degree higher than it is in summer. This will also cause the seasonal dependence of the hiss occurrence.

The decrease of hiss occurrence frequency in summer can be attributed to the ionospheric absorption, as suggested by HARANG and HAUGO (1965). When the ionosphere electron density increases by ten times of quiet value at 80 km height, the absorption of VLF waves with frequency of 10 kHz amounts to 30 dB as calculated by ONDOH (1963). However, there are some questions whether the seasonal variations of occurrence of auroral hiss emission can be attributed fully to the ionospheric absorption. For example, chorus emissions with frequencies from a few hundred Hz to a few kHz are observed in the day time in all seasons. When the ionospheric absorption is not large enough to permit both chorus and hiss emissions to pass through the ionosphere, both emissions less than one kHz may be observed on the ground. However, chorus emissions are

strongly observed in summer whereas auroral hiss with a similar low frequency rarely appears at Syowa Station in summer. Furthermore, the seasonal dependence of the occurrence of low latitude hiss is small, as shown by TANAKA *et al.* (1976). From Injun 3 observations, GURNETT (1966) reported that the occurrence of auroral hiss emissions shows no seasonal variation. We also examined the VLF emission data from ISIS 1 and 2 and found that the occurrence frequency of auroral hiss in summer tends to be less than in winter. Since both GURNETT (1966) and we examined only a few examples, it is necessary to examine in greater detail the seasonal variations of auroral hiss observed at satellite altitudes in order to reach a definite conclusion. The seasonal dependence possibly indicates the effect of generation of hiss emission rather than the effect of the ionospheric absorption. We will discuss this problem in detail in Chapter 7.

## 2.2. Types of auroral hiss

At high latitudes auroral hiss emissions are observed in a wide frequency range from a few hundred Hz to one hundred kHz. As pointed out (MOROZUMI, 1965; KOKUBUN *et al.*, 1972; TANAKA *et al.*, 1976), night time hiss emissions in the VLF-LF range can be classified into two types. In this section, the spectral structure of these types of hiss will be discussed in detail. Figs. 16 and 17 show examples of chart records of VLF-LF emissions at frequency bands of 0.4, 0.75,

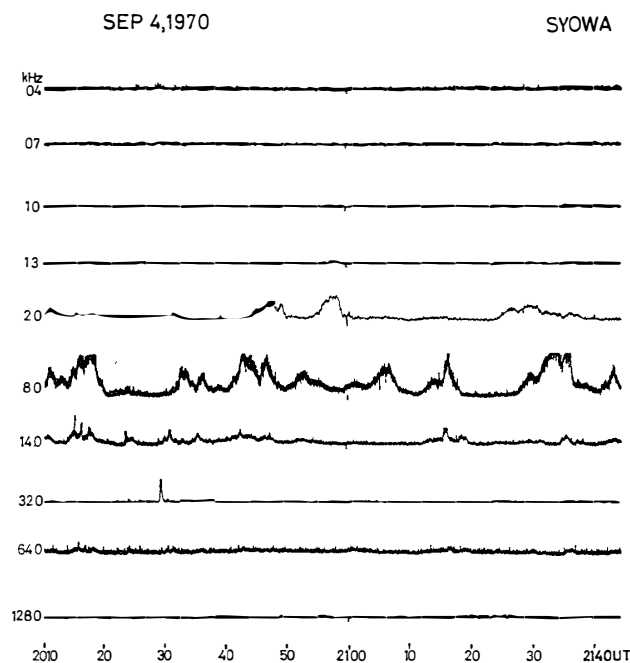


Fig. 16. The temporal variation of auroral hiss intensity at the 0.4, 0.75, 1.0, 1.3, 2.0, 8.0, 14.0, 32.0, 64.0 and 128 kHz bands. Auroral hiss at the 2.0, 8.0 and 14.0 kHz bands shows strong intensity.

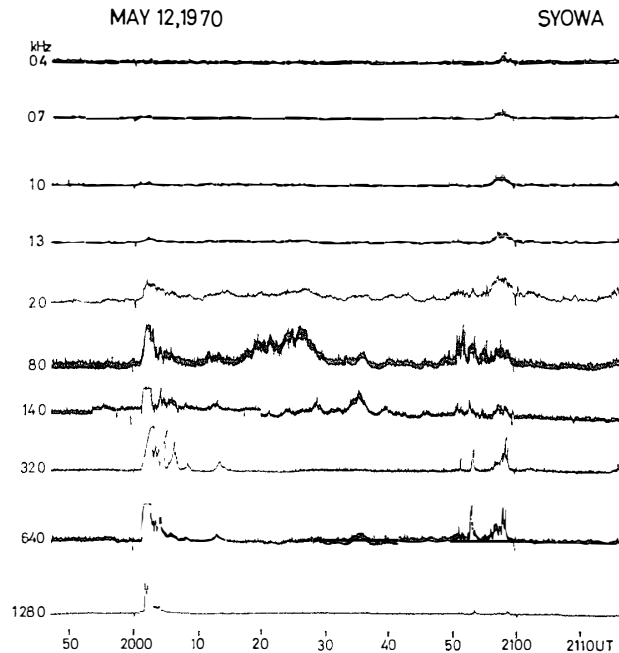


Fig. 17. Temporal variation of auroral hiss intensity. The format is the same as that in Fig. 16. Strong auroral hiss intensities are recognized in the frequency range from 0.4 to 128 kHz.

1.0, 1.3, 2.0, 8.0, 14.0, 32.0, 64.0 and 128 kHz. The auroral hiss observed at Syowa Station can be divided into two types on the basis of its frequency-spectrogram. In Fig. 16, auroral hiss with a rather narrow band of frequency, 2–14 kHz, was seen from 2010 UT to 2140 UT. The emission was observed steadily for an hour or more. The center frequency of this emission was about 8 kHz. We call this type of auroral hiss a narrow-band continuous hiss. Fig. 17 shows another example of hiss events. Hiss emissions with a wide-band frequency (1.0–64 kHz) were impulsively observed around 2002 UT. The increase in intensity was seen in frequencies as high as 128 kHz in this event. The duration of this emission was several minutes. We call this type a wide-band impulsive hiss. The continuous hiss was also observed from 2010 UT to 2050 UT. This emission is characterized by its narrow-band frequency spectrum, that is, the increase in intensity at the frequency band lower than 1.3 kHz and higher than 32 kHz was not clearly seen. The impulsive hiss was again observed around 2052 UT. In this event, the low frequency band (0.4–2.0 kHz) and the high frequency band (32 kHz–64 kHz) were clearly intensified. From many other examples, we could easily classify two types of hiss emission. Several examples of dynamic spectra of auroral hiss are illustrated in Figs. 18–20 in order to confirm the characteristic differences between continuous and impulsive hiss emissions. Note that the recording range of the tape recorder used in this observation is limited to a frequency

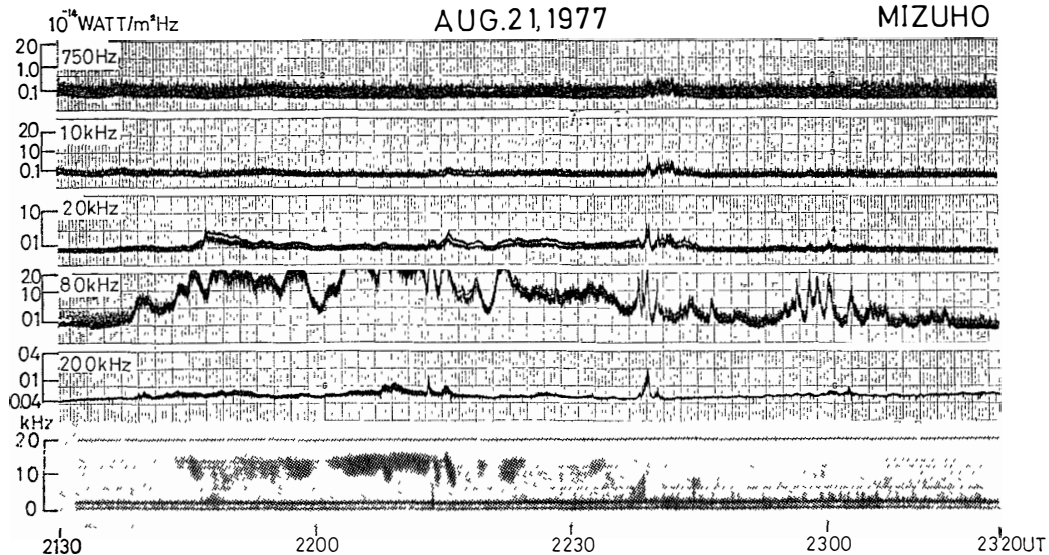


Fig. 18. The band limited intensity of auroral hiss at 0.75, 1.0, 2.0, 8.0 and 20.0 kHz along with the frequency spectrogram observed at Mizuho Station. The maximum frequency of the frequency-time spectrum is about 17 kHz.

of  $\sim 17$  kHz. The maximum frequency of the frequency-time spectra shown in Figs. 18–20 is about 17 kHz. Fig. 18 shows the band limited intensity of auroral hiss at several frequency bands (top panel) along with the frequency-time spectrum (bottom panel) from 2140 UT to 2230 UT. As seen in this figure, the narrow-band continuous hiss with center frequency of about 8 kHz was observed. During this period a weak impulsive hiss with a lower frequency extending to 1 kHz was also observed around 2215 UT. A typical impulsive hiss of a wide-band frequency occurred around 2240 UT and rapidly faded out with a short duration. Another hiss event was observed around 2300 UT. This emission occurred impulsively, but the width of its frequency band was narrow. This emission may belong to the narrow band continuous hiss in spite of an impulsive appearance. Fig. 19 shows a typical continuous hiss event. Auroral hiss emissions whose center frequencies were about 8 kHz were observed from 2200 UT to 2430 UT. The frequency-time spectrum of these emissions is characterized by the narrow frequency, and the center frequency varies slowly with time. Fig. 20 shows a continuous and impulsive hiss example. The narrow-band continuous hiss was observed for a long time from 2040 UT to 2140 UT. A strong impulsive hiss with a wide frequency band appeared at 2200 UT and the duration of this emission was about 20 minutes.

We examined several time expanded frequency spectrograms of auroral hiss emission in order to study the characteristics of hiss spectra in detail. Typical examples of continuous and impulsive hiss are represented in Figs. 21 and 22.

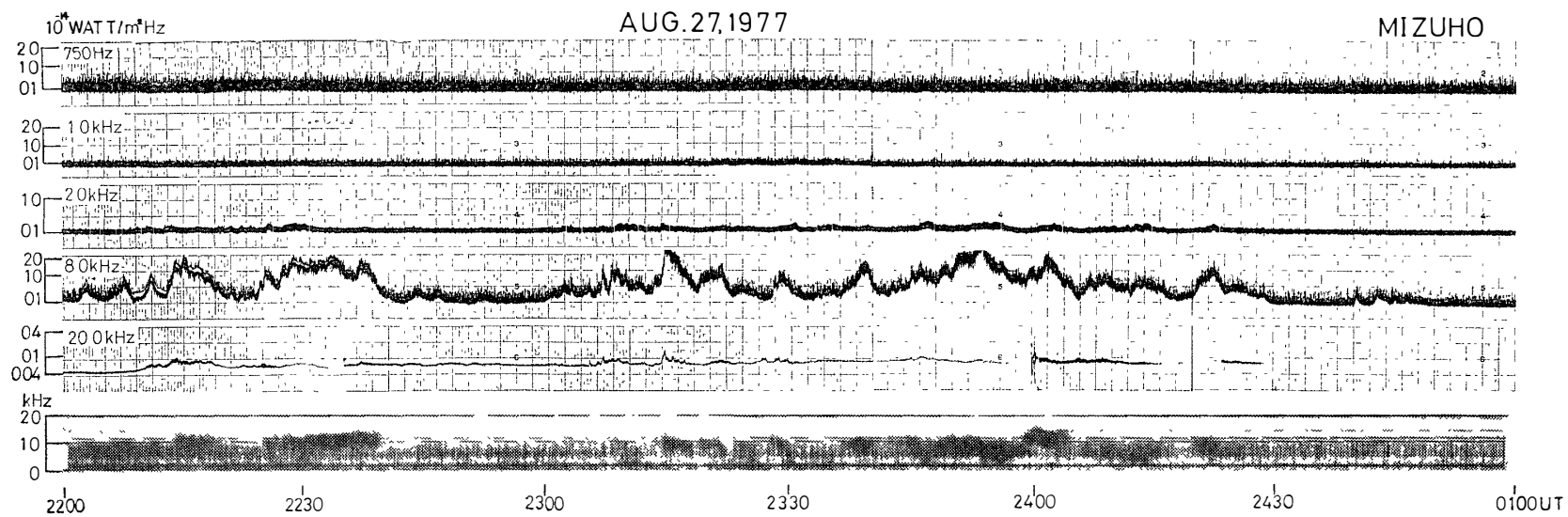


Fig. 19. The band limited intensity of auroral hiss and the frequency-time spectrum. The format is the same as that in Fig. 18.

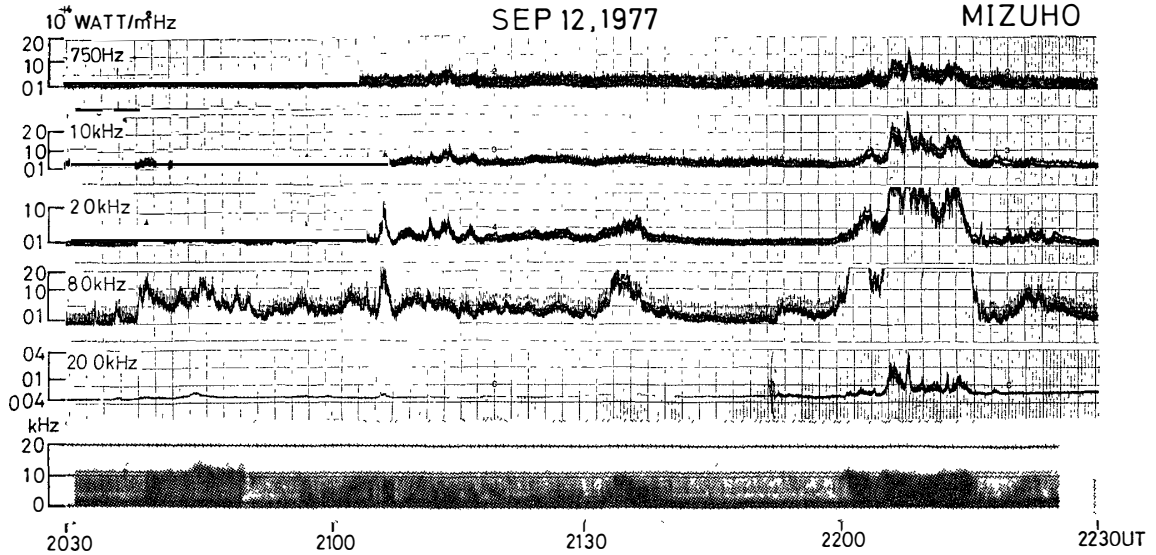


Fig. 20. The band limited intensity of auroral hiss and the frequency-time spectrum. The format is the same as that in Fig. 18.

Other examples are shown in Appendix: Fig. A-7–Fig. A-10. Fig. 21 shows the frequency-time spectrum of narrow-band continuous hiss that occurred from 1947 UT to 1953 UT along with the temporal variation of intensity at 8 kHz band. The center frequency of this emission was about 8 kHz, the band width about 4 kHz, and the typical variation of frequency spectrum was not seen in this interval. In contrast, Fig. 22 illustrates the frequency-time spectrum of wide-band impulsive hiss that occurred from 0033 UT to 0039 UT and from 0048 UT to 0054 UT along with the temporal variation of intensity at the 8 kHz band.

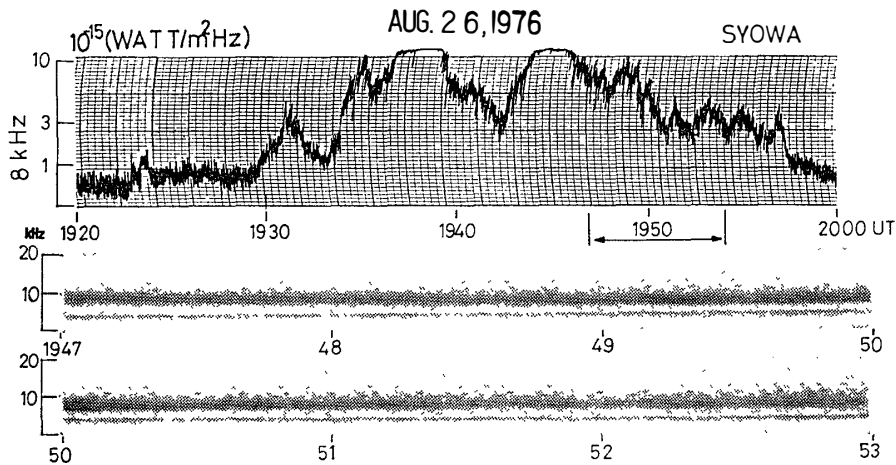


Fig. 21. The band limited intensity at 8 kHz (top panel) and the frequency-time spectra (bottom panel) of the continuous hiss observed at Syowa Station.

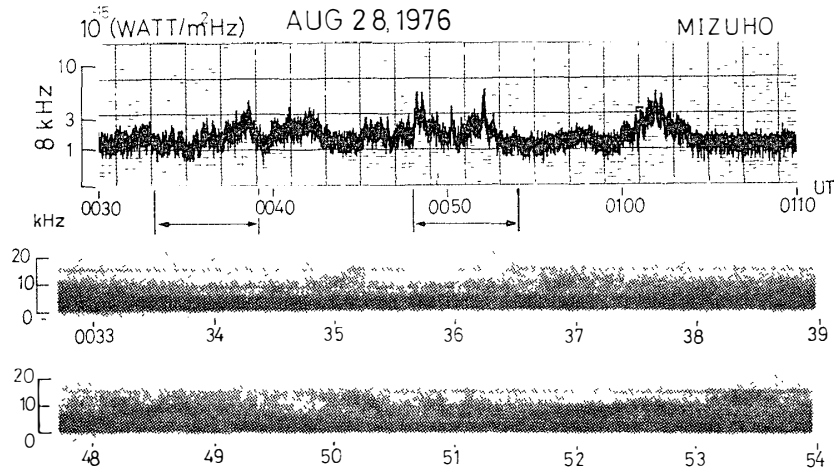


Fig. 22. The band limited intensity at 8 kHz (top panel) and the frequency-time spectra (bottom panel) of the impulsive hiss observed at Mizuho Station.

Remarkably complex frequency spectra were seen. The time scale of this dispersive emission was less than 10 seconds.

As seen in these frequency-time spectra and the fashion of its temporal variations in the band limited intensities of hiss emissions, the classification of auroral hiss emissions into two categories is reasonable. The frequency time spectrum of impulsive hiss was characterized by the wide-band frequency, dispersive spectrum and its sharply intensified emission. On the other hand, the continuous hiss was characterized by the narrow-band frequency and no dispersive spectrum. The difference in the power-spectral densities and the duration time between the narrow-band continuous hiss and the wide-band impulsive hiss were also examined. Fig. 23 represents the frequency spectrograms including both continuous and impulsive hiss emissions. The typical continuous hiss spectrum observed from 2106 UT to 2112 UT is shown in this figure. Both continuous and impulsive hiss were detected from 2135 UT to 2141 UT and a typical impulsive hiss was seen around 2140 UT. Fig. 24 represents examples of the power spectral densities of the continuous and impulsive hiss observed around 2110 UT and 2140 UT on Aug. 30, 1976 at Mizuho Station; the event described in Fig. 23. The power spectrogram was obtained by one second averaging. The power spectrum of the continuous hiss described in Fig. 23 had a spectral peak around 12 kHz. The intensity fell under the receiver's threshold level around 5 kHz and 20 kHz. Artificial noise was seen at less than 5 kHz. The intensity of the emission at the spectral peak was about 20 dB stronger than the threshold intensity. The frequency where the intensity dropped by 6 dB from peak value was seen around 10 kHz and 14 kHz. On the other hand, the frequency of the spectral peak of the impulsive hiss described in Fig. 23 was also seen around 12 kHz. However,

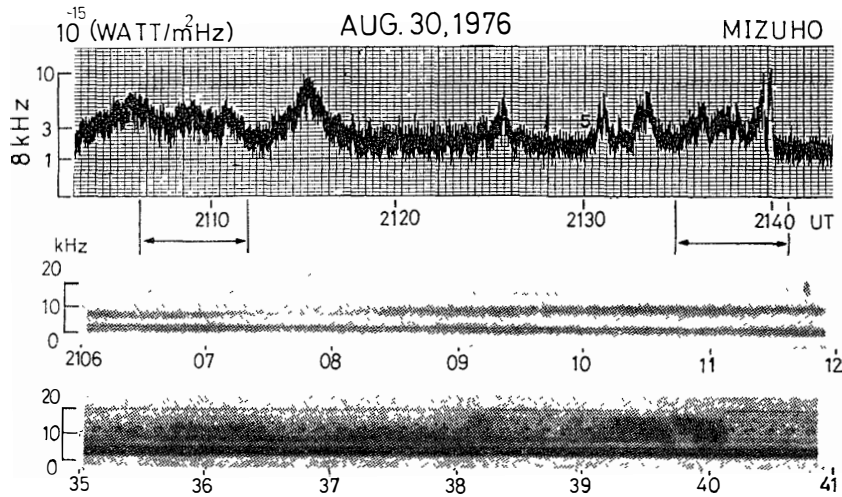


Fig. 23. The band limited intensity at 8 kHz (top panel) and the frequency-time spectra (bottom panel) of the continuous hiss and the impulsive hiss observed at Mizuho Station.

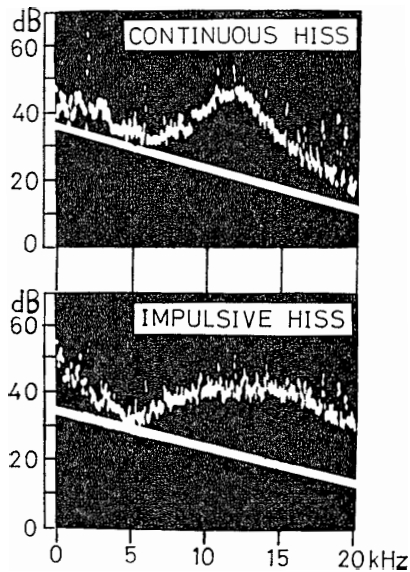


Fig. 24. The power spectral densities of the continuous hiss (top panel) and the impulsive hiss (bottom panel) observed around 2110 UT and 2140 UT on August 30, 1976 at Mizuho Station.

the frequency range where the intensity dropped by 6 dB from peak value was broader than 10 kHz. The spectral characteristics in an even broader frequency range can be examined by using the chart records. Fig. 25 shows the average spectra of continuous and impulsive hiss emissions each of which were obtained from ten typical events. We chose the strong continuous and impulsive hiss events and examined the peak intensity of them. The shaded region indicates the receiver's threshold. The peak intensity of the narrow-band continuous hiss is seen at about 10 kHz and its intensity amounts to about  $\sim 2 \times 10^{-14}$

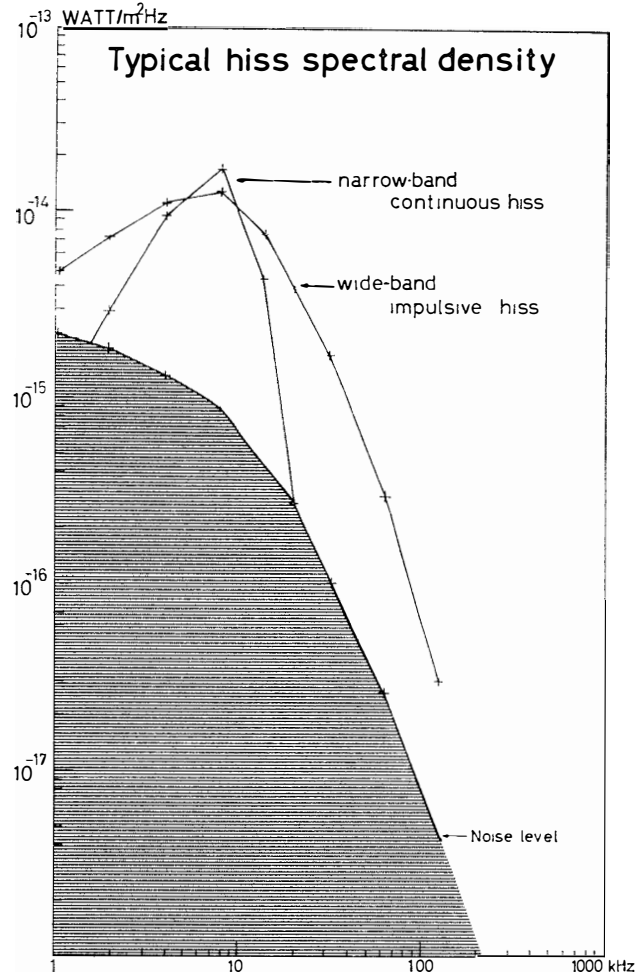


Fig. 25. The average power spectral density of continuous and impulsive hiss emissions. The shadow region is the receiver's threshold level.

W/m<sup>2</sup> Hz. This type of emission usually dominates in the frequency range of 3–15 kHz. The wide-band impulsive hiss emission also has its intensity peak around 10 kHz. However, its spectral slope is flat and can usually be observed over receiver's threshold, in the frequency range of 1–100 kHz.

On the other hand, a definitive difference is clearly seen in the duration between two types. Fig. 26 shows the histogram of the duration of continuous and impulsive hiss. The classification here is made by examining whether the intensity at the 64 kHz band is observed or not; *i.e.*, the emission with an enhancement at the 64 kHz band is classified as the impulsive hiss, and the emission without the band dominating at near 8 kHz as the continuous hiss. All events stronger than the receiver's threshold level during the period from June to October 1970 were examined. As seen in Fig. 26, the duration of impulsive hiss (with enhancement at 64 kHz band) is the order of or less than ten minutes or less. The

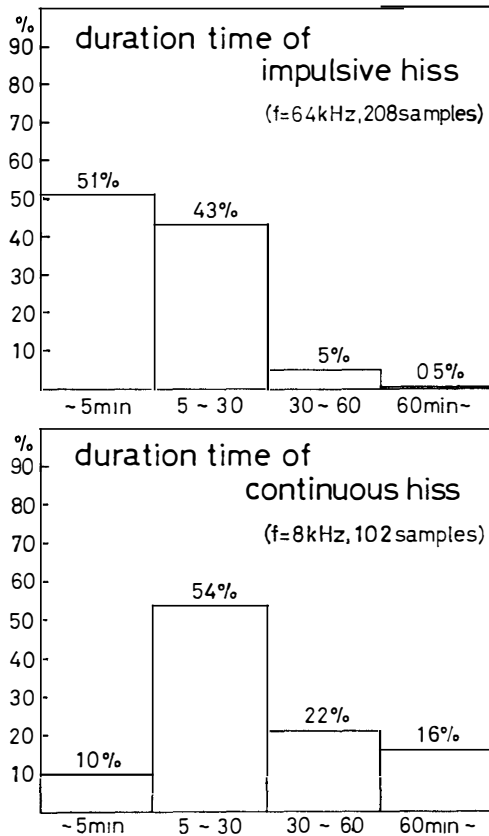


Fig. 26. The histogram of the duration of continuous and impulsive hiss.

duration of the continuous hiss, on the other hand, is several tens of minutes, 16% of the continuous hiss being known to have a duration longer than one hour. On the basis of these statistical results, it is evident that the impulsive hiss and the continuous hiss have a meaningful difference in their durations.

### 2.3. Latitudinal dependence of occurrences of auroral hiss

We examined the latitudinal dependence of the occurrence frequency of hiss emissions based on the records from Syowa (mag. lat.  $-70.38^\circ$ , long.  $79.39^\circ$ ) and Mizuho Stations (mag. lat.  $-72.32^\circ$ , long.  $80.62^\circ$ ) during the period from June 1976 to December 1977. Fig. 27 shows the diurnal variation of auroral hiss at the 8 kHz band observed at Syowa and Mizuho Stations. We selected events higher than  $1.0 \times 10^{-15}$  W/m<sup>2</sup> Hz at 8 kHz. The data used here was obtained during the period from June to August in 1976. Furthermore, we examined the events that occurred between 1930 UT and 0230 UT because the artificial noise occasionally disturbed the observation of auroral hiss at Mizuho Station during the rest of the time. Auroral hiss was most frequently observed from 2200 to 2300 UT at both stations. There is no systematic difference in the diurnal variation between Mizuho and Syowa Stations. Further, there is no

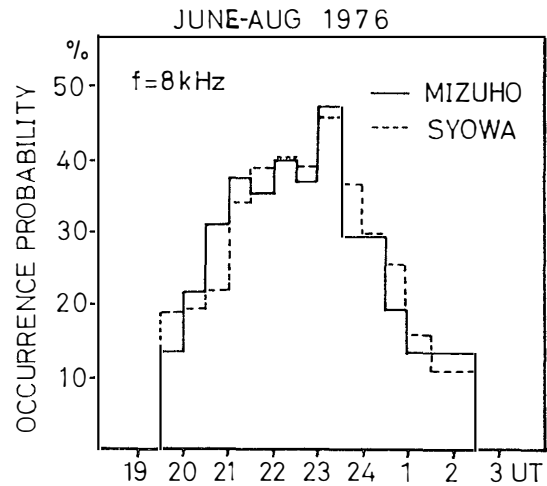


Fig. 27. The diurnal variation of auroral hiss at the 8 kHz band observed at Syowa and Mizuho Stations.

meaningful difference in the occurrence number of auroral hiss between Mizuho and Syowa Stations. The intensity, however, observed at Mizuho and Syowa Stations is not the same. Figs. 28a and b show the intensity of auroral hiss at the 0.75, 1.0, 2.0, 8.0 and 20 kHz bands and the frequency-time spectrum at both stations. These are examples of continuous hiss observed intermittently for a long time at both stations. At about 2230 UT, the intensity of hiss at Mizuho Station was stronger than that at Syowa Station. After 2300 UT, the intensity of hiss at both Stations became similar. The intensity ratio of hiss between the two stations varied temporarily, but the spectral shape and the time variations of lower and upper cutoff frequencies, were very similar between the two stations. Figs. 29a and b also show the intensity of hiss and the frequency-time spectrum at both stations. This is an example of continuous hiss with a narrow-band frequency range (2 kHz–15 kHz). Before 2114 UT auroral hiss was observed only at Mizuho Station. After 2114 UT, a similar variation of intensity of continuous hiss was observed at both stations. During this interval, similar spectra were also seen at the two stations. As the spectral shape of the continuous hiss emissions observed at both stations were very similar generally, the observable distance of the similar continuous hiss emission may be larger than 300 km. Figs. 30a and b show the intensity of hiss and the frequency spectrogram at both stations as before. From 2040 UT to 2150 UT, the continuous hiss emissions with a narrow frequency range (2 kHz–15 kHz) were observed at both stations. The spectral shape and the time variations of lower and upper cut off frequencies were very similar between the two stations. After 2200 UT, typical impulsive hiss with a wide frequency range occurred. The intensity of impulsive hiss at Mizuho Station was stronger than that at Syowa Station. The intensity of impulsive hiss between the two stations was usually different.

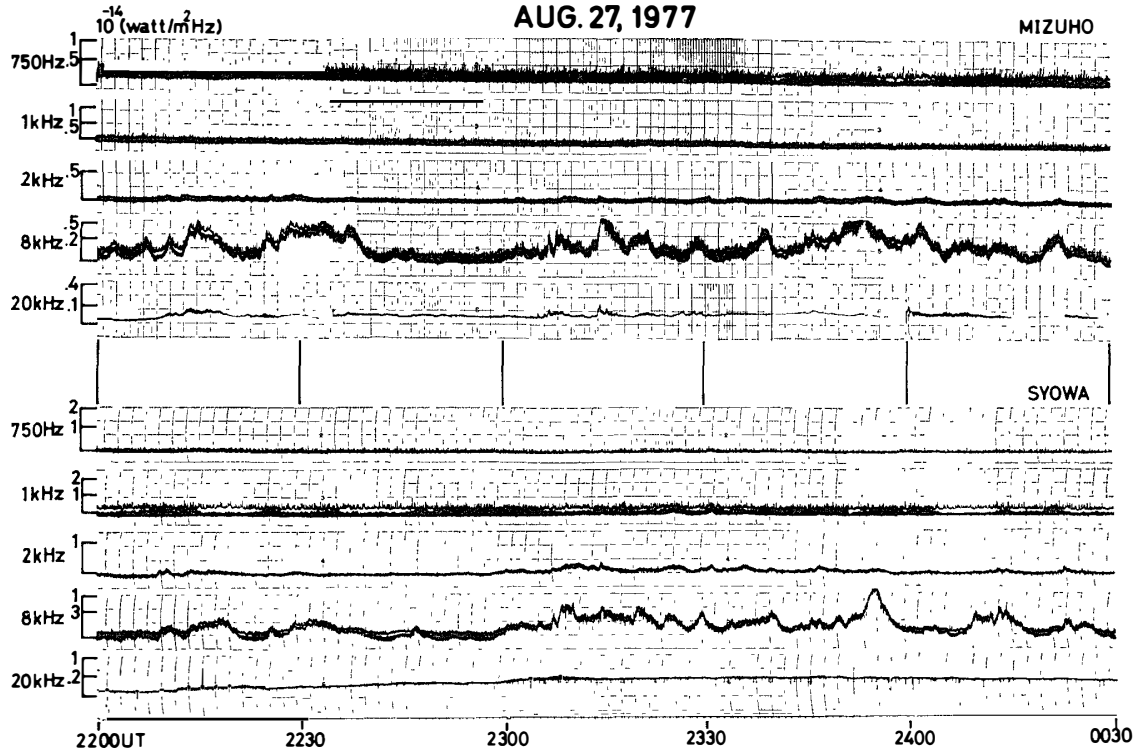


Fig. 28a. The intensity of auroral hiss at the 0.75, 1.0, 2.0, 8.0 and 20 kHz bands observed at Syowa and Mizuho Stations.

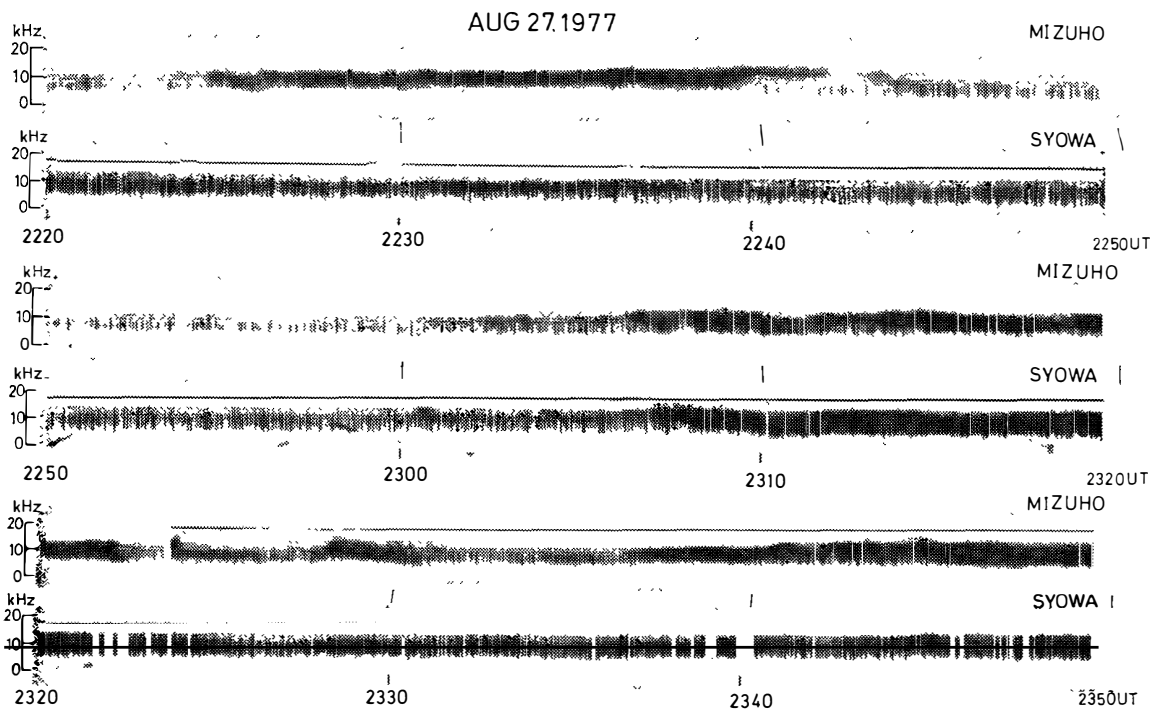


Fig. 28b. The frequency-time spectra of auroral hiss observed at Syowa and Mizuho Stations from 2220 UT to 2350 UT.

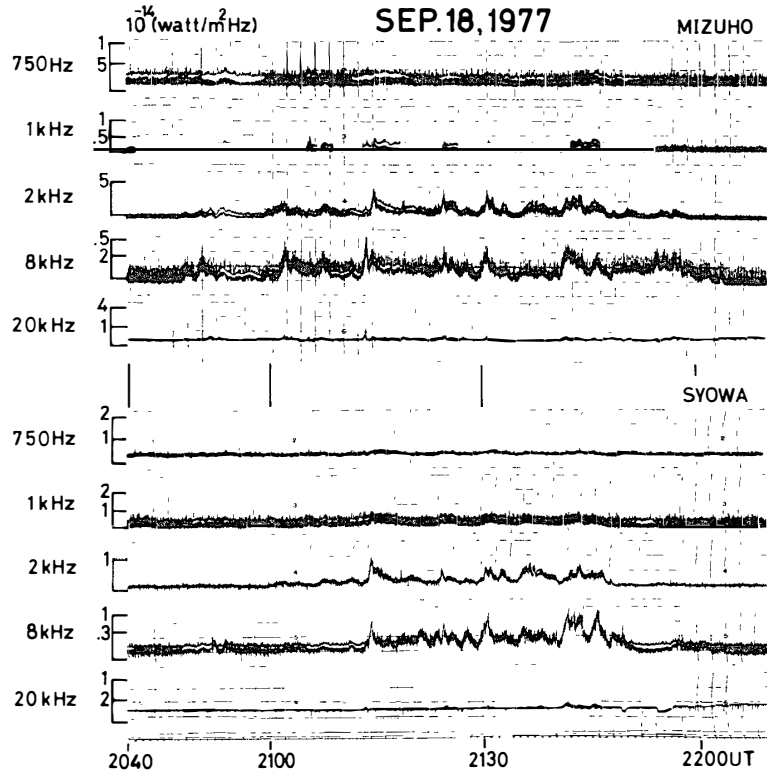


Fig. 29a. The intensity of auroral hiss at the 0.75, 1.0, 2.0, 8.0 and 20 kHz bands observed at both stations. The format is the same as that in Fig. 28a.

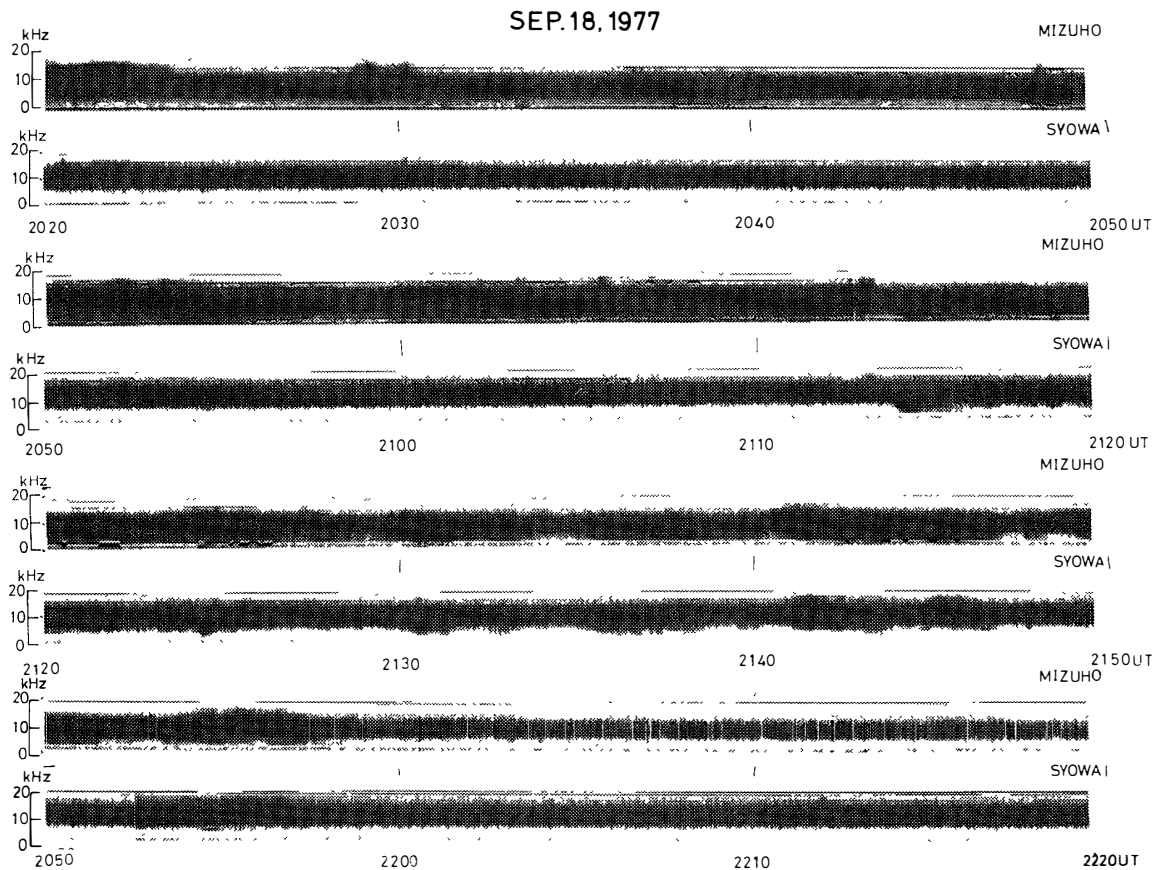


Fig. 29b. The spectral intensity of auroral hiss from 0 to 20 kHz at MIZUHO and SYOWA stations on SEP. 18, 1977.

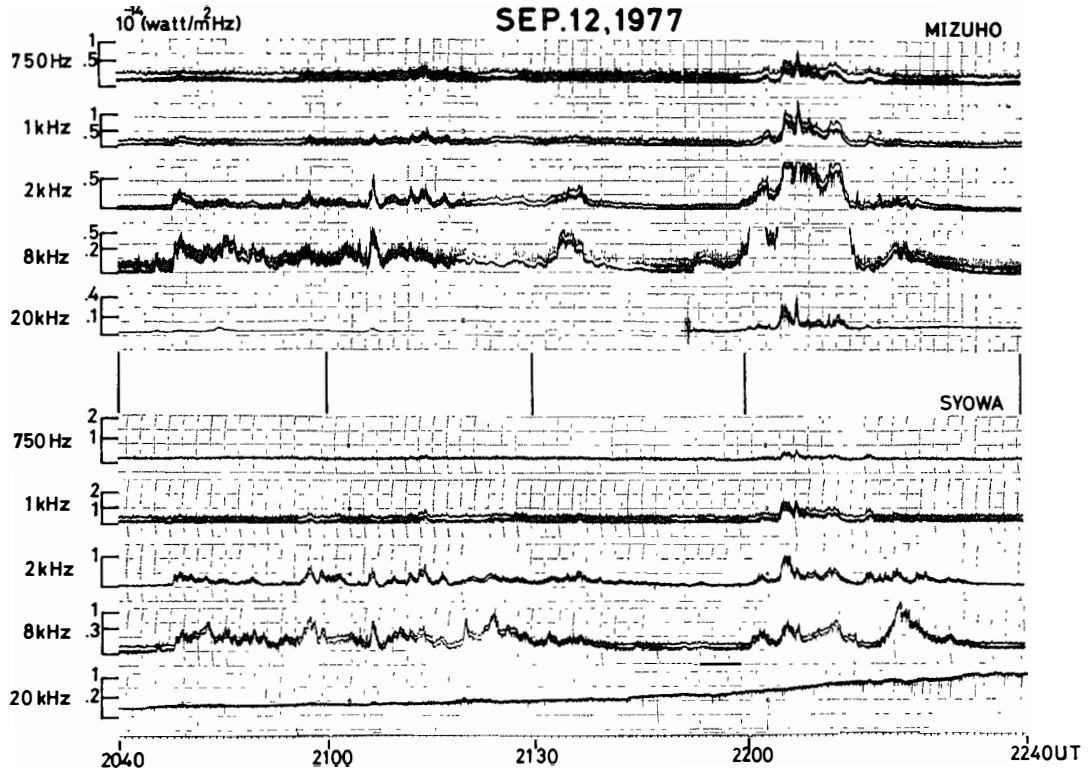


Fig. 30a. The intensity of auroral hiss observed at both stations. The format is the same as that in Fig. 28a.

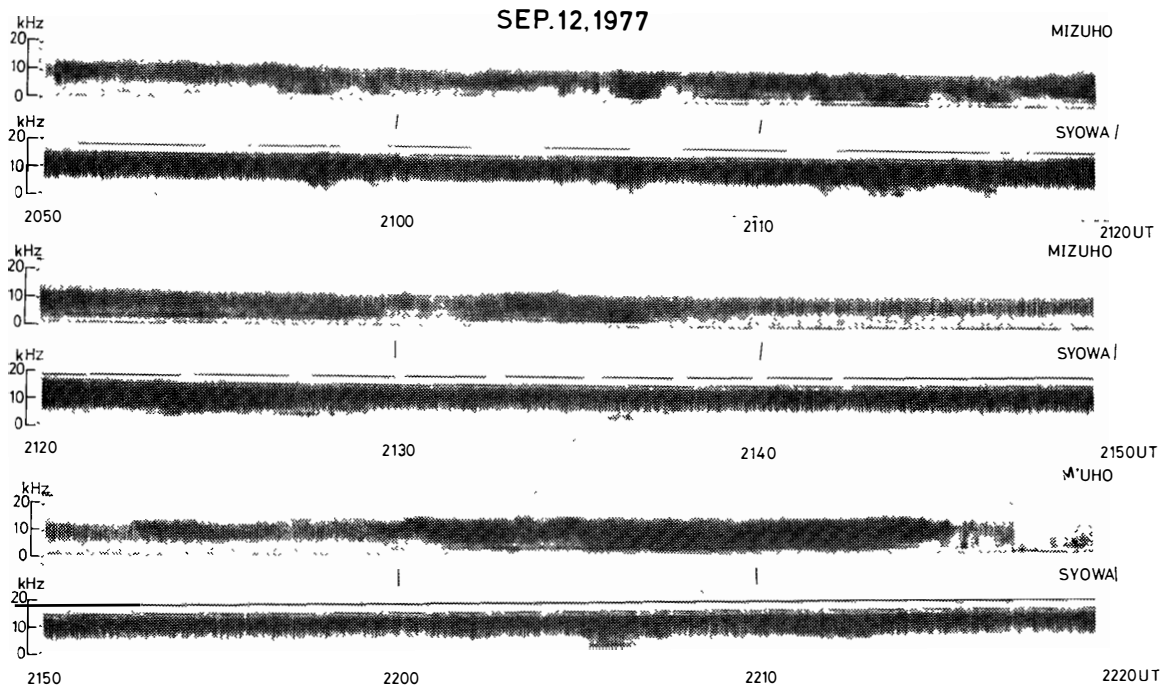


Fig. 30b. The frequency-time spectra observed at both stations from 2050 UT to 2220 UT.

#### **2.4. Summary**

It is evident that auroral hiss emissions are divided into two types; the narrow-band continuous hiss and the wide-band impulsive hiss. The seasonal and diurnal variations of the two types show similar tendencies, but the frequency spectra and the duration time of the two types are quite different. From Mizuho and Syowa Stations' observations, the spectral shape of the continuous hiss emission obtained at both stations is generally similar. However the spectral shape and the intensity of the impulsive hiss are occasionally different at both stations. These results show that the observable distance of the similar continuous hiss emission may be larger than that of the impulsive hiss emission.

### 3. Relationships between Auroral Hiss Emissions and Aurora

The relationships between auroral hiss and aurora have been examined by many investigators, including MARTIN *et al.* (1960), JØRGENSEN (1966) and OGUTI (1974). MARTIN *et al.* (1960) has showed that the intensity and band-width of hiss vary with the ionospheric absorption and may also vary with the intensity of aurora. However, it is not easy to examine the relationships between the luminosity of aurora and the intensity of auroral hiss because auroral hiss propagates for a long distance but the auroral brightness cannot be recognized if the station is far away (more than a few hundred km) from the auroral location. Furthermore, ionospheric absorption may act on the intensity of auroral hiss. Therefore, the relationships between the luminosity of aurora and the intensity of auroral hiss are not yet clear enough to reach a conclusion regarding the emission mechanism of auroral hiss. According to the recent satellite observations, LAASPERE and HOFFMAN (1976) suggested that auroral particles with energy of less than 1 keV are more frequently related to the occurrence of auroral hiss. If this is the case, the electrons which excite the visual aurora and the auroral hiss would be different. In this chapter, we will examine the relationships between the intensity of auroral hiss and the spatial and temporal variations of auroral display and luminosity.

#### 3.1. Aurora associated with auroral hiss

The two different power spectra of auroral hiss mentioned previously may correspond to precipitating auroral electrons with different energy spectra. This type of aurora may also differ between the aurora related to the impulsive hiss and that related to the continuous hiss. Fig. 31 shows the temporal variations of the auroral hiss intensity at the 0.75, 8 and 64 kHz bands along with the sequential all-sky photographs of aurora. The emission event seen at the 8 kHz band is the typical narrow-band continuous hiss. A steady auroral arc was concurrently seen near the poleward horizon of Syowa Station during this interval. The frequency-time spectra of hiss along with the sequential all-sky photographs of aurora are shown in Fig. 32. These emissions dominated in the frequency range of 5–15 kHz and their center frequencies were seen at around 10 kHz.

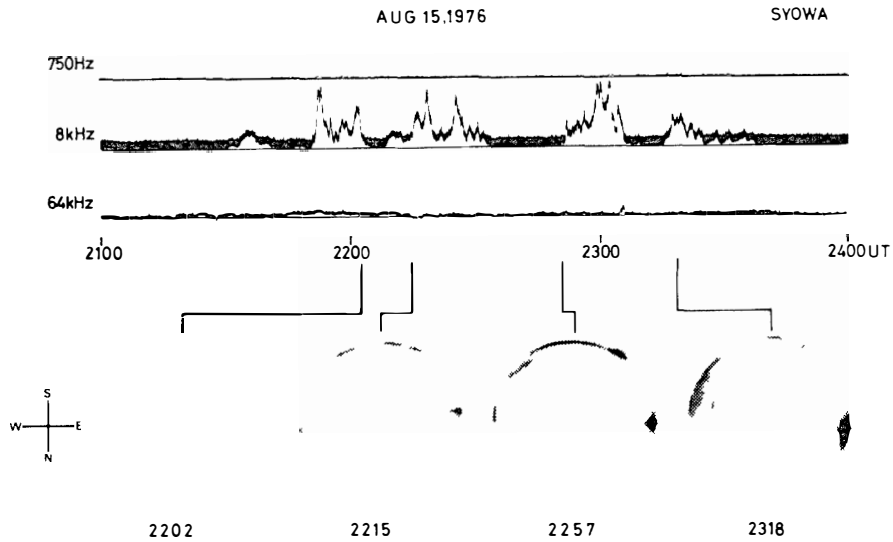


Fig. 31. The auroral hiss intensity at the 0.75, 8 and 64 kHz bands along with the sequential all-sky photographs of aurora observed at Syowa Station.

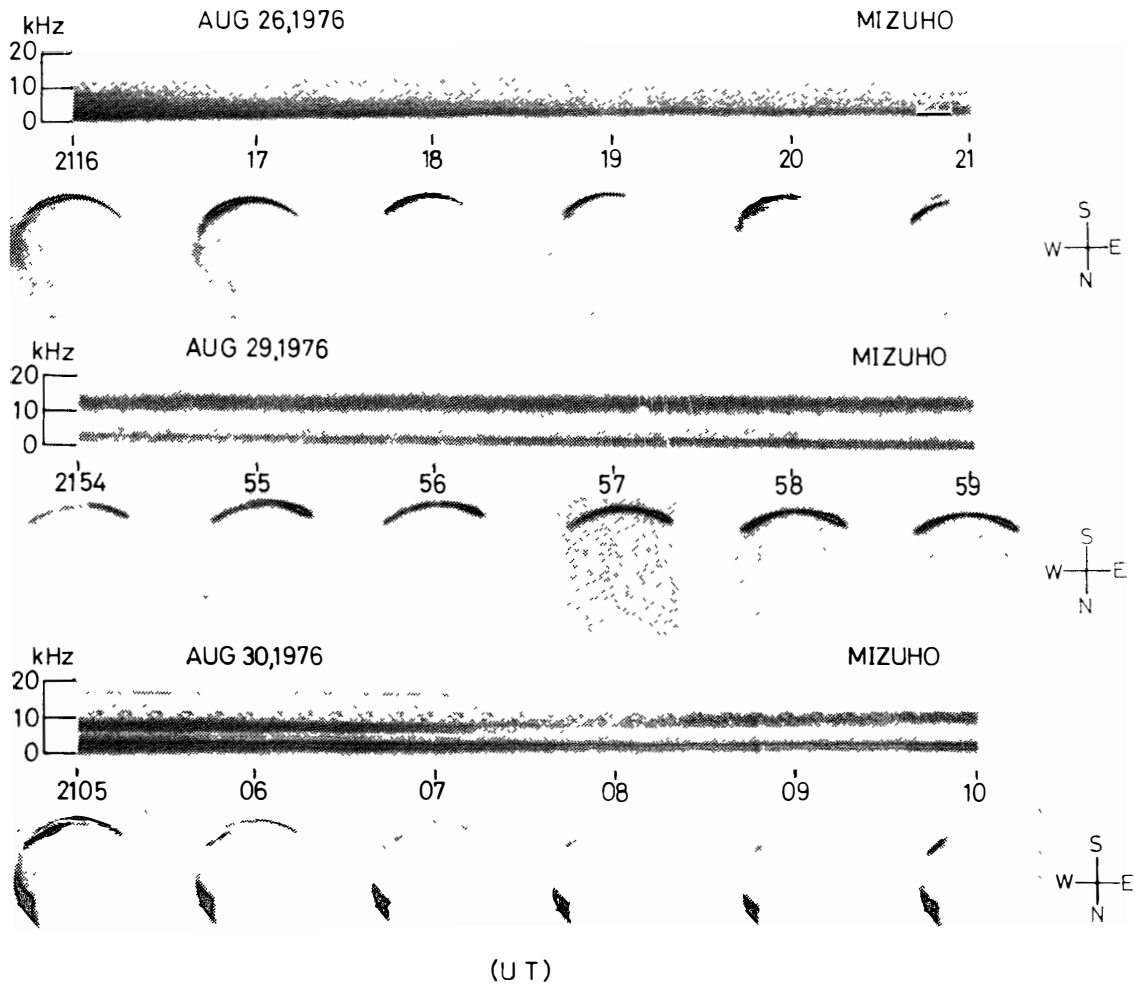


Fig. 32. The frequency-time spectra of continuous hiss observed at Mizuho Station and the sequential all-sky photographs of aurora observed at Syowa Station. Signals lower than 5 kHz in the  $f-t$  spectra are the artificial noise.

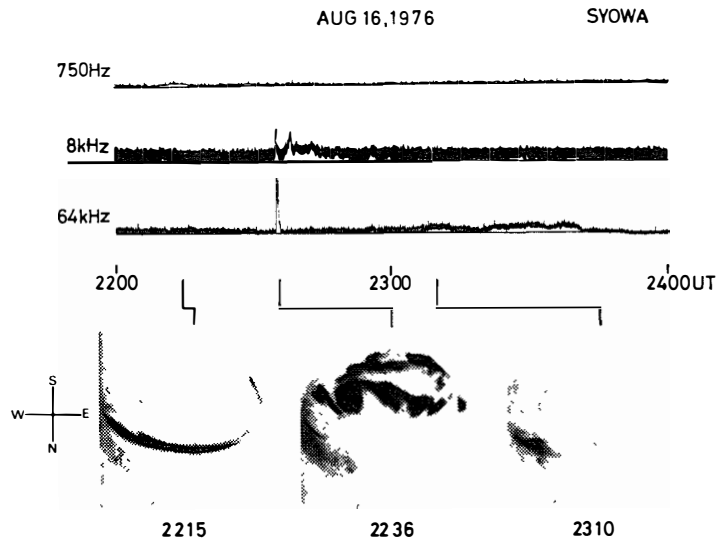


Fig. 33. The auroral hiss intensity at the 0.75, 8 and 64 kHz bands and all-sky auroral photographs.

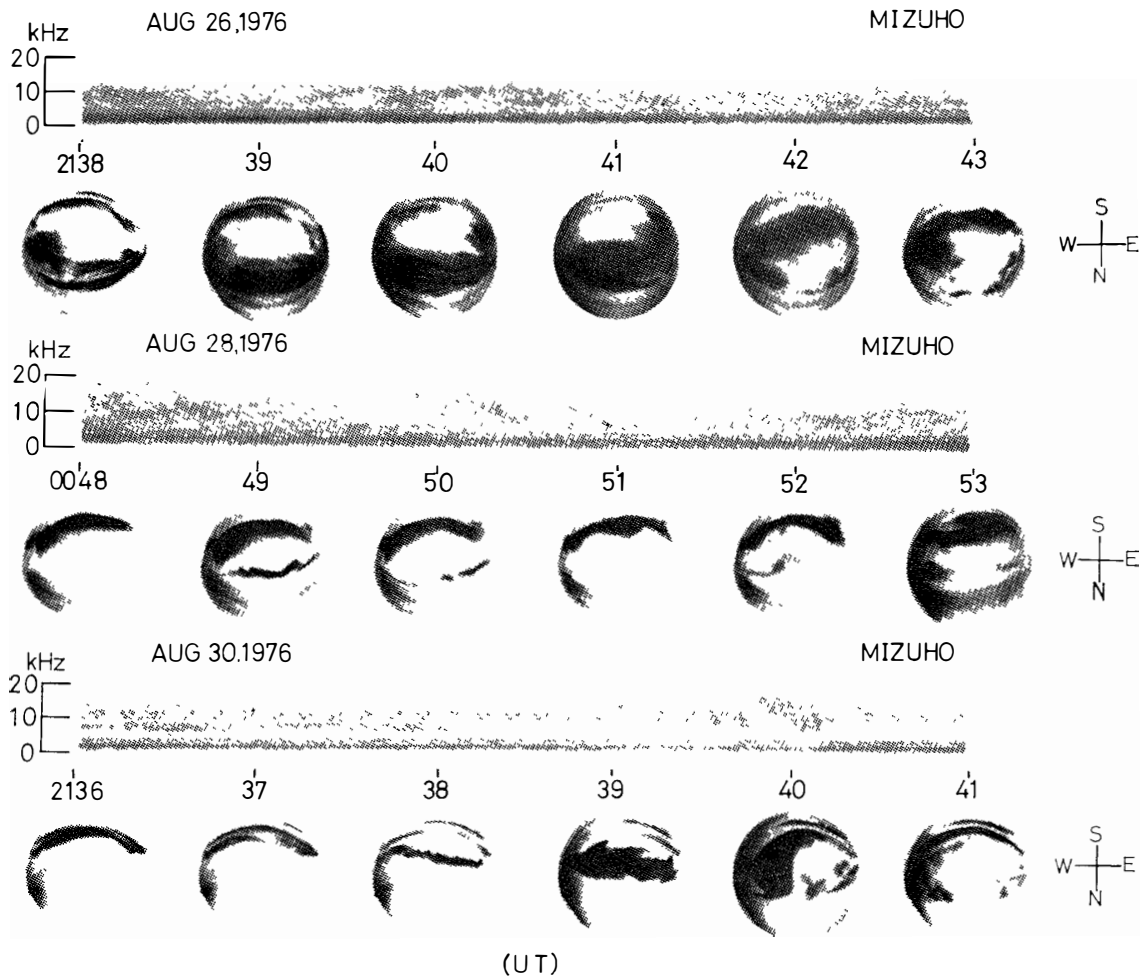


Fig. 34. The frequency-time spectra of impulsive hiss observed at Mizuho Station and the sequential all-sky photographs of aurora observed at Syowa Station. Signals lower than 5 kHz in the  $f-t$  spectra are the artificial noise.

During this interval, the steady auroral arc was seen near the poleward horizon of Syowa Station. These results clearly show that the continuous hiss occurs in association with the steady auroral arc.

Similarly, the continuous hiss also occurs when the multiple auroral arcs are seen near the zenith (shown later in Fig. 43). However, when the steady auroral arc is seen at the lower latitude of the station, the continuous hiss is rarely observed, or weak if it appears. Fig. 33 shows the intensity of auroral hiss at the 0.75, 8 and 64 kHz bands and the all-sky auroral photographs. Although the steady auroral arc was seen near the lower latitude of Syowa Station around 2215 UT, auroral hiss was not recognized. An impulsive hiss occurred simultaneously with the initiation of auroral brightening around 2236 UT. The impulsive hiss disappeared within a few minutes. Similar examples of the impulsive hiss and the related aurora were recognized in many other events. Frequency-time spectrograms of the impulsive hiss and all-sky photographs of aurora are shown in Fig. 34. The wide-band impulsive hiss emissions as seen in the frequency-time spectrogram were accompanied by occurrences of active bright aurora in all-sky photographs. An important point is that the impulsive enhancement of hiss occurs around the initiation of auroral brightening. This active bright aurora here belongs to discrete aurora similar to rayed-band, corona or the westward traveling surge. From these results, it can be said that the continuous hiss emission occurs accompanied by the steady auroral arc located at the higher latitude of the station, and the impulsive hiss emission occurs accompanied by the local auroral activities of discrete aurora observed near the zenith. The impulsive hiss occurs almost simultaneously with the initiation of the auroral breakup which is usually followed by sharp and large fluctuations of the magnetic field. The relationships between auroral hiss and the magnetic fluctuations will be described in Chapter 6.

### 3.2. Fluctuation of auroral luminosity and auroral hiss occurrence

The intensity of hiss emissions are not always associated with the fluctuations of auroral luminosity. Here, the luminosity of the auroral green line ( $5577 \text{ \AA}$ ) obtained by the scanning photometer and related changes in intensity of the VLF emission are examined. Generally speaking, the change in intensity of the impulsive hiss is correlated more with the fluctuations of auroral luminosity than is continuous hiss. This may be due to the fact that the steady arc which is associated with the continuous hiss usually appears near the poleward horizon, considerably far from Syowa Station. In such a case it is difficult to obtain the real fluctuations of luminosities by use of the scanning photometer because of its limited spatial resolution. The photometer used here scans meridionally from north to south every 30 s and the peak and background luminosities for one scanning interval are obtained. Since the range of the photometer view is  $5^\circ$ , then the bright aurora

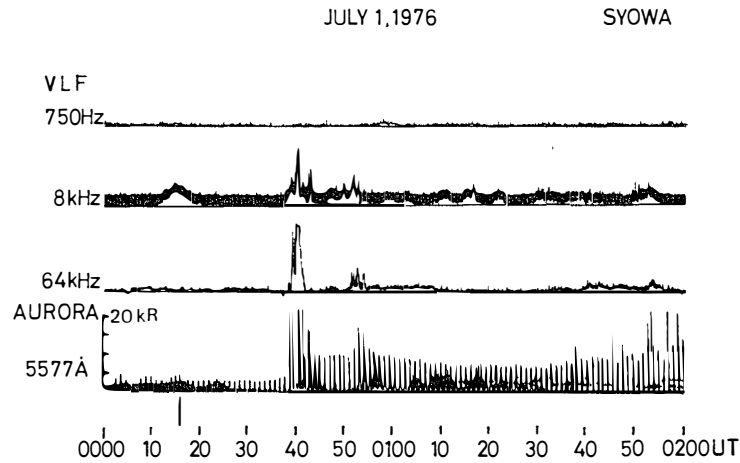


*Fig. 35. The auroral hiss intensity at the 0.75, 8 and 64 kHz bands and the luminosity of the auroral green line (5577 Å) obtained by the meridian scanning photometer at Syowa Station.*

which is not situated near the meridian plane is not recognized by the photometer. For this reason it is necessary to use the all-sky photographs of aurora in order to examine the relationships between the auroral luminosity and the intensity of hiss. An example of the relation between the intensification of impulsive hiss and luminosity of the auroral green line (5577 Å) is shown in Fig. 35. An impulsive hiss with a frequency band extending to 64 kHz occurred at 0040 UT. According to all-sky photographs, the steady auroral arc was seen near the lower latitude of Syowa Station around 0035 UT. A poleward expansion of aurora began at 0040 UT. The enhancement of auroral brightening whose luminosity

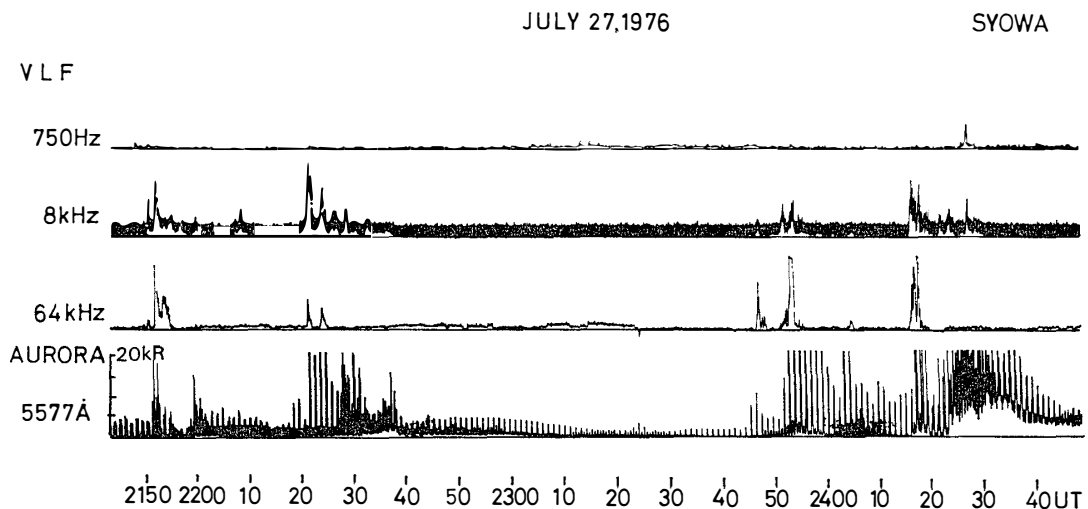


*Fig. 36. The auroral hiss intensity and aurora. The format is the same as that in Fig. 35.*

was greater than 20 kR, was seen at that moment. The occurrence of impulsive hiss seems to be associated with the initiation of auroral poleward expansion. Around 0055 UT, a weak impulsive hiss, related to another poleward expansion of aurora, was recognized. Fig. 36 shows another example of hiss intensity and related changes in auroral luminosity. At 2150 UT, an impulsive hiss was observed, followed by the enhancement of the auroral luminosity higher than 20 kR. At 2220 UT another impulsive hiss accompanied by the enhancement of auroral brightness near the poleward region again occurred. The intensity of the impulsive hiss soon became weak as the discrete auroral structure changed to the diffuse bright aurora after 2225 UT. At 2345 UT, 2352 UT and 0018 UT, impulsive events were received in association with the enhancement of the auroral brightness which exceeded 20 kR. After 2420 UT, although the auroral luminosity was higher than 20 kR, the impulsive hiss was not observed. This may be due to absorption in the ionosphere. In this case, a riometer at the frequency band of 30 MHz indicated the ionospheric absorption of 2 dB during this interval. This result indicates that the rapid disappearance of impulsive hiss may be due partly to the effect of the ionospheric absorption. The possible change in energy spectra of the precipitating electrons may be another reason. The energy spectrum of precipitating electrons may change from the developing stage to the full expansion stage of an auroral breakup causing the concurrent change in characteristics of the emissions. This will be discussed in Chapter 7.

The intensity of continuous hiss and auroral luminosity are shown in Fig. 37. From 1900 UT to 2200 UT, continuous hiss emissions were intermittently observed and faint auroral arcs appeared near the poleward horizon of Syowa Station. The peak to peak correspondence between the fluctuations of auroral

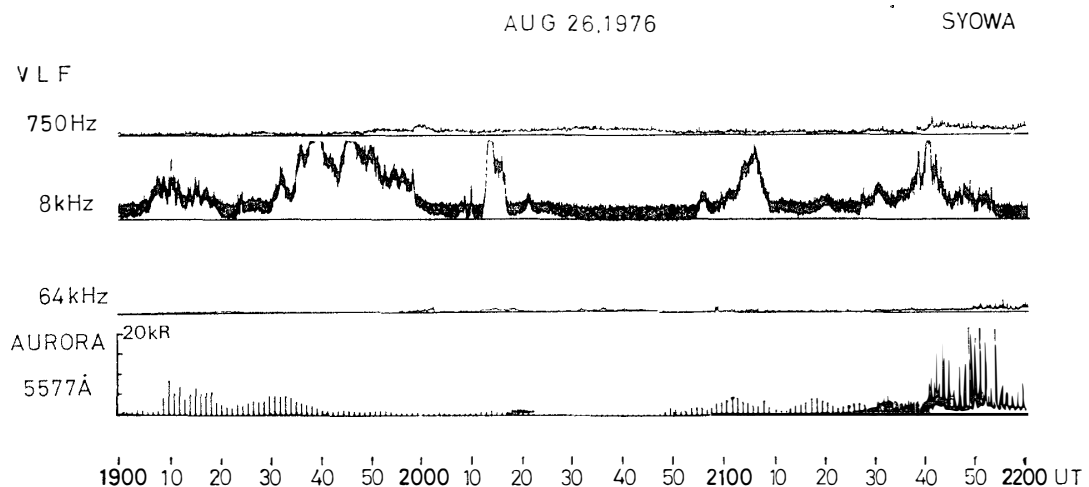


Fig. 37. The auroral hiss intensity and the aurora. The format is the same as that in Fig. 35.

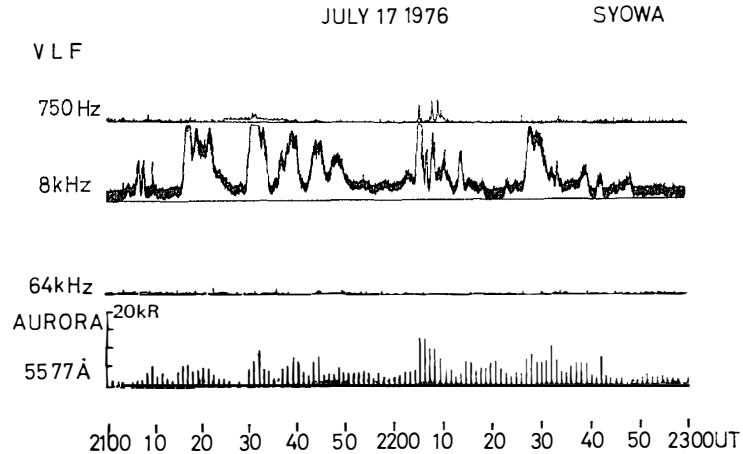


Fig. 38. The auroral hiss intensity and the aurora. The format is the same as that in Fig. 35.

luminosity and the VLF intensity at the 8 kHz band could not be recognized. For example, from 1930 UT to 2020 UT, an intense emission seen at the 8 kHz band was not accompanied by any significant enhancement of auroral luminosity. This is likely due to the fact that the auroral arc moves away beyond the poleward horizon, namely to the outside field view of the scanning photometer. However, there are some events which show a good correlation between the fluctuations of auroral arc luminosity appearing at the poleward horizon of Syowa Station and the VLF intensity as shown in Fig. 38. From 2100 UT to 2250 UT, the intensity of the hiss increased as the luminosity of the auroral green line (5577 Å) increased. A steady auroral arc with a luminosity less than 10 kR was seen at the poleward horizon of Syowa Station during this interval. Especially from 2129 UT to 2142 UT, peak to peak correspondence between the fluctuations of auroral luminosity and the hiss intensities was recognized at the 8 kHz band. Fig. 39 shows the all-sky photographs of aurora from 2105 UT to 2142 UT along with the intensity of hiss at the 8 kHz band. As seen in this figure, the fluctuation of the auroral arc luminosity shows good a relationship to the fluctuation of the intensity at the 8 kHz band. This example indicates that continuous hiss emission is also correlated with the luminosity of the auroral arc. Based on a number of events we examined, it can be said that the intensity of hiss increases as the luminosity of the steady auroral arc increases, or the movement of aurora is seen. Our results showed that some of the fluctuations in both impulsive and continuous hiss intensity, are clearly related to the fluctuations of auroral luminosities. However, there are also many other events which show no significant correlation between the fluctuation of auroral luminosity and the VLF intensity. These results may be explained partly by the ionospheric absorption, and partly by the possibility that hiss emissions related to the aurora situated beyond the poleward horizon

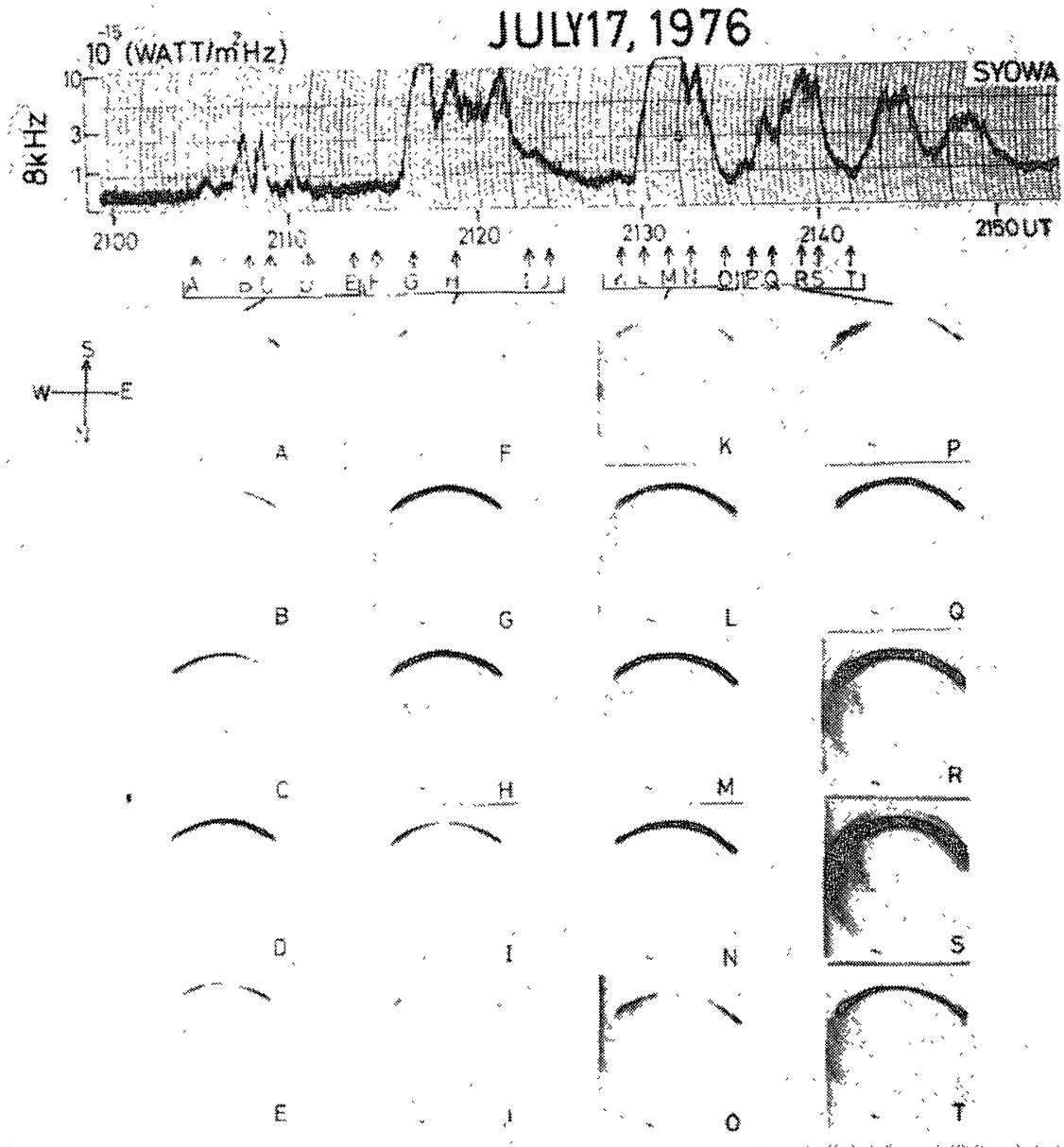


Fig. 39. The intensity of hiss at 8 kHz and sequential all-sky photographs of aurora observed at Syowa Station.

can still be observed at Syowa Station. Another possibility also must be considered; that the electrons that excite visible aurora can be different from the electrons which excite the auroral hiss emission, as suggested by MOSIER and GURNETT (1972). If this is the case, so many rarities of the relationships, between the auroral luminosity and the intensification of hiss emission, some of which are excellently related but others are not, may be ascribed to the change in the energy spectrum

of the precipitating electrons from one event to another.

### 3.3. Spatial distribution of aurora and the emission region of auroral hiss

We reported that continuous hiss is observed associated with the steady auroral arc located at the poleward region, and impulsive hiss is observed associated with the active bright aurora near the zenith. These tendencies are statistically examined and shown in Fig. 40. The 50 events with strong intensities

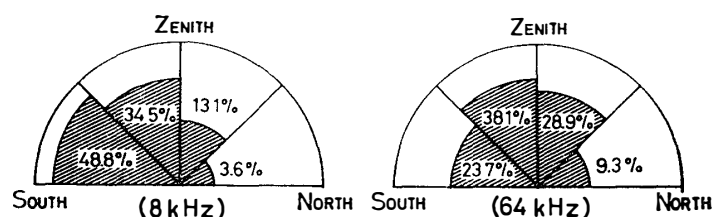


Fig. 40. The relationship between the two types of hiss emissions (the continuous hiss and the impulsive hiss) and the location of aurora.

at the 8 kHz ( $>10^{-15}$  W/m<sup>2</sup> Hz) and 64 kHz bands ( $>10^{-16}$  W/m<sup>2</sup> Hz) are selected and compared with the distribution of aurora observed by the all-sky camera. The all-sky camera photographs are divided into four parts along the geomagnetic latitude. They are the regions with elevation angles of 0° to 45° and 45° to 90° both in the north and south directions. If the altitude of aurora is assumed to be 100 km, the region of aurora with the elevation angle of 45° is 100 km away from the zenith in the N–S direction. In this analysis, we counted all regions when the aurora like multiple arcs located around several regions divided. Despite some ambiguities between the hiss emissions and the locations of the related aurora, our calculations clearly show the tendency that hiss emissions at the 8 kHz band well associated with the aurora located around the poleward region. About 50% of all the continuous hiss emissions correlate to the aurora located around the poleward region more than 100 km away from the zenith. On the contrary, more than 60% of all the hiss emissions observed at 64 kHz are related to the aurora located within 100 km in N–S direction from the zenith.

In order to make these tendencies more clear, further examinations are made on the relationships between the distribution of aurora and the relative intensity of hiss emissions observed at Syowa and Mizuho Stations. Fig. 41 shows intensity variations of hiss observed at the two stations and the aurora observed at Syowa Station. The narrow-band continuous hiss emissions were observed for a long time at both stations (The frequency-time spectrum of this event was already shown in Fig. 28b). When a steady auroral arc appeared from the zenith to the poleward region of Syowa Station, almost the same intensity hiss emission was recorded at both stations. Another example of the relationships between intensities of

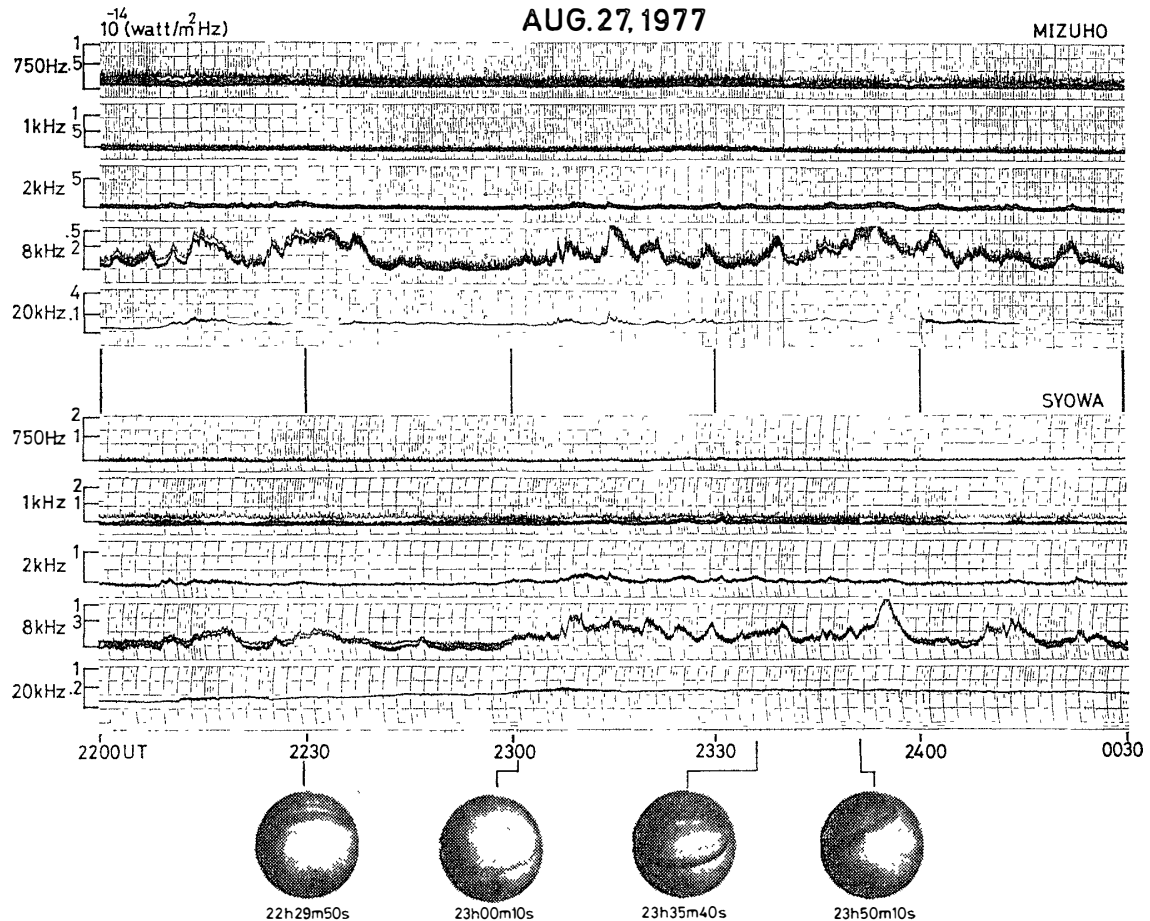


Fig. 41. The auroral hiss intensity at the 0.75, 1, 8 and 20 kHz bands observed at Syowa and Mizuho Stations. The all-sky auroral photographs observed at Syowa Station during this interval are also shown.

VLF emissions at the 8 kHz band and auroral distributions are shown in Fig. 42. From 2100 UT to 2200 UT, the intensity of the continuous hiss emissions at both stations were almost same. A bright auroral arc was located in the higher latitude region of Mizuho Station during this interval. The intensity of hiss at the 8 kHz band at Mizuho Station increased to a level higher than that at Syowa Station after 2140 UT when the aurora expanded into the higher latitude region.

Fig. 43 shows the change in intensity of hiss at the 8 kHz band when multiple arcs appear over Syowa Station. The intensity of continuous hiss was intermittently enhanced for a long time at both stations. Similar enhancements of continuous hiss associated with multiple arcs over Syowa Station were observed at both stations.

The relationships between the impulsive hiss and the location of active bright

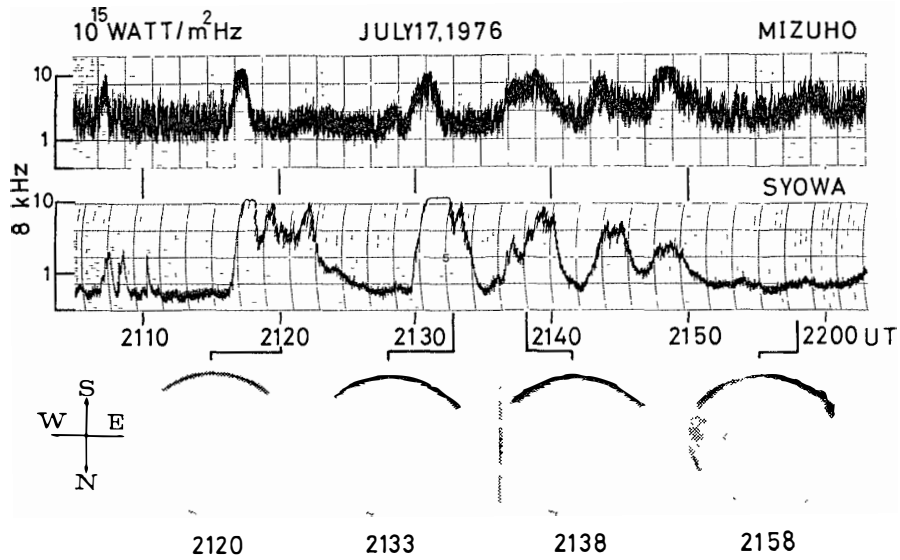


Fig. 42. The intensity of hiss at the 8 kHz band observed at Syowa and Mizuho Stations and the sequential all-sky photographs of aurora observed at Syowa Station.

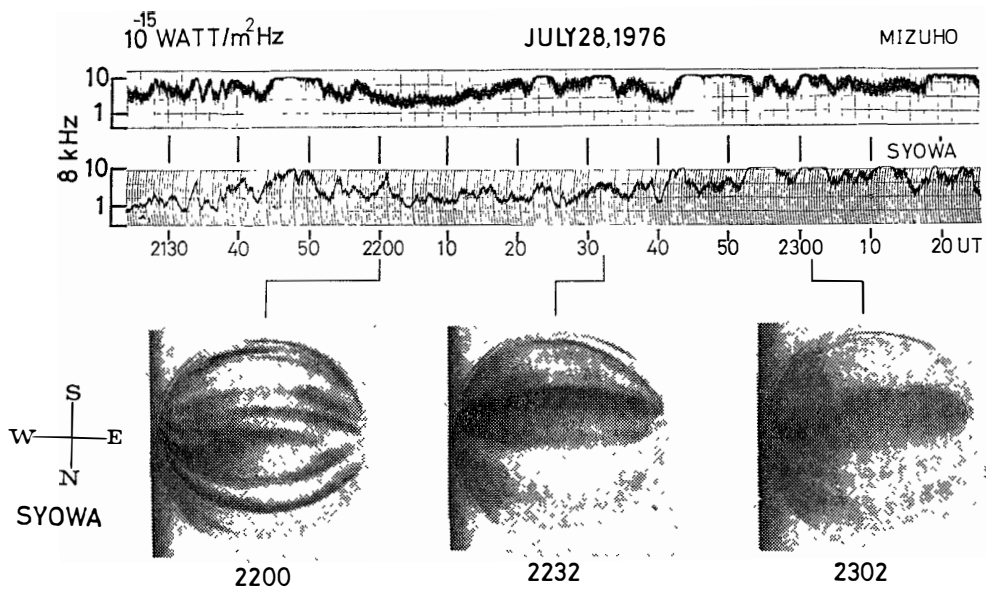


Fig. 43. The intensity of hiss at 8 kHz observed at Syowa and Mizuho Stations and the sequential all-sky photographs of multiple auroral arcs observed at Syowa Station.

aurora are also examined. The intensity of auroral hiss obtained at the two stations and the all-sky photographs of aurora are shown in Fig. 44. The frequency-time spectrum of this hiss event is shown in Fig. 30b. An almost similar intensity of continuous hiss was observed at both stations from 2040 UT to 2130 UT as an auroral band was located on the higher latitude side of Syowa

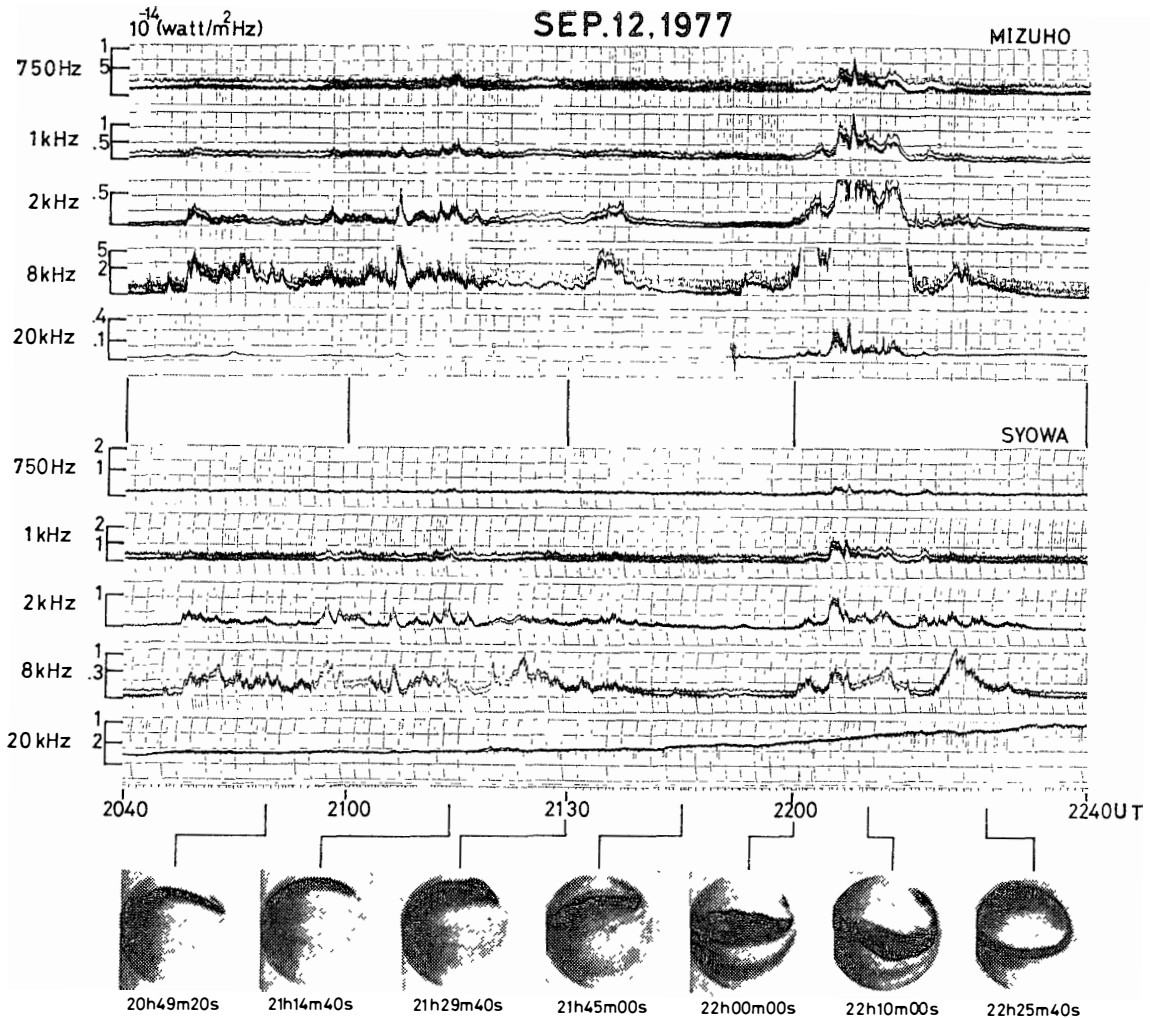


Fig. 44. The auroral hiss intensity at the 0.75, 1, 8 and 20 kHz bands observed at Syowa and Mizuho Stations. The all-sky auroral photographs observed at Syowa Station during this interval are also shown.

Station and near the zenith of Mizuho Station. Around 2200 UT, impulsive hiss occurred at Mizuho Station and a weak impulsive hiss was also observed at Syowa Station. Concurrently an enhancement of auroral brightness was seen near the zenith of Syowa Station. As shown in this figure, a greater difference in emission intensity was seen for the impulsive hiss between Syowa and Mizuho Stations than for the continuous hiss emission. This may indicate that the penetration region of impulsive hiss through the ionosphere is more localized than that of continuous hiss. Fig. 45 shows the typical impulsive hiss event associated with a poleward expansion of aurora. The auroral arc was seen on the lower latitude side of Syowa Station from 2238 UT to 2240 UT. A weak auroral hiss

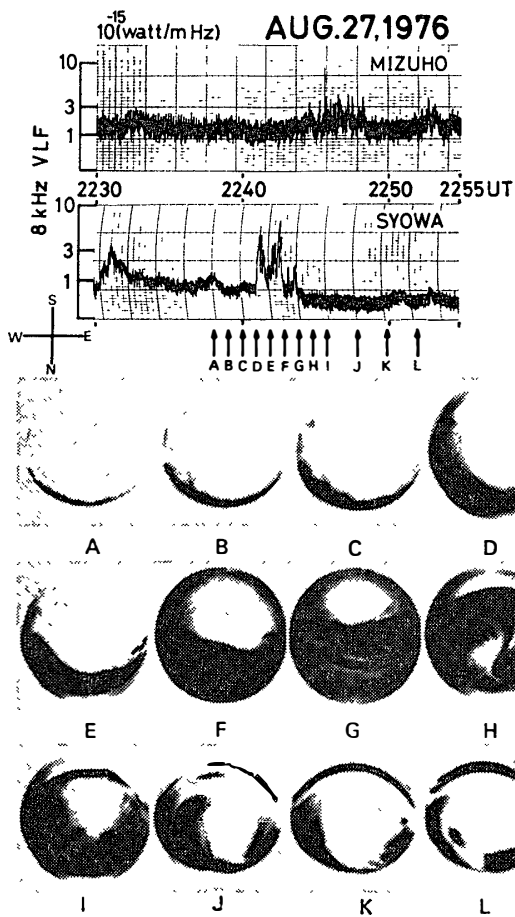


Fig. 45. The top panel shows the intensity of auroral hiss at the 8 kHz band observed at Syowa and Mizuho Stations. The bottom panel shows the sequential all-sky photographs of aurora observed at Syowa Station. Each auroral photograph (A~L) correspond to the time indicated by each of the arrows from A to L.

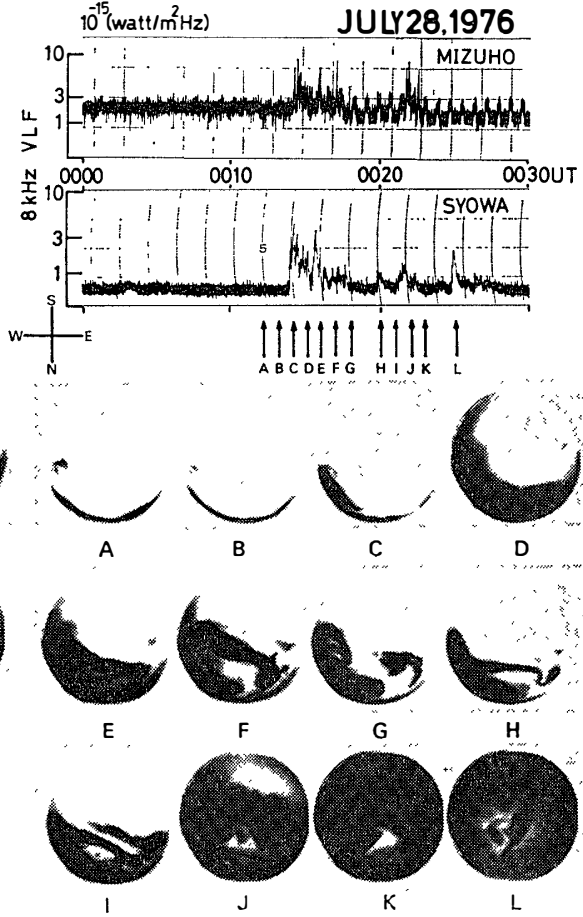


Fig. 46. The intensity of auroral hiss at the 8 kHz band observed at Syowa and Mizuho Stations. The sequential all-sky photographs of aurora observed at Syowa are shown in the bottom panel. The format is the same as that in Fig. 45.

was observed during the interval. When the auroral poleward expansion occurred at 2241 UT over Syowa Station (D), an impulsive hiss simultaneously appeared at Syowa Station. However, enhancement of hiss emissions were not seen at Mizuho Station. A slight enhancement of impulsive hiss began at 2245 UT at Mizuho Station when the front of active bright aurora arrived at Mizuho Station (G), while the emission activity at Syowa Station disappeared after the passage of poleward expanding auroras over the zenith. It is clearly seen that a time lag between the occurrence of hiss emission at Syowa and Mizuho Stations

correlates with the auroral movement. An example similar to Fig. 45 is also given in Fig. 46. Auroral hiss was not observed before 0014 UT when the arc was located on the lower latitude side of Syowa Station. An impulsive hiss event began at 0014 UT, in association with the initial brightening of an auroral substorm at both stations (C). The intensity of hiss at Mizuho Station became stronger than that at Syowa Station at 0022 UT when the front of bright aurora reached at Mizuho Station (J). It can be said that the difference of hiss intensity between the two stations generally depends on the location of the front of bright aurora. However, there are some impulsive hiss events associated with the active bright aurora located around the poleward horizon of Syowa Station. Fig. 47 shows such an example. The impulsive hiss was observed at 2309 UT at Syowa Station when the auroral brightness was enhanced near the zenith of Mizuho Station. During this interval, the intensity of impulsive hiss at Mizuho Station was much less than that at Syowa Station. When the enhancement of auroral brightness occurred again at 2332 UT on the higher latitude side of Mizuho Station, the intensity of impulsive hiss at Mizuho Station began to rise above that at Syowa Station. This example shows that the impulsive hiss received is related to the active aurora located not only near the zenith but also at the poleward horizon of the station. In this event, the strong intensity of impulsive hiss observed is related to the active aurora located on the poleward side of the station.

In order to clarify the relationships between the hiss intensity and the location of aurora, we must compare the relative intensities of hiss emissions at Syowa and Mizuho Stations with respect to the location of auroras. We statistically examine the continuous hiss emissions accompanied by the steady auroral arc, for the steady auroral arc is seen in the narrower meridian plane more than

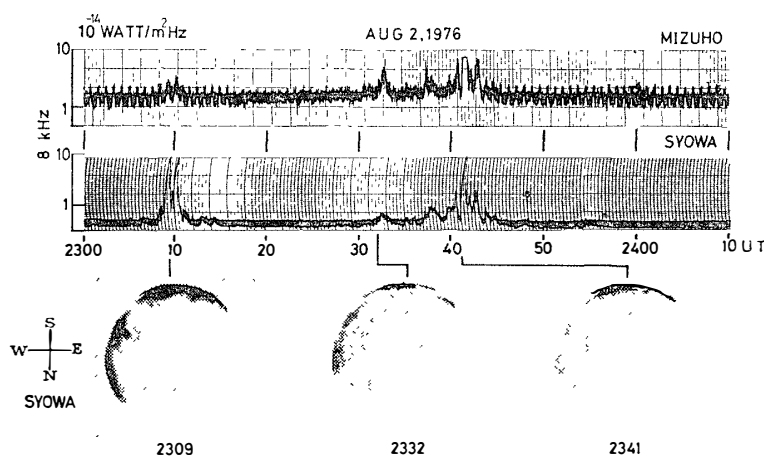


Fig. 47. The band-limited intensity of auroral hiss at the 8 kHz band observed at Syowa and Mizuho Stations along with the all-sky photographs of aurora.

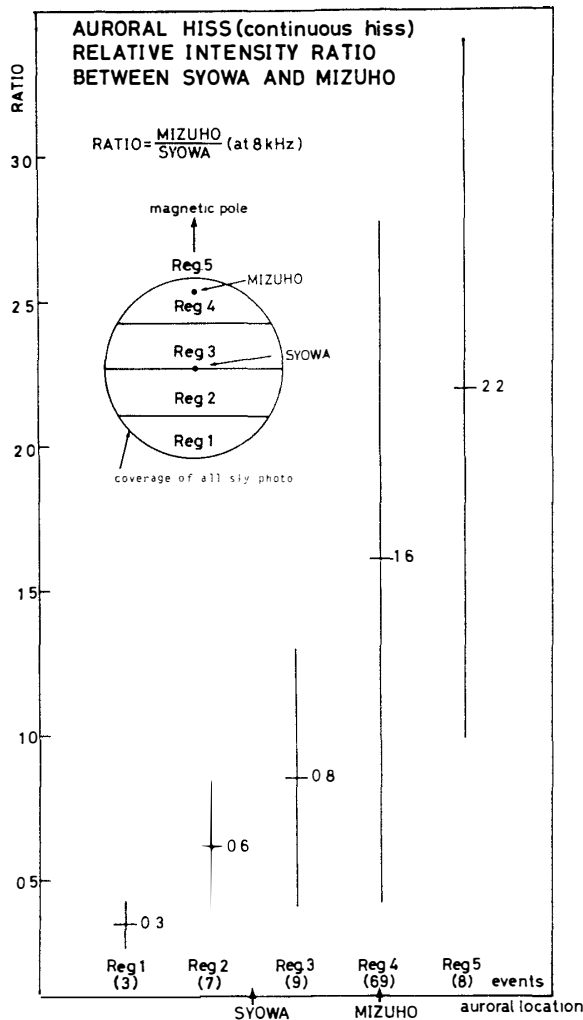


Fig. 48. The relationships between the relative intensity ratio of continuous hiss at the 8 kHz band obtained at Syowa and Mizuho and the locations of the steady auroral arc. The average ratio and the error bar are also shown in each region respectively. The region 5 is beyond the high latitude horizon of Syowa.

the active bright aurora and is suitable for deciding the location of aurora. The data of VLF emission here were obtained from June to August in 1976 at Syowa and Mizuho Stations. An all-sky camera photograph was divided into four parts according to the elevations below or above 45° from Syowa Station in a N-S direction as described before. In addition, one more region (*i.e.* high latitudes), beyond the coverage of the all-sky camera was taken into consideration. As the aurora located in this region could not be recognized by the all-sky camera photograph at Syowa Station, we used the auroral data of visual observation at Mizuho Station and this covered the region beyond the high latitude horizon from Syowa Station. The relationships between the relative intensity ratio of hiss emission at the 8 kHz band obtained at Syowa and Mizuho Stations and the locations of steady auroral arc are shown in Fig. 48. According to this result, it is evident that the intensity of hiss at Syowa Station is significantly stronger

than that at Mizuho Station, when the aurora appears on the lower latitude side of Syowa Station. On the other hand, when the aurora appears in high latitudes more than 100 km apart from the zenith of Syowa Station, the intensity of hiss at Mizuho Station becomes the same or slightly stronger than that at Syowa Station. If the steady auroral arc is distributed in an extensive area, the relative intensity ratio is scattered in a wide range. However, the general tendency that the relative intensity at Mizuho (high latitude) increases as the steady auroral arc is located in higher latitudes holds statistically.

#### 3.4. Summary

It is clear that two types of emission, the continuous hiss and the impulsive hiss, corresponding to the steady auroral arc, appeared at the higher latitude side of the station and the bright active aurora appeared near the zenith. Some of the fluctuations both of impulsive and continuous hiss intensity are clearly related to the fluctuations of auroral luminosities. However, many other examples show no meaningful correlation between the fluctuation of auroral luminosity and the VLF intensity at 8 kHz. These results may be partly explained in terms of the ionospheric absorption and the limitation of coverage of the scanning photometer. Another possibility that the electrons that excite the visual aurora and the auroral hiss emissions are different, should be considered. As for the relationships between the intensity of auroral hiss and the distribution of aurora, the intensity of the two types of hiss depends on the location of aurora. It is statistically clear that an increase in the continuous hiss intensity at a high latitude station is seen as a steady auroral arc is located in high latitudes. The impulsive hiss is frequently observed when the front of the active bright aurora appears near the zenith of the station. These results show that the penetration region of impulsive hiss may be more localized than that of continuous hiss.

#### 4. Arrival Direction of Auroral Hiss Emissions

It is important to examine the arrival direction of auroral hiss in order to study its generation region, propagation path and generation mechanism. HARANG (1968) observed auroral hiss using two loop antennas (N–S and E–W components) and showed that the intensity of auroral hiss detected by an E–W component loop antenna is usually stronger than that detected by a N–S antenna at Tromsø. From these results, he suggested that auroral hiss propagates mainly in the meridian direction. VERSHININ (1970) has observed VLF hiss emissions at stations in Siberia and also found that the change in direction of a magnetic antenna strongly affects the level of the received signal. The magnetic antenna oriented in the geomagnetic N–S picked up the stronger signal. TANAKA (1972) has observed the arrival direction of hiss emissions with a technique in which the TE (transverse electric field) component in the output signal of loop antennas is eliminated at the moment when the vertical component of the electric field  $E_z$  crosses the zero line. He found that auroral hiss propagates from low latitudes nearly along the magnetic meridian plane with a small deviation and that its incident angle is not very large. This method requires the observed wave to be monochromatic. However the auroral hiss is actually a signal with a broad frequency band. Therefore the contamination of random-noise and waves with different frequencies seriously degrades the accuracy of the results.

TSURUDA and HAYASHI (1975) have developed a new direction finding system in which the TE component is eliminated by taking simple algebraic combinations among the  $B_{N-S}$ ,  $B_{E-W}$  and  $E_z$  components (see Chapter 1). This method gives a reasonable arrival direction for non-monochromatic waves though it cannot be applied to linear polarization waves. OGUTI *et al.* (private communication, 1977) observed the arrival direction of VLF emissions at Churchill and Thompson in Canada using this new method. They showed that the exit point of a kind of hiss coincides roughly with the auroral active region. In this chapter, we examine the relationships between the location of aurora and the arrival direction of hiss. The local time variation of the arrival direction of hiss observed at Syowa Station in 1976 is also statistically examined.

#### 4.1. Relation between luminous region of aurora and the arrival direction of auroral hiss

In the previous chapter, we described that the occurrence of most auroral hiss is well correlated with the increase in luminosity of aurora. In order to clarify the relationships between aurora and auroral hiss in more detail, we examine the relation between the location of aurora and the exit point of simultaneous hiss emission through the ionosphere. Fig. 49 shows the intensity of hiss emission at the 750 Hz, 8 kHz and 64 kHz frequency bands, the arrival direction and the polarization of auroral hiss at the 8 kHz band, and the all-sky photographs of aurora with the exit area indicated by a rectangle in each picture. The arrival directions are shown in the middle panel.  $\theta$  is the incident angle measured from the zenith and  $\phi$  is the azimuthal angle measured from the north. The exit area on an all-sky camera photograph shown in the bottom panel is deduced from the arrival directions, assuming the exit level to be 100 km. An exit area shown here indicates the fluctuation of the arrival direction in one minute interval for hiss emissions with an intensity of  $>5 \times 10^{-15} \text{ W/m}^2 \text{ Hz}$ . The narrow-band continuous hiss was intermittently observed from 2100 UT to 2300 UT. In these events, peak to peak correspondence between the fluctuations of auroral luminosities and hiss intensities at 8 kHz band were clearly recognized, (as shown in Fig. 38, Chapter 3), and it is considered that the continuous hiss emission may be generated by these auroral particles. During this time interval, however, the arrival direction of auroral hiss was seen in the lower latitude of Syowa Station whereas the auroral active region was located near the poleward horizon. The polarization was right handed and circular ( $p \sim 0.5$ ). A similar example is given in Fig. 50. Steady auroral arcs were seen near the poleward horizon of Syowa Station from 2130 UT to 2330 UT and the narrow-band continuous hiss was observed during this time interval. The exit area of the hiss wave was at the lower latitude of Syowa Station and sometimes a little west, though the auroral arc was seen near the poleward horizon of Syowa Station. In most of the continuous hiss events examined here, the arrival directions associated with the auroral arc near the poleward region were generally seen near the zenith or at a latitude a little lower than of Syowa Station's.

Next, the relationships between the arrival direction of impulsive hiss and the associated auroral activity are examined. Fig. 51 represents the intensity of VLF hiss emission, the arrival direction of the hiss at the 8 kHz band and the all-sky camera photographs of aurora. The isolated impulsive hiss emission occurred around 2236 UT, associated with the initiation of auroral brightening near the zenith. In association with the poleward movement of auroras around 2236 UT, the arrival direction of hiss changed from the north to the south rapidly. After 2237 UT, the arrival direction turned to the north again. In this example, the arrival direction of impulsive hiss was much closer to the location of the auroral

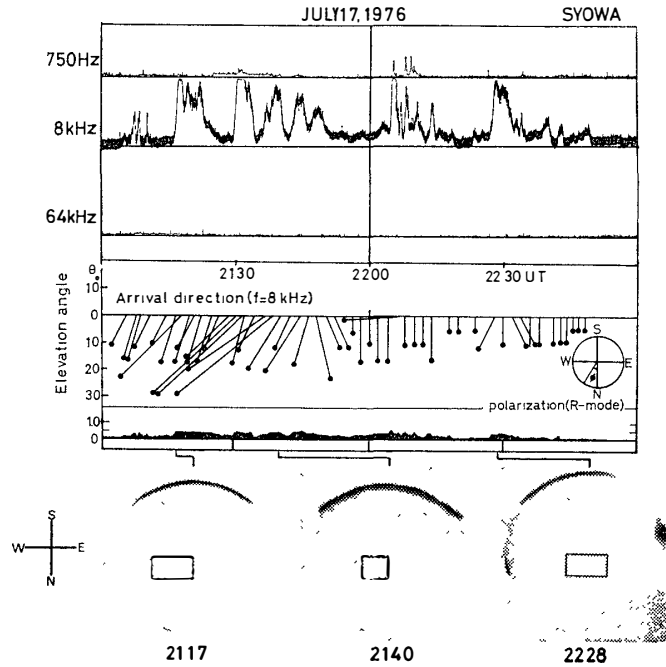


Fig. 49. The top panel shows the intensity of auroral hiss at the 0.75, 8 and 64 kHz bands. The middle panel shows the arrival direction and the polarization of hiss emissions at the 8 kHz band. The bottom panel shows the all-sky photographs of the related aurora observed at Syowa Station during this interval. The exit areas in one minute intervals are also shown on the all-sky photographs.

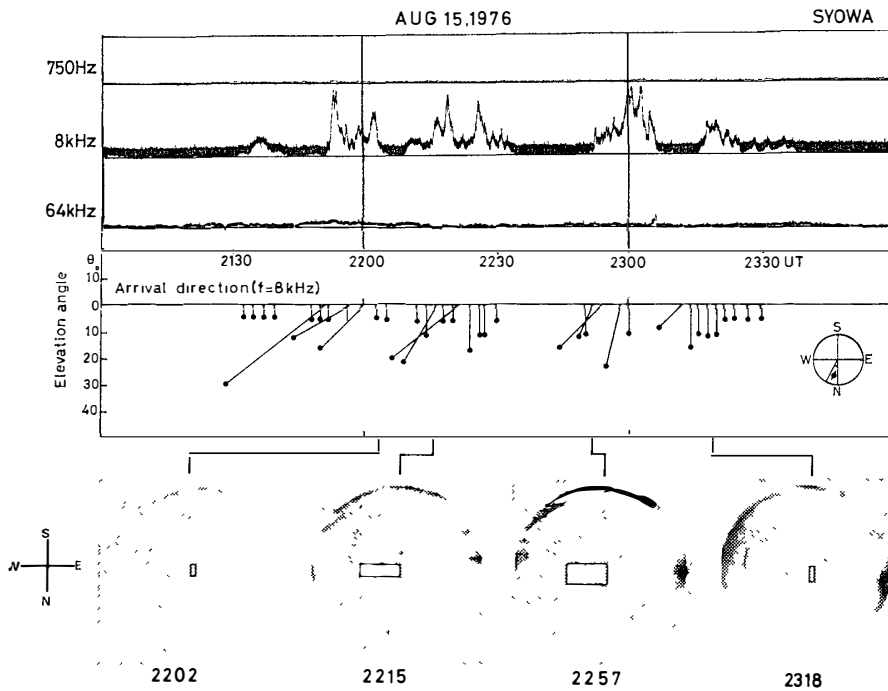


Fig. 50. The auroral hiss intensity, the arrival direction of aurora hiss at the 8 kHz band and the all-sky photographs of the related aurora. The format is the same as that in Fig. 49.

## VLF-LF Hiss Emissions Associated with Aurora

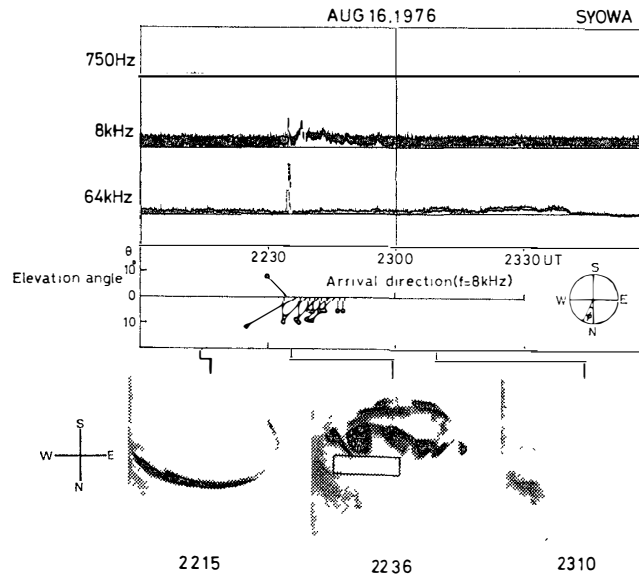


Fig. 51. The auroral hiss intensity, the arrival direction of auroral hiss at the 8 kHz band and the all-sky photographs of the related aurora. The format is the same as that in Fig. 49.

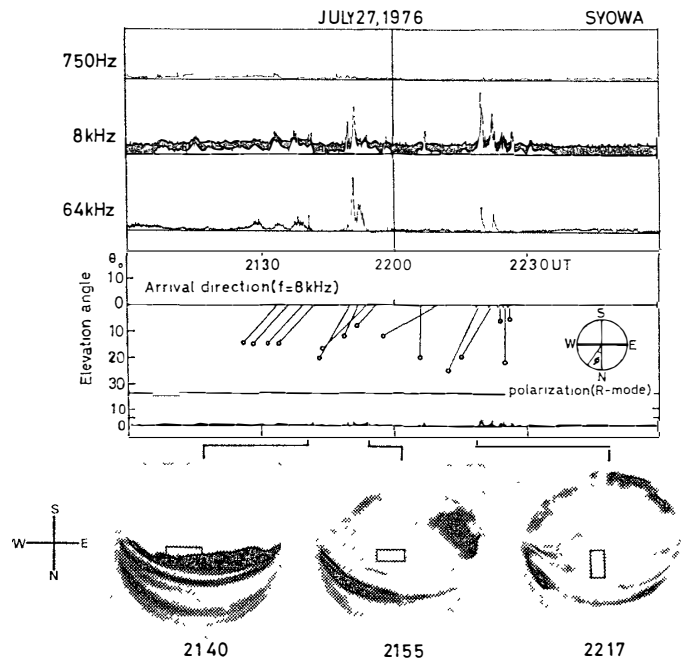


Fig. 52. The auroral hiss intensity, the arrival direction of auroral hiss at the 8 kHz band and the all-sky photographs of the related aurora. The format is the same as that in Fig. 49.

active region than that of continuous hiss. Another example of the relation between the arrival direction of impulsive hiss and the location of aurora is shown in Fig. 52. Several impulsive hiss emissions were intermittently observed from 2130 UT to 2230 UT. During these intervals, the auroral enhancements were seen near the zenith of Syowa Station. In this case, the arrival direction of impulsive hiss did not change so much and the exit area continued to be region near the zenith or at a latitude slightly lower than Syowa Station's. Fig. 53 shows another example similar to that shown in Fig. 52. The figure represents the intensity of impulsive hiss at the 8 kHz band observed at Mizuho and Syowa Stations, the arrival direction of hiss and all-sky camera photographs of aurora obtained at Syowa Station. Although the active bright aurora was seen near the zenith of Mizuho Station around 2310 UT, the arrival direction of hiss measured at Syowa Station pointed to the lower latitude of Syowa Station in this interval. Around 2340 UT, the active auroral region moved toward the higher latitude of Mizuho Station, and the arrival direction of hiss still continued to be near the lower latitude of Syowa Station. The polarization was right-handed and almost circular ( $p \sim 0.5$ ). The arrival direction of impulsive hiss was often found to point out the location of aurora when active bright auroras appeared near the zenith of Syowa Station. However, the arrival direction of impulsive hiss associated with the poleward bright aurora showed a different region from the auroral location.

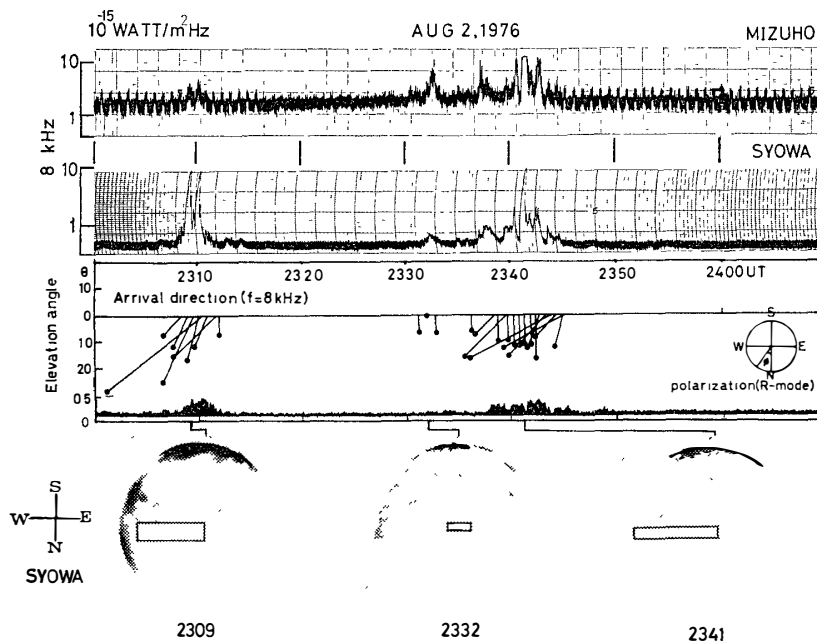


Fig. 53. The auroral hiss intensity, the arrival direction of auroral hiss at the 8 kHz band and the all-sky photographs of the related aurora. The format is the same as that in Fig. 49.

Note the fact that the values of the elevation angle and the azimuthal angle depend on integration time. When the integral time is longer than the duration of hiss phenomena, the arrival direction obtainable from this system tends to point near the zenith region. In our observations, we took 5 seconds for the integral time. This time constant is too long to examine the hiss phenomena whose arrival direction fluctuates within a few seconds. As the duration time of the continuous hiss is usually longer than a few tens of seconds, the error in the computed arrival direction should be small. On the other hand, as impulsive hiss emissions rapidly fluctuate within a few seconds, the error in arrival direction is larger compared with that in the case of continuous emissions. Although there are some ambiguities and limitations concerning the computed arrival direction, the tendency of the arrival direction obtained from this system namely whether hiss emissions arrive from the north or the south, is true. Similar results were also obtained by OGUTI *et al.* (private communication, 1977) using a similar technique. They observed the arrival direction of auroral hiss at Churchill and Thompson in Canada. They showed that the auroral hiss emissions were categorized into two kinds on the basis of the relationships between the arrival direction and the associated auroral locations. These results are summarized as follows.

- 1) The exit point of the wide-band hiss ( $f > 2$  kHz, possibly identical the impulsive hiss here) accompanied by the local auroral activation is roughly identical to the region of local auroral activity.

- 2) The arrival direction of the narrow-band hiss ( $4 \text{ kHz} < f < 20 \text{ kHz}$ , especially its low frequency band) which usually occurs in the evening region is not related to the region of auroral activity.

These results are consistent with our results here at Syowa Station, but some differences do exist. One of the differences is that the arrival direction of hiss observed at Churchill frequently coincides with the region of local auroral activity, while the hiss waves at Syowa Station are usually considerably equatorward of the associated auroral activity. This difference may come from the differences in dip angle of the geomagnetic field line at Churchill and at Syowa Station. According to the international geomagnetic reference field (IGRF) in 1975 the dip angle of Churchill is  $83^\circ$  and that of Syowa Station is  $65.5^\circ$ . Generally speaking, the auroral particles precipitate along the field line, and the VLF wave whose wave normal is perpendicular to the ionospheric plane efficiently propagates to the ground. Therefore the region of electron precipitation (the region of auroral activity) may deviate markedly from the region of wave incidence in the area where the magnetic dip is small. This may explain why a good relationship is found between the auroral region and the exit point of hiss at Churchill, whereas the region of wave incidence is equatorward of the auroral location at Syowa Station. We will discuss this problem in more detail in Chapter 7.

#### 4.2. Local time dependences of arrival direction of auroral hiss

In the previous section, we examined the arrival direction of hiss emission in the N–S direction and showed the arrival direction of continuous hiss at Syowa Station was mostly seen near the lower latitude of Syowa Station even when the related aurora appears near the poleward horizon of Syowa Station. In this section, the local time variations of arrival direction, especially in the E–W direction, are examined. Fig. 54 represents the intensity of auroral hiss emission at the 0.75, 8 and 64 kHz bands and the arrival direction of hiss at the 8 kHz band. From 1800 UT to 2400 UT, the narrow-band continuous hiss emissions were intermittently observed. During these time intervals, the arrival direction of hiss emissions was near the zenith or in a little lower latitude of Syowa Station except around 2050 UT and 2215 UT. Around 2215 UT, the arrival direction rapidly changed from north to south and was related to the occurrence of an impulsive hiss. An important point seen in this figure is a slow variation in the E–W component of the arrival direction with the local time. The arrival direction was eastward in the early evening (1800 UT–1900 UT). From 2000 UT to 2200 UT, the wave came from both the east and the west. After 2200 UT, most of the arrival directions of hiss were the westward region. In this example, the change in the arrival direction from the east to the west occurred around 2130 UT. A similar example is shown in Fig. 55. From 1800 UT to 2100 UT, a faint auroral arc was seen near the poleward horizon of Syowa Station and after 2130 UT a bright arc appeared near the zenith of Syowa Station. Continuous hiss emissions were observed from 1800 UT to 2300 UT intermittently. The arrival direction of these emissions was mostly in the lower latitude of Syowa Station in the N–S component except around 2015 UT. The example also showed a systematic variation in the E–W component of the arrival direction with the local time. Namely, in the early evening (1800 UT to 1900 UT) the arrival direction of hiss was the east and it changed from east to west around 2000 UT. After 2000 UT, the arrival directions of hiss were westward region.

The similar variations of arrival direction with local time were seen in many other examples. We examine statistically the local time variation of the narrow-band continuous hiss at the 8 kHz band. We selected 27 days' auroral hiss phenomena which were observed during 1800 UT to 2400 UT from June to August in 1976 and examined the arrival directions of 54 hiss events whose intensities were stronger than  $5 \times 10^{-15}$  W/m<sup>2</sup> Hz. The statistical change in arrival direction of hiss at the 8 kHz band with the local time thus obtained is shown in Fig. 56. The statistical result also indicated that the hiss came from the east in the early evening (1800 UT–1900 UT) and the arrival direction changed from the east to the west around 2030 UT in the lower latitude of Syowa Station. From the fact that the change in the arrival direction from the east to the west was seen around 2030 UT, it may indicate that strong continuous hiss emissions occur

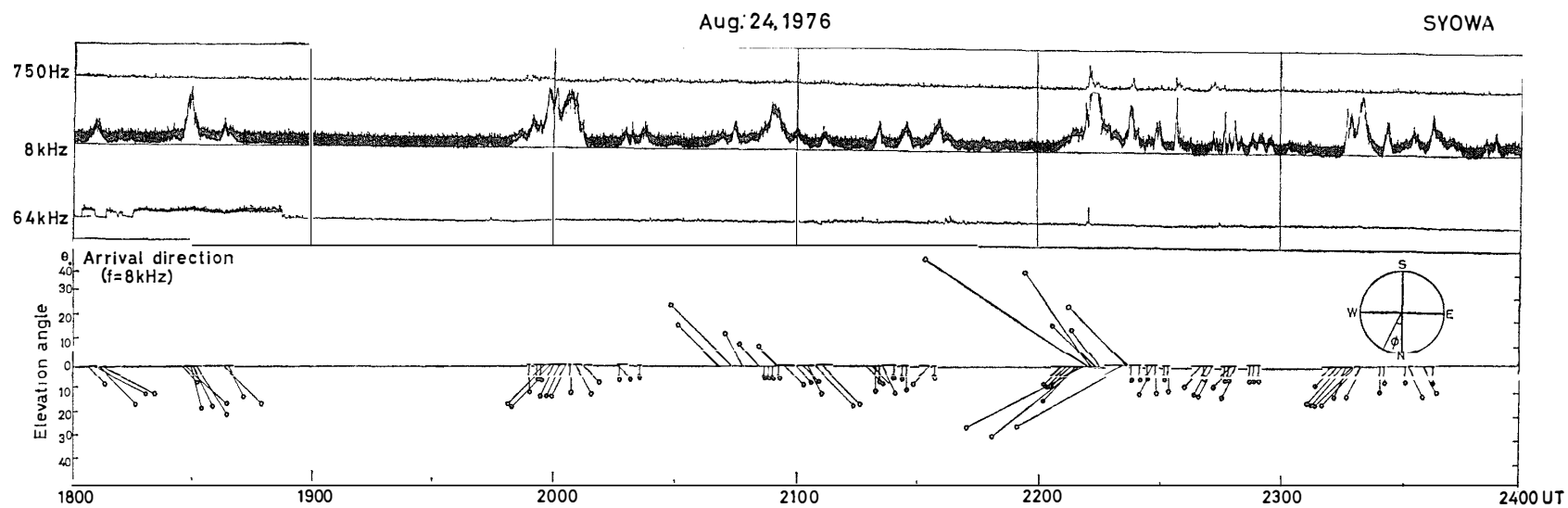


Fig. 54. The intensity of auroral hiss emissions at the 0.75, 8 and 64 kHz bands and the local time variations of the arrival direction of hiss at the 8 kHz band. The change in the arrival direction from the east to the west occurred around 2130 UT.

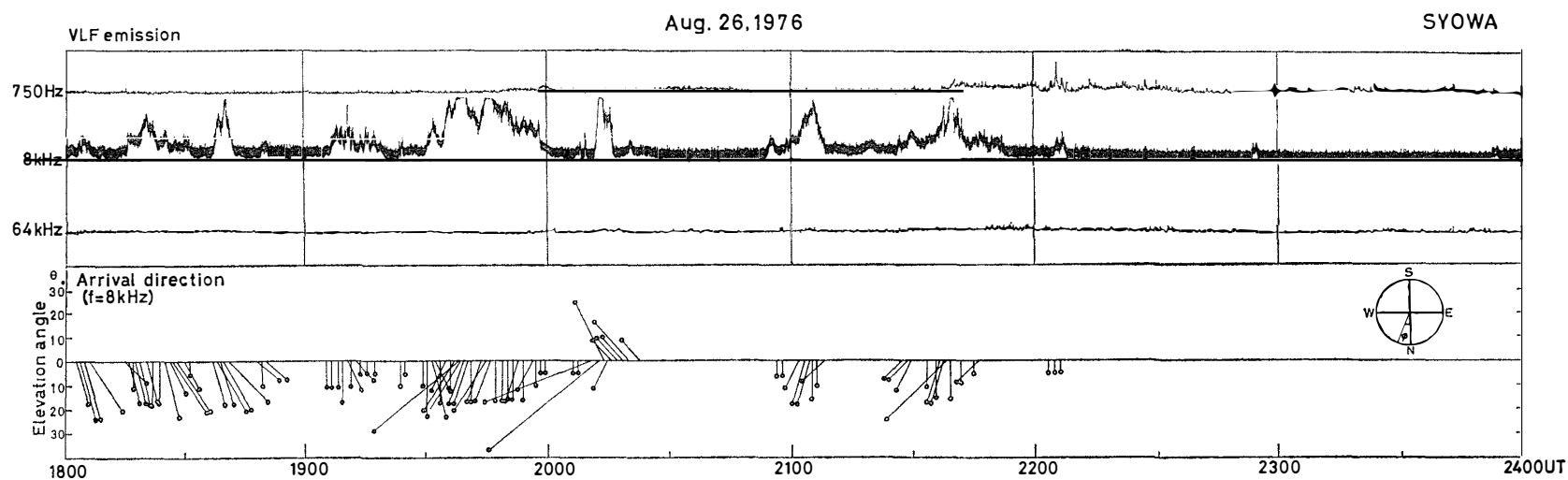


Fig. 55. The intensity of auroral hiss emissions and the arrival directions of hiss at the 8 kHz band. The format is the same as that in Fig. 54. The change in the arrival direction from the east to the west occurred around 20h UT.

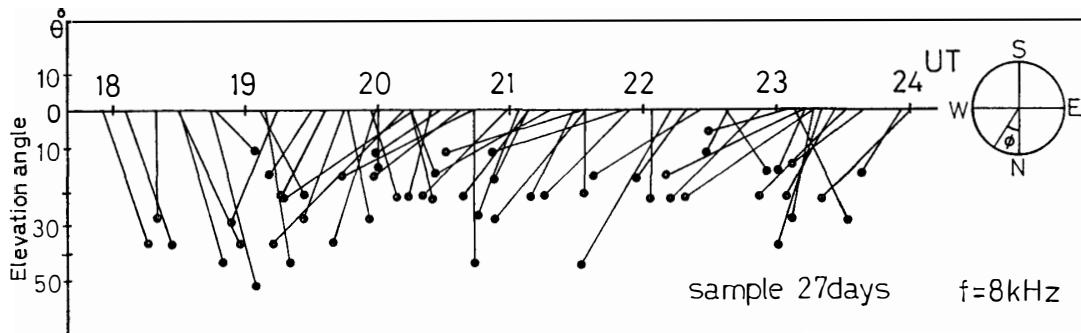


Fig. 56. The statistical change in the arrival direction of continuous hiss at the 8 kHz band with local time. 27 days' auroral hiss phenomena during 18h to 24h from June to August 1976 were examined.

frequently around this local time. This result may be supported by the energetic particle observations reported by MCDIARMID *et al.* (1975).

They examined the average intensity contour for 1.3 keV precipitating electrons detected on the Alouette 2 Satellite as shown in Fig. 57. It showed one of the peak fluxes of precipitating electrons ( $\sim 10^7$  electron/cm<sup>2</sup>·s·sr·keV) was seen around 2100 UT in the evening sector. If the strong hiss emissions may be excited by the precipitating electrons around this local time and they propagate in every region, the change in arrival direction from the east to the west occurring around 2030 UT mentioned above, may be reasonably explained.

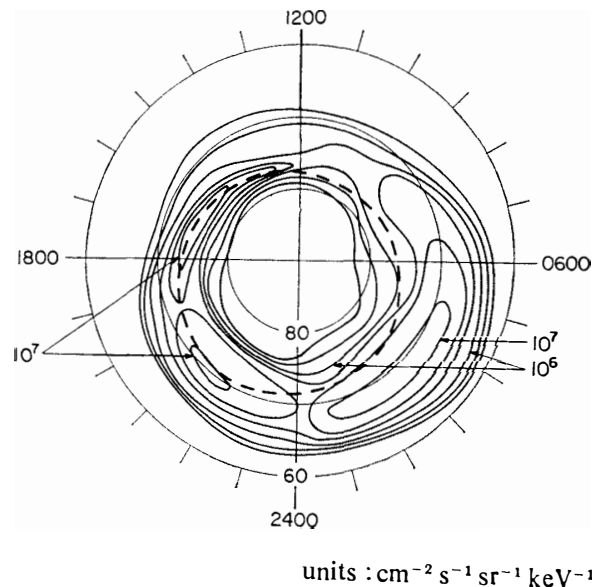


Fig. 57. Average intensity contours for 1.3 keV electrons. Intensity units are  $\text{cm}^{-2} \text{s}^{-1} \text{sr}^{-1} \text{keV}^{-1}$ , and adjacent contours differ in intensity by a factor of about 2.2. The dashed line is the 35 keV Alouette 2 background boundary:  $K_p \leq 3_0$  and  $\theta < 45^\circ$  (after MCDIARMID *et al.*, 1975).

#### 4.3. Summary

The arrival direction of both continuous and impulsive hiss emissions measured at Syowa Station was seen mostly near the zenith or in a little lower latitude of Syowa Station. The exit point of the continuous hiss at Syowa Station was usually seen around several hundreds of km equatorward of the associated aurora. On the other hand, the arrival direction of impulsive hiss which is related to the bright aurora appeared near the zenith, indicated near the region of aurora. The difference between the auroral location and the arrival direction may be understood in terms of the inclination of the geomagnetic field. Namely the auroral particles precipitate along the field line, whereas the VLF emissions excited and/or guided along the field line above thousands of km may gradually deviate from the field line below, propagating along a non-ducted path roughly perpendicular to the ionosphere. The fact that a good coincidence between the exit point of hiss and the active region of aurora was found at Churchill where the dip is large ( $\sim 83^\circ$ ) (OGUTI *et al.*, private communications, 1977) seems to support the interrelation mentioned above. A systematic local time variation of the arrival direction of hiss was found both in individual events and in statistics. In the early evening (1800 UT–1900 UT), the arrival direction was the east and it changed from the east to the west around 2030 UT. After 2100 UT, most of the hiss emissions came from the westward region. This local time variation of the arrival direction seems to be related to the distribution of precipitating electron flux with an energy 1.3 keV (MCDIAMID *et al.*, 1975) which may excite continuous hiss emissions.

## 5. Coordinated Ground-Satellite Observations of Auroral Hiss Emissions

### 5.1. Introduction

From the observations of low-altitude polar-orbiting satellites, it has been shown that there are several types of electrostatic and electromagnetic waves (auroral hiss, saucer, LHR emissions etc.) on auroral field lines (GURNETT, 1966; McEWEN and BARRINGTON, 1976; TAYLOR and GURNETT, 1968; LAASPERE and JOHNSON, 1973; JIRICEVK and TRISKA, 1976).

MOSIER and GURNETT (1972) examined the relationship between five VLF hiss events measured with Injun 3 and auroras observed on the ground (Churchill). One of these five events occurred near auroral arcs with significant changes in the hiss spectrum in the immediate vicinity of the auroral arcs. In the remaining four events, auroral hiss emissions were not associated with any detectable auroral light emissions. From this result, MOSIER and GURNETT (1972) suggested that auroral hiss and auroral light emissions are usually generated by electrons with somewhat different energies, and that when the energy spectrum of precipitating electrons includes high energy components, VLF hiss and auroral light emissions are simultaneously generated.

MOSIER (1971) showed by means of the Injun 5 Poynting flux measurement technique that auroral hiss emissions propagate downward (toward the earth), while saucer emissions propagate upward, *i.e.*, they suggested that a part of VLF hiss is generated above Injun 5, while saucer is generated below the satellite. GURNETT and FRANK (1972) reported that saucer emissions are usually observed on a lower latitude side than the V-shaped VLF hiss region. However, they did not discuss the relationship between the location of saucer emissions observed on satellite and locations of auroras observed on the ground. We will examine such a relationship by using VLF data obtained with ISIS 2 and auroral data observed at Syowa Station.

In order to understand the relationship between VLF hiss emissions observed on the ground and on the satellite, coordinated ground and satellite observations of VLF hiss are very important. In this chapter, from the simultaneous frequency-

time spectrum data of VLF emissions observed on ISIS 2 and on the ground, we will examine the conditions in which VLF emissions are simultaneously observed on the satellite and on the ground.

The ISIS 2 satellite was launched on April 1, 1971 on a circular polar orbit with an inclination of  $88.18^\circ$ , an apogee altitude of 1424 km and a perigee altitude of 1354 km. VLF wave data measured by a wide-band (50 Hz–30 kHz) receiver with an electric dipole antenna of 79 m length were received at Syowa Station, Antarctica in 1976.

### 5.2. Coordinated observations of auroral hiss and aurora

Fig. 58 shows the 8 kHz VLF intensity records from Syowa Station. Large enhancements of the continuous hiss at the 8 kHz band were observed in the four events (B, E, F, G). However, the 8 kHz intensity was low in the remaining three events (A, C, D). In the G event, the location of ISIS 2 was far away from Syowa Station when a large enhancement of the 8 kHz intensity was observed at Syowa Station. Therefore, this event is not a good example for comparing the VLF emissions observed on the ground and on satellite. We shall describe

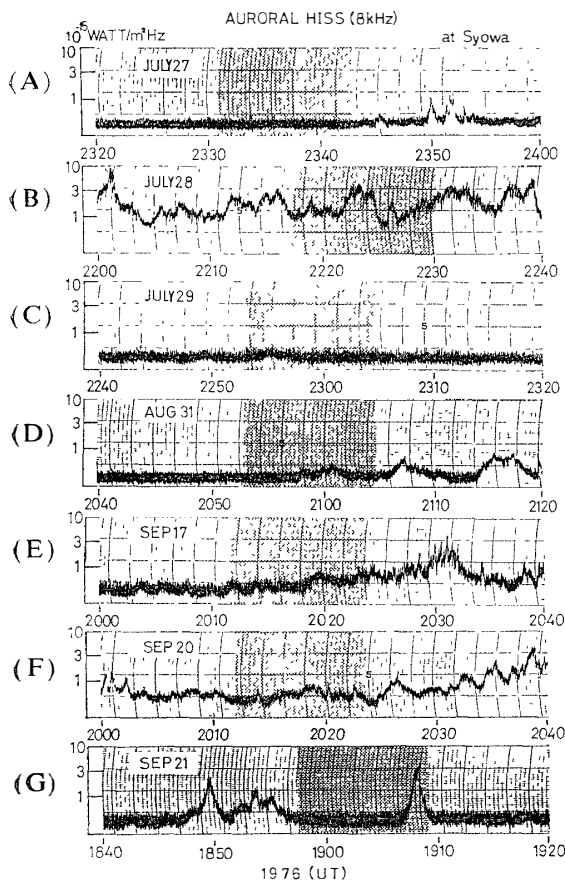


Fig. 58. The 8 kHz intensity observed at Syowa Station. Shadow regions show the period of simultaneous ground-satellite observations of VLF hiss emissions.

the three events (B, E, F) in detail as a case study and the remaining four events (A, C, D, G) will be presented in Appendix: Fig. A-11–Fig. A-14.

–September 17, 1976 event–

Fig. 59 gives frequency-time spectra of continuous hiss emissions on ISIS 2 and all-sky photographs taken at Syowa Station. The foot point of the geomagnetic field lines through ISIS 2 was computed at an altitude of auroras using the 1975 IGRF model. Here, the altitude of auroras is assumed to be 100 km. The position of the satellite foot point at 100 km level is illustrated by a circle on the all-sky photographs in Fig. 59. It is apparent in Fig. 59 that wide-band hiss emissions were observed continuously on ISIS 2 when the satellite was located in the latitude region higher than the location of the northern-most auroral arc, while saucer emissions were observed just after the satellite traversed the northern-most auroral arc at 2021:53 UT.

Such a relationship is presented again in Fig. 60. The frequency-time spectra of VLF emissions observed on ISIS 2 and on the ground (Syowa Station) are given in the top and bottom panels of Fig. 60, respectively. The middle panel shows the orbit and the geomagnetic latitude of the subsatellite point of ISIS 2, and the locations of Syowa and Mizuho Stations. The middle panel also shows the locations of auroral arcs and the geomagnetic field lines through these arcs. The  $f$ - $t$  spectrum at the bottom in Fig. 60 indicates that auroral hiss emissions with a narrow-band structure were observed continuously at Syowa Station during the ISIS 2 passage.

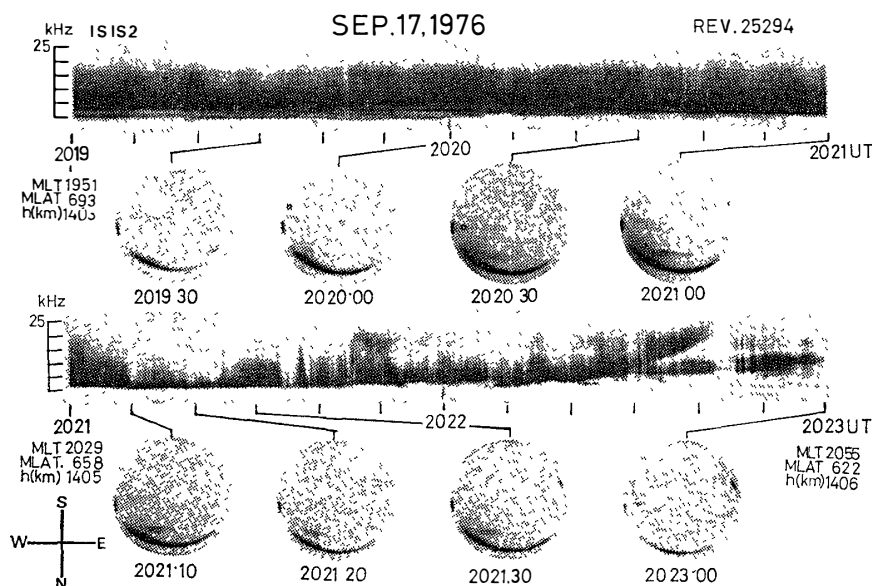


Fig. 59. All-sky camera photographs at Syowa Station and VLF frequency-time spectrum observed on ISIS 2. The satellite foot point along the geomagnetic-field line is plotted on the all-sky camera photographs with circles.

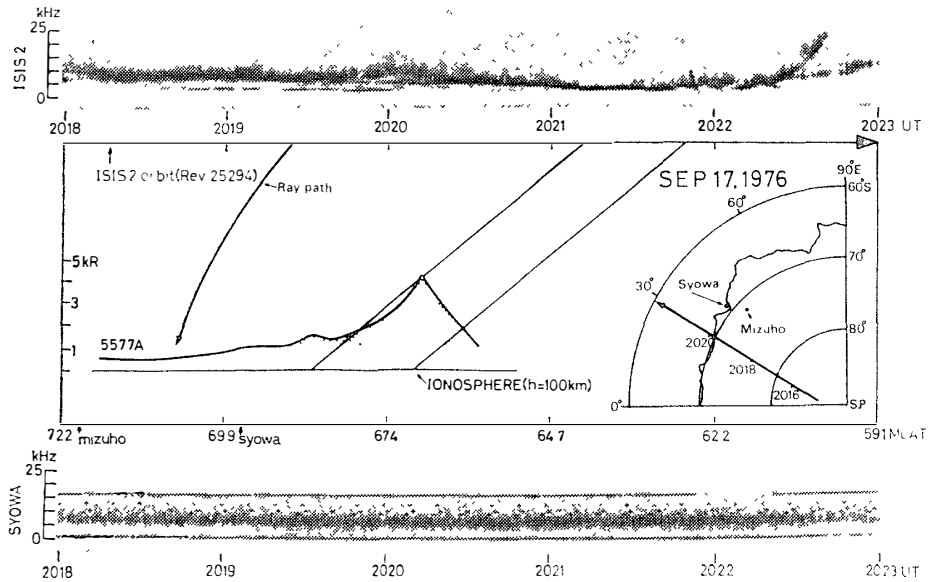
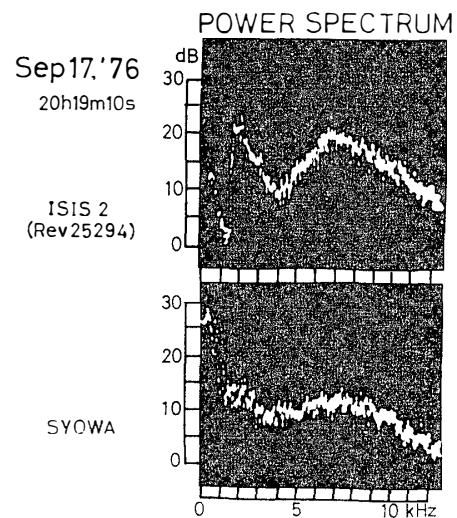


Fig. 60. Relationships between auroral hiss emissions simultaneously observed at an altitude of  $\sim 1400$  km and on the ground. Top and bottom panels give frequency-time spectra of VLF waves on ISIS 2 and on the ground (Syowa), respectively. The middle panel shows the intensity profile of  $5577 \text{ \AA}$  emissions which were observed by a meridian-scanning photometer at Syowa Station at 2020 UT. The location of auroral arcs is indicated by dotted areas. Geomagnetic field lines through arcs and a calculated ray path of an 8 kHz whistler mode wave are also illustrated schematically. The location of ISIS 2 is shown by the ground track of the subsatellite point in the middle panel. The locations of Syowa and Mizuho Stations are given at the bottom of the middle panel.

Fig. 61. Power spectra of VLF emissions simultaneously observed at 20h19m10s on the ISIS 2 and on the ground. Top and bottom panels give the power spectra of ISIS 2 and the ground (Syowa Station) respectively.



If the continuous hiss observed on the ground result from the VLF waves which propagate along the geomagnetic field lines, the  $f$ - $t$  spectrum on ISIS 2 at 2021:10 UT would be similar to the spectrum on the ground. The spectrum of auroral hiss obtained from ISIS 2 at 2021:10 UT showed a narrow-band structure with a center frequency of 2 kHz and a band-width of 1 kHz. However, the power spectrum observed on the ground at the same time had a different band structure with a center frequency of 8 kHz and a band-width of 5 kHz. The spectrum similar to the spectrum on the ground was seen on ISIS 2 when the subsatellite point of ISIS 2 was located near the same geomagnetic latitude as that of Syowa Station. Fig. 61 shows the power spectra observed both on ISIS 2 and on the ground at 2019:10 UT. Hiss spectrum on the ground showed a band structure with a center frequency of 7 kHz and a band-width of 5 kHz. VLF emissions obtained from ISIS 2 had two band structures whose center frequencies were 2 and 7 kHz. The spectral band around 7 kHz is similar to the spectrum observed on the ground.

–September 20, 1976 event–

Figs. 62 and 63 give relationships among VLF emissions at the altitude of  $\sim 1400$  km, auroras and continuous hiss observed on the ground. The low cutoff frequency of VLF emissions at the satellite altitude shows a clear latitude dependence (*cf.* Fig. 63). In the high latitude region, the cutoff frequency decreased with decreasing latitude, reaching a minimum at 2018:50 UT and then the cutoff frequency increased toward low latitudes. Saucer emissions were observed at 2020:45 UT when the satellite traversed the geomagnetic field lines threading the northern-most auroral arc.

Fig. 64 shows the continuous hiss spectra observed on satellite and on the ground at 2019:20 UT. ISIS 2 hiss spectrum had a peak frequency of 2 kHz and a narrow band-width of 1 kHz. The ground hiss spectrum also showed a similar peak frequency at 2 kHz and a band-width of 1 kHz. These results strongly suggested that continuous hiss emissions with similar spectral structures

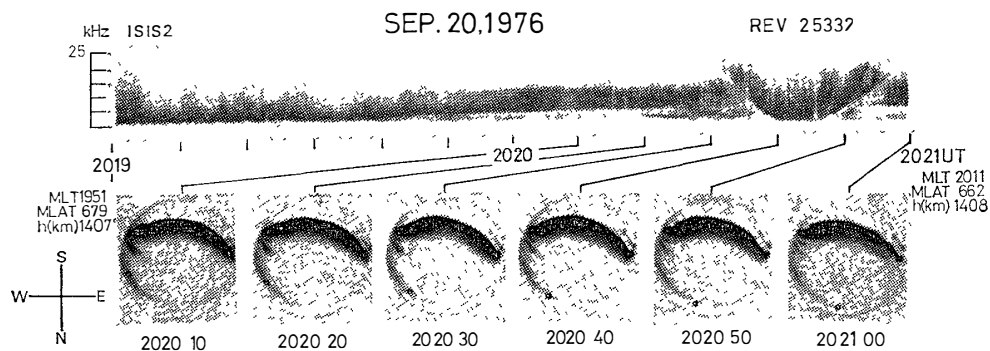


Fig. 62. All-sky camera photographs at Syowa Station and VLF frequency-time spectrum observed on ISIS 2. The notation is the same as that in Fig. 59.

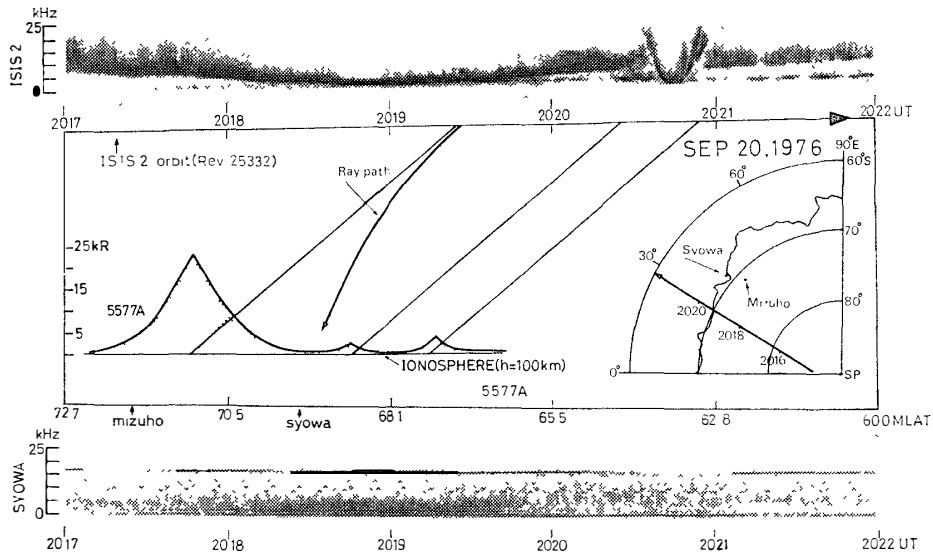
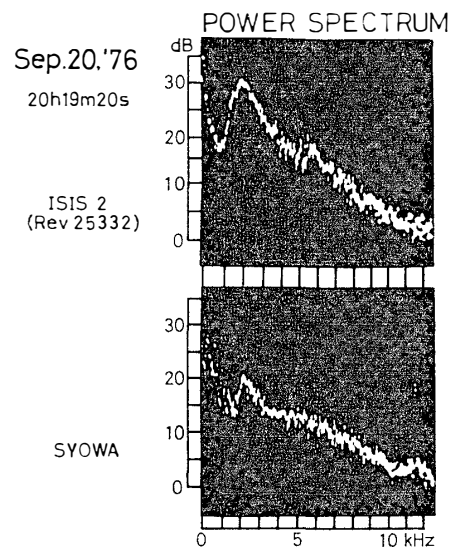


Fig. 63. Relationships between auroral hiss emissions simultaneously observed at an altitude of  $\sim 1400$  km and on the ground. The intensity profile of  $5577 \text{ \AA}$  emissions was observed at 20h21m UT. The notation is the same as that in Fig. 60.

Fig. 64. Power spectra of VLF emissions simultaneously observed at 20h19m20s UT on the ISIS 2 and on the ground. Top and bottom panels give the power spectra of ISIS 2 and the ground (Syowa Station) respectively.



as those at satellite altitude are observed when the ground station is located near the same geomagnetic latitude as that of the satellite.

–July 28, 1976 event–

Figs. 65 and 66 show the relationship between VLF emissions observed on ISIS 2 and auroras and continuous hiss observed on the ground. In this event, multi-auroral arcs were seen and intense continuous hiss emissions with a band structure were observed at Syowa Station. The center frequency varied from

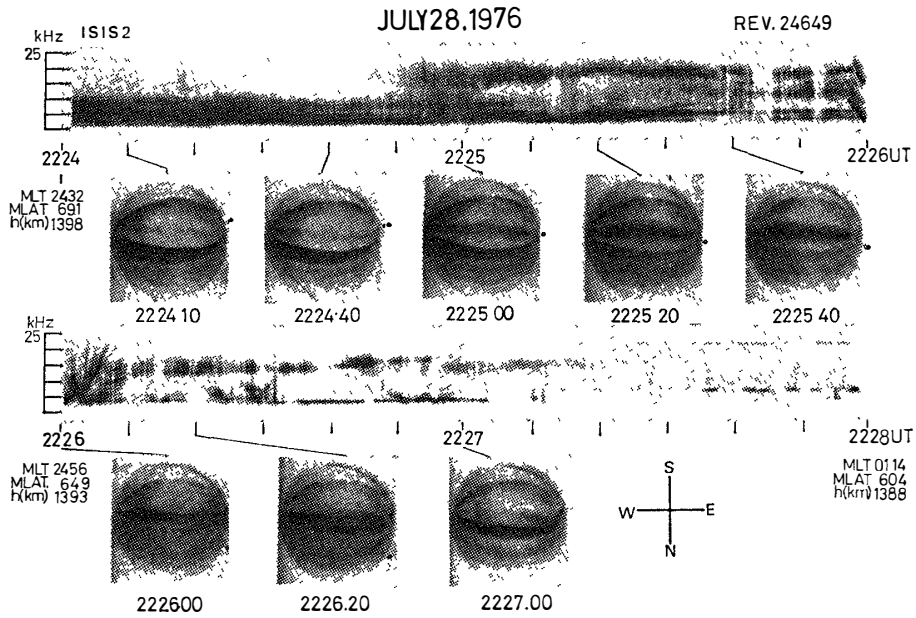


Fig. 65. All-sky camera photographs at Syowa Station and VLF frequency-time spectrum observed on ISIS 2. The notation is the same as that in Fig. 59.

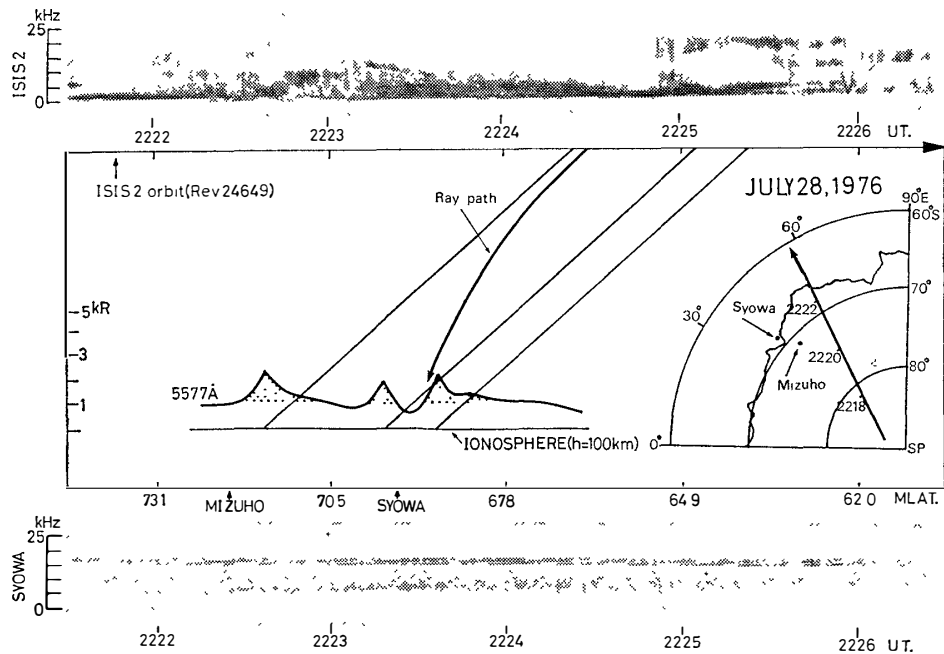
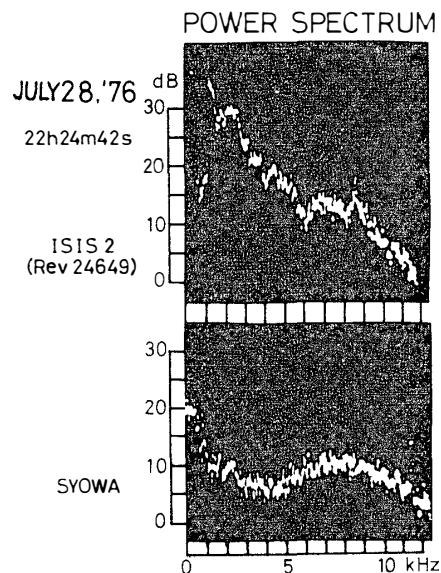


Fig. 66. Relationships between auroral hiss emissions simultaneously observed at an altitude of  $\sim 1400$  km and on the ground. The intensity profile of  $5577 \text{ \AA}$  emissions was observed at 2225 UT. The notation is the same as that in Fig. 60.

Fig. 67. Power spectra of VLF emissions simultaneously observed at 22h24m42s UT on the ISIS 2 and on the ground. Top and bottom panels give the power spectra of ISIS 2 and the ground (Syowa Station) respectively.



5 kHz to 10 kHz within a few minutes. Auroral hiss emissions with a similar spectral structure were also observed at Mizuho Station (the  $f-t$  spectrum is not given here). The ISIS 2 orbit was outside of the all-sky camera coverage from Syowa Station. However, the location of ISIS 2 was within 100 km of the edge of the all-sky photographs. In the following discussion, the auroral arcs are assumed to extend toward the outside of the all-sky coverage along the latitude.

Fig. 67 shows the power spectra of continuous hiss at 2224:42 UT, when the ground hiss spectrum had a peak frequency of 7.5 kHz and a band-width of 5 kHz. ISIS 2 hiss spectrum was more complicated than on the ground, having intensity peaks around 2 kHz. However, a band structure around 7 kHz seems to correspond to the ground hiss spectrum. On the other hand, if VLF waves propagate along the geomagnetic field line, the  $f-t$  spectrum on ISIS 2 at about 2225:20 UT would be similar to the spectrum on the ground. The hiss spectrum on ISIS 2 had a band structure emission with a peak frequency of 2 kHz. This spectrum was quite different from the spectrum on the ground which showed a narrow-band emission with a peak frequency of 7.5 kHz and a band width of 5 kHz.

When the satellite passed the region connected to the bright arcs through the geomagnetic field lines at 2224:55 UT, impulsive VLF emissions with wide-band frequency components from  $\sim 1.0$  kHz to 25.0 kHz were observed. These emissions were continuously observed until 2227:00 UT. Saucer emissions were observed after 2226:00 UT, when ISIS 2 passed near the field lines threading the northern-most faint arc.

### 5.3. Summary

Simultaneous observations of VLF emissions on ISIS 2 and the ground were carried out at Syowa Station in 1976. From these observations, 7 events were selected in order to study the relationship between VLF emissions and auroras. We have already described the relationships of the 3 typical events in the previous section. The remaining 4 events are given in Fig. A-11–Fig. A-14. The results are summarized as follows.

1) Occurrence regions of hiss and saucer emissions observed with ISIS 2 are localized in latitude. Hiss emissions are generally observed on the higher latitude side of the geomagnetic field lines through the northern-most auroral arc, while saucer emissions are observed on the lower latitude side of these field lines.

2) In general, hiss emissions are continuously observed during ISIS 2 traverse across the auroral zone on the night side. The latitude range of hiss emissions is about a thousand kilometer, while the latitude range of saucer emissions is much narrower than that of the hiss emissions. A typical latitude range of the saucer emission region is a few tens of kilometers.

3) A hiss spectrum on ISIS 2 similar to the ground continuous hiss spectrum at Syowa Station was seen when the subsatellite point was located near the same geomagnetic latitude as that of Syowa Station. However, the ISIS VLF spectrum observed on the Syowa field lines was quite different from the ground hiss spectrum.

The observed result that saucer emissions occur on the lower latitude side of the field lines through the northern-most auroral arc is consistent with JAMES' result (1976). He suggested that saucers are excited by upward ionospheric thermal electrons. In order to examine JAMES' suggestion, it is necessary to measure simultaneously both low-energy electrons and VLF waves.

GURNETT and FRANK (1972) and LAASPERE and HOFFMAN (1976) reported that hiss emissions are closely associated with precipitating electrons with energies of a few hundred eV. From DMSP auroral particle observations, MENG (1976) and MENG *et al.* (1978) showed that a large number of soft electrons with energies of several hundred eV precipitate in a wide latitude range around auroral arcs. In our ISIS 2 VLF observations, hiss emissions were frequently observed in the wide latitude range higher than the field lines through the northern-most auroral arc. From these results, it is suggested that soft precipitating electrons efficiently excite the auroral hiss emissions.

The relationships between VLF emissions observed at high altitudes and on the ground were studied by GURNETT (1966), SRIVASTAVA (1976) and JØRGENSEN (1968). GURNETT (1966) examined only two events and indicated a lack of correspondence between VLF emissions observed on Injun 3 and on the ground (Great Whale River). SRIVASTAVA (1974) compared eight VLF emission events observed on Injun 5 with VLF data obtained at College and Barter Island.

However, he was also unable to find a good correspondence between the ground and satellite data. On the other hand, JØRGENSEN (1968) showed a similar spectrum of VLF emission observed at high altitude and on the ground. We examined 51 VLF emission data and could find three events which had similar spectra at the high altitude and on the ground. These results show that similar auroral hiss emissions between ground-satellite were not obtained very often. When the narrow-band spectrum was observed at the high altitude near the zenith of the ground station, there was a good correspondence between ground and satellite VLF spectrum. However, there is a lack of correspondence between saucer and LHR emissions observed on satellite and VLF emissions observed on the ground.

There were no data of impulsive hiss emission simultaneously observed on the ISIS 2 satellite and on the ground. Therefore it is not clear whether the impulsive hiss propagates along the field line or not in our analysis.

VLF emissions are not so frequently observed on the ISIS 2 satellite at the night side in summer. Electron density near the altitude of the ISIS 2 satellite increases one or two orders of magnitude in summer (N. MATUURA, private communication, 1977). These back-ground electron density variations may change a condition of the hiss excitation process as described later. Therefore, it is necessary to study the seasonal variation of hiss emissions and its relationship to background plasma variations in the future.

## 6. Geomagnetic and Global Auroral Activities and Auroral Hiss Emissions

Many workers have demonstrated that there are close relationships between auroral hiss emission and geomagnetic disturbance (ELLIS, 1959, 1961; MOROZUMI, 1965; HARANG and LARSEN, 1965; KOKUBUN *et al.*, 1972). ELLIS (1959, 1961) showed that the occurrence of hiss emissions in the frequency band of 4–10 kHz increases during geomagnetic disturbances at the subauroral zone. MOROZUMI (1965) classified the night time sequence of VLF emission into three phases  $N_1$ ,  $N_2$ ,  $N_3$ , by comparing VLF emissions with auroral activity, geomagnetic pulsation and cosmic noise absorption at Byrd Station. The  $N_1$  phase before midnight is characterized by the appearance of intense hiss and diffuse arc-like auroras. The ionospheric absorption during the  $N_1$  phase is usually small, and one to one correspondence between hiss bursts and positive magnetic variations of 50–100  $\gamma$  is sometimes observed in this phase (HARANG and LARSEN, 1965). The  $N_2$  phase, when impulsive hiss bursts occur almost simultaneously with a sudden increase in brightness of aurora, Pi bursts and a sharp onset of cosmic noise absorption, is interpreted as the expansion phase of a substorm in accordance with the recent concept of magnetospheric substorm (AKASOFU, 1968). In the  $N_3$  phase, chorus type emissions are often observed near 1 kHz after the breakup phase, accompanied by an intensive cosmic noise absorption and irregular geomagnetic pulsations (HAYASHI and KOKUBUN, 1971).

AKASOFU (1968) proposed a model of a VLF substorm on the basis of MOROZUMI's result. In his model the  $N_1$  phase is interpreted as a phenomenon associated with the development of westward traveling surge. However, it is not evident whether or not hiss in the evening region is related directly to the development of the expansion phase of a substorm. The purpose of the first section in this chapter is to examine the relationships between the hiss emission and the development of a magnetospheric substorm.

Previously we described that there are two kinds of hiss emissions which are related to the steady auroral arc and the active bright aurora (Chapter 4). This result is obtained from the examination of the local auroral activity data

(all-sky camera photograph). Then we reexamine this result using the global auroral activity data (DMSP) in the second section.

### 6.1. Occurrence of auroral hiss and the development of a magnetospheric substorm

Recently, many investigators have showed that there are three stages: the growth phase, expansion phase and recovery phase, in the development of a magnetospheric substorm (IJIJIMA and NAGATA, 1972; MCPHERRON, 1973, NISHIDA and NAGAYAMA, 1973). According to AKASOFU's criterion (AKASOFU, 1968) the onset time of the expansion phase was determined from the sudden brightening and

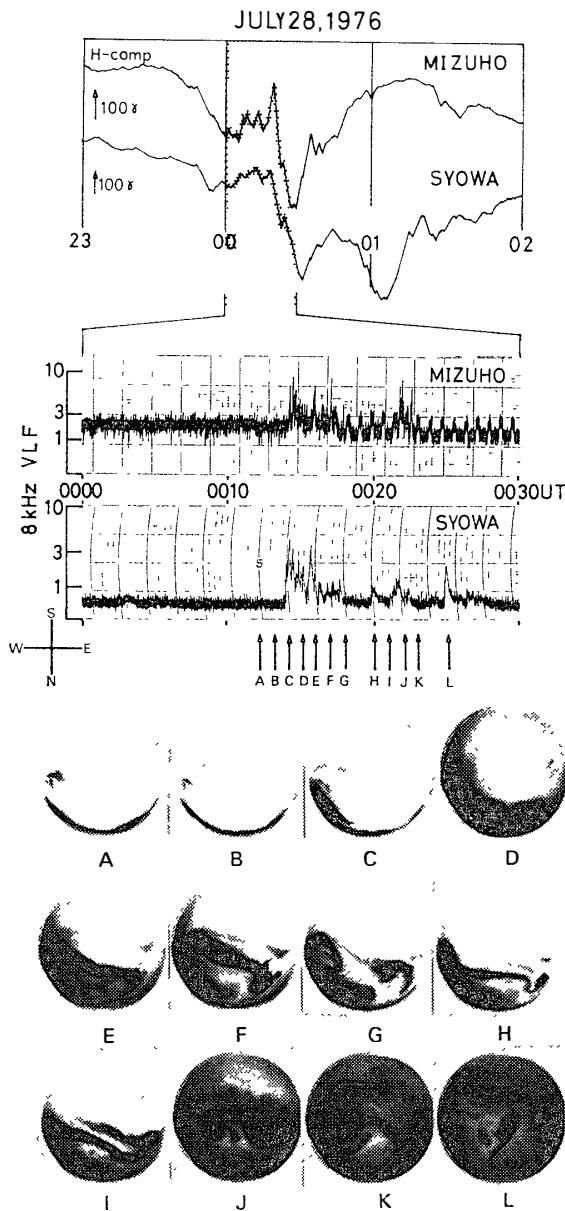


Fig. 68. The top panel shows the magnetograms at Mizuho and Syowa Stations. The middle panel shows the intensity of auroral hiss at the 8 kHz band observed at both stations and the bottom panel shows the sequential all-sky photographs of aurora obtained at Syowa Station. Each auroral photograph (from A to L) corresponds to the time indicated by each of the arrows from A to L.

spreading of auroras associated with the sharp negative disturbance in the  $H$  component of the magnetic field. Since the characteristics of the precipitating auroral particles and the background electron densities temporarily vary in the development of the magnetospheric substorm, it is important to know the relationships between the occurrence of hiss and the development of the substorm in order to understand the generation mechanism of hiss emissions. Fig. 68 represents a typical example of the relationships between the auroral breakup and hiss emissions. It shows the magnetograms and VLF emissions at the 8 kHz band

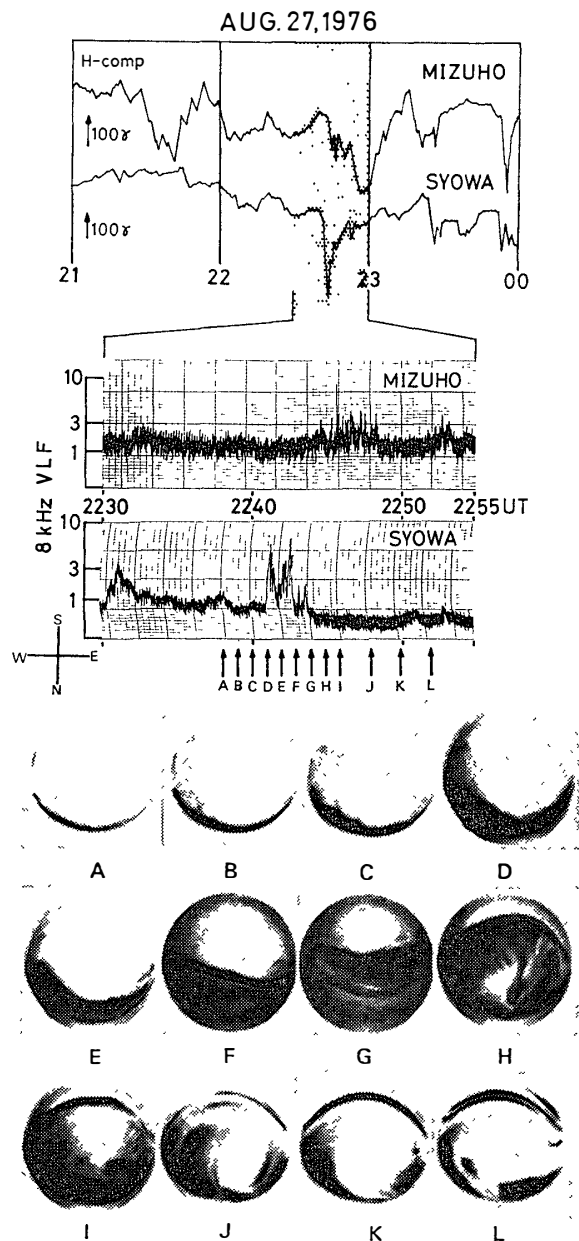


Fig. 69. The top panel shows the magnetograms and the middle panel shows the intensity of auroral hiss at the 8 kHz band observed at Syowa and Mizuho Stations. The bottom panel shows the auroral photographs observed at Syowa. The notation is the same as that in Fig. 68.

observed at Mizuho and Syowa Stations and the auroral photographs observed at Syowa Station. The steady auroral arc was seen on the lower latitude side of Syowa Station before 0014 UT. When the initial brightening of the auroral arc was seen at 0014 UT in the lower latitude of Syowa Station (C) and the sharp negative bay occurred at both stations simultaneously, the impulsive hiss which extended from a few kHz to a few tens kHz suddenly appeared. The intensity of hiss emissions became weak after the poleward expansion of the aurora. The disappearance of hiss may partly be due to absorption by the ionosphere. This example shows that impulsive hiss emissions occurred simultaneously with the local auroral break-up and the onset of the expansion phase. A similar example is shown in Fig. 69. The format is the same as that of Fig. 68. Before 2241 UT, a steady auroral arc was seen in the lower latitude of Syowa Station. Weak auroral hiss emissions were observed before this time. The sharp negative bay and the initial brightening of aurora began at 2241 UT (D). In this case, however, the impulsive hiss associated with this initial brightening of aurora appeared only at Syowa Station. The strong hiss emission appeared 4 minutes later at Mizuho Station. This time was coincident with the arrival time of active auroras near the zenith of Mizuho Station. This example shows that the hiss region seems to be related to the front region of active aurora. Generally speaking, impulsive hiss emissions occur associated with the initial brightening of aurora and onset time correlates with the beginning of the negative bay disturbance. It can also be said that the impulsive hiss is observed near the localized region where the active aurora occurs.

Next, the relationships between the occurrence of the continuous hiss emissions and the development of a substorm are examined. As described before, these emissions are related to a steady auroral arc located near the poleward

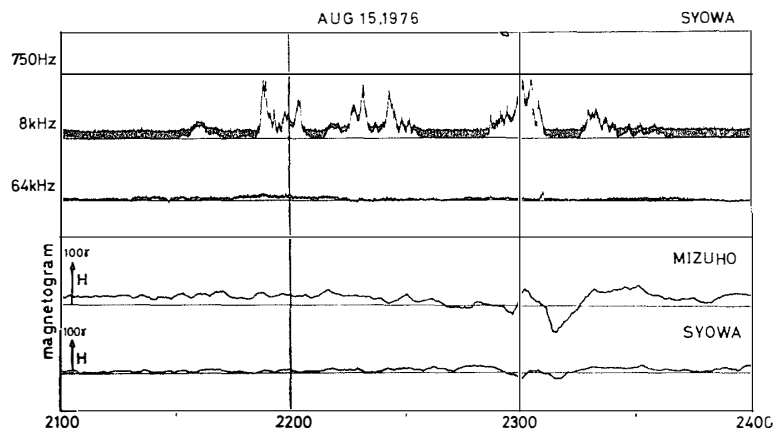


Fig. 70. The intensity of auroral hiss at the 0.75, 8 and 64 kHz bands observed at Syowa Station and the magnetic variations observed at both Syowa and Mizuho Stations.

horizon and the local magnetic disturbance is usually small. Fig. 70 represents the records of VLF emissions at the 750 Hz, 8 kHz and 64 kHz bands observed at Syowa Station and the magnetic variations observed at Syowa and Mizuho Stations. The continuous hiss emissions were seen from 2130 UT to 2330 UT.

In this interval, small positive and negative deflections of the magnetic field were observed. Their magnitudes were less than  $50 \gamma$  at both stations and they had no relation to the enhancements of hiss emissions, except around 2308 UT. A weak impulsive hiss was recorded around 2308 UT and was followed by a small negative bay of about  $70 \gamma$  at Mizuno Station. A similar example is shown in Fig. 71. It also represents the poor relations between VLF and the magnetic variations as in Fig. 70. Several enhancements of continuous hiss at the 8 kHz band occurred from 2100 UT to 2300 UT at Syowa Station. Weak magnetic fluctuations with magnitudes of about  $50 \gamma$  were seen at both stations during this interval, but no clear relation between VLF enhancements and magnetic variations were recognized. A steady auroral arc was seen near the poleward horizon of Syowa Station (Fig. 39, Chapter 3) during this interval. As seen in these examples and in many others as well, it can be said that the enhancements of continuous hiss emissions are poorly related to magnetic variations at Syowa and Mizuho Stations. Since we did not examine the world-wide geomagnetic activity data, it was not clear whether the continuous hiss emissions occurred in the expansion phase or not. Then we examined the relationships between the world-wide geomagnetic activity (*AE* index) and the occurrence of the continuous hiss emissions. Fig. 72 shows the intensity of VLF emission at the 4, 8, 14, 32 and 64 kHz bands, *AE* index and the magnetic field variations at Syowa Station. Continuous hiss emissions with peak intensities around the 4 and 8 kHz

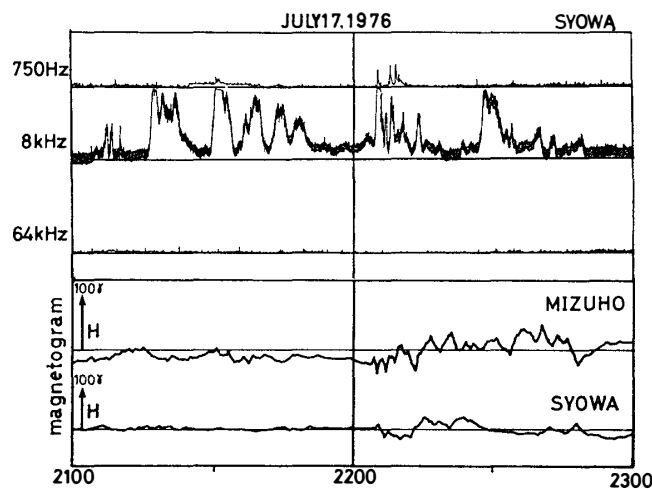


Fig. 71. The intensity of auroral hiss at the 0.75, 8 and 64 kHz bands observed at Syowa Station and the magnetic variations at both Syowa and Mizuho Stations.

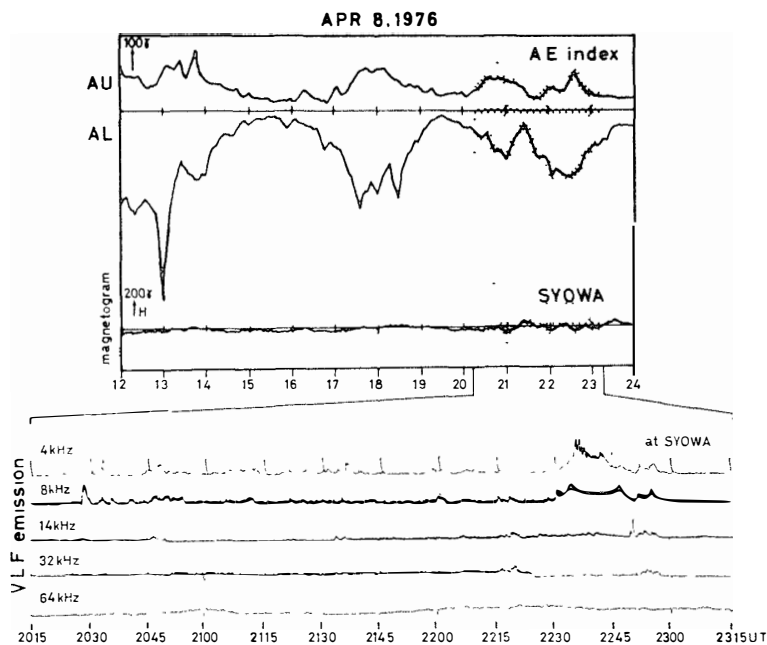


Fig. 72. The top panel shows the *AE* index and the *H*-component magnetogram at Syowa Station. The intensity of auroral hiss at the 4, 8, 14, 32 and 64 kHz bands is shown in bottom panel.

bands were observed in a period from 2030 UT to 2300 UT. Although the magnetic variation at Syowa Station was not remarkable in this interval, disturbances with a magnitude of  $300 \gamma$  were seen in the *AE* index. The *AE* index indicates that two negative bays occurred from 2030 UT to 2300 UT, beginning around 2030 UT and 2130 UT respectively. The enhancements of continuous hiss were found to occur during the developing stages of the two substorms. Fig. 73 represents another example of continuous hiss emissions observed at Syowa Station and the *AE* index. The continuous hiss emissions with a spectral peak around 14 kHz were followed by weak magnetic disturbances at Syowa Station while the *AE* index indicates a typical substorm with a depression of about  $500 \gamma$  in the horizontal component at 2030 UT. The onset of *AL* depression was nearly coincident with the appearance of the continuous hiss emissions. These results suggest that most of continuous hiss emissions are also observed during the expansion phase of a substorm. When an enhancement of the continuous hiss emission occurs in the evening, a related enhancement of the auroral luminosity is often seen although the aurora pattern is different from the active bright aurora observed near the auroral breakup region. The enhancement of the continuous hiss emission, concurrent with the enhancement of the auroral luminosity in the evening, would be a manifestation of the initiation of a substorm in the midnight sector. Although many example indicates that most of the continu-

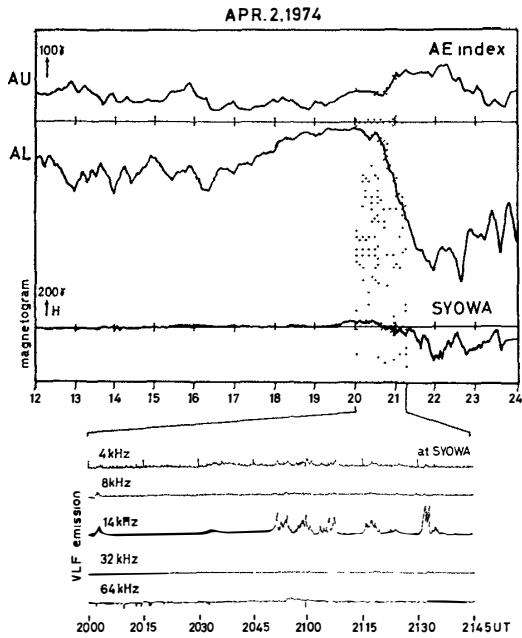


Fig. 73. The AE index and the H-component magnetogram are shown in the top panel and the intensity of auroral hiss at several bands is shown in the bottom panel. The format is the same as that in Fig. 72.

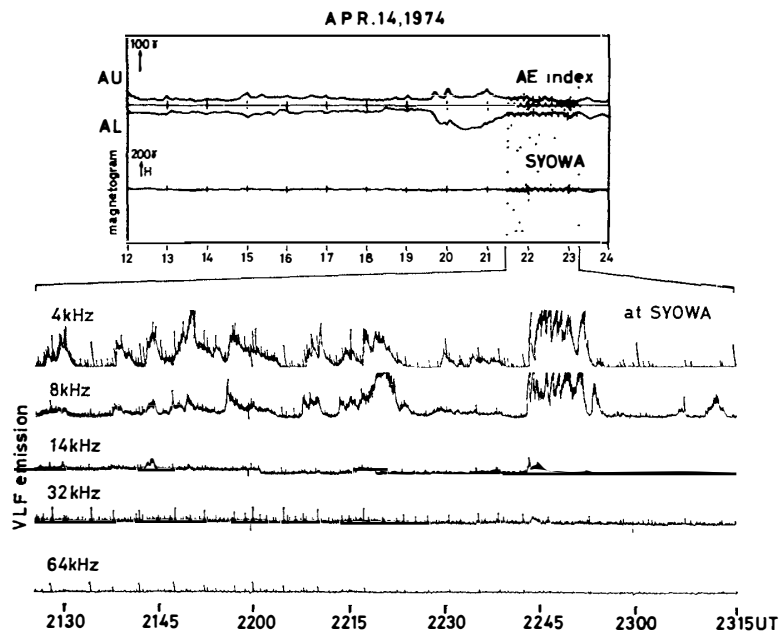


Fig. 74. The AE index and the H-component magnetogram are shown in the top panel and the intensity of auroral hiss at several bands is shown in the bottom panel. The format is the same as that in Fig. 72.

ous hiss emissions are related to the initiation of a substorm, there are a few examples continuous hiss that are not directly followed by the global initiation of a substorm. Fig. 74 shows an example of this kind. VLF emissions and

$AE$  indices, along with a magnetogram obtained at Syowa Station are shown here. Strong continuous hiss emission in the 4 and 8 kHz bands were seen from 2130 UT to 2315 UT in the lower panel. However, both the  $AE$  index and the magnetic variation at Syowa Station were less than  $50 \gamma$  in this time interval. Any indication of an auroral breakup was not seen during or after this time interval.

In order to elucidate the relationships between auroral hiss emission and the local breakup of auroras, the magnetic disturbance and hiss emissions observed at Syowa Station are examined using 25 days data from May to August in 1969. Isolated negative bays with deflections greater than  $200 \gamma$  at Syowa Station were selected. The deviation of the horizontal component was less than  $40 \gamma$  during the 2.5 hours before and after the breakup time. Fig. 75 represents changes

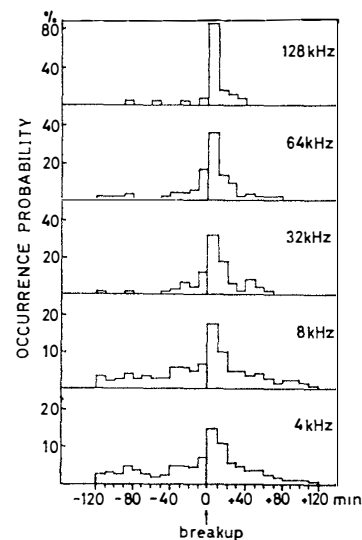


Fig. 75. Occurrence probabilities of intensity increases at five frequency bands before and after breakup.

in occurrence probability of hiss at 5 frequency bands with the initiation of breakup defined above. As seen in this figure the hiss emission with higher frequencies has a higher probability of occurrence in association with the onset of an auroral breakup. Other interesting features are that the hiss emissions with lower frequencies (4 and 8 kHz) tend to increase to a fairly high level before the breakup, and that the enhancement related to the local breakup is not as remarkable as in higher frequencies. The association of higher frequency components with the initiation of the local breakup suggests that the hiss with higher frequencies are generated in the region closer to the auroral precipitation that causes the breakup of auroras. On the other hand, the hiss with lower frequencies is not always generated in the region closer to the auroral precipitation that causes the local breakup.

## 6.2. Global auroral activity and auroral hiss

The relationships between auroral activity and enhancements of hiss emissions observed at Syowa Station were described in Chapter 3. However, the coverage of all-sky camera photographs is limited within a thousand km and is not enough to study the relationships between the auroral activities and hiss emissions on a global scale. Hence, photographs of aurora obtained by a polar-orbiting U. S. Air Force satellite (in  $99^\circ$  inclination sun-synchronous orbit with altitudes ranging between 815 and 852 km, the orbital period is about 102 minutes) were examined to study the relationships between hiss emissions at Syowa Station and auroral activities in the premidnight sector. The photographs are produced by a line-scanning technique. The field of view is about 3.2 km to 100 km altitude and the longitudinal width of the photographs is approximately 2500 km at 100 km altitude (PIKE and WHALEN, 1974). The spectral range of the detector is approximately 4000–11000 Å, peaking near 8000 Å (MORSE *et al.*, 1973). Photographs used here are obtained on the nightside when the satellite was in 1900 UT to 2000 UT magnetic local time traveling near Syowa Station, Antarctica in 1974 and 1975.

Fig. 76 represents an auroral photograph, *AE* index, VLF emission at 8 and 32 kHz bands and magnetic variations at Syowa Station. A westward traveling surge was seen near the zenith of Syowa Station around 2000 UT. From 2000 UT to 2010 UT, an impulsive hiss with high frequency components beyond 32 kHz was observed, and the *AE* index showed the onset of a negative bay. A negative bay with a depression of about  $100\gamma$  was also recorded on the magnetogram at Syowa Station. Fig. 77 represents an auroral photograph, *AE* index, VLF emissions at 8 and 64 kHz bands and magnetic variations obtained at Syowa Station in the same format as in Fig. 76. A strong impulsive hiss emission with a high frequency component above 64 kHz was seen around 2050 UT. The auroral photograph shown in this figure, however, was taken from 2121 UT to 2129 UT, 20 minutes after the occurrence of the hiss emission. A bright aurora covered the zenith of Syowa Station and the auroral hiss emissions were not observed on the ground. According to the magnetic field data at Syowa Station and the *AE* index, this time interval corresponds to a recovery phase. The enhancement of the impulsive hiss may be an indication of an auroral breakup that occurred 20 minutes before. From these analyses, it can be said that the appearance of impulsive hiss relates to the active bright aurora observed near the zenith of the station. This result is consistent with the conclusion obtained from the all-sky photograph data described in Chapter 3.

We described in previous sections that the continuous hiss emission appears corresponding to the enhancement of luminosity of the auroral arc located near the poleward horizon of Syowa Station. An auroral photograph from the satellite also leads to a similar result. Fig. 78 shows the auroral photograph, *AE* index,

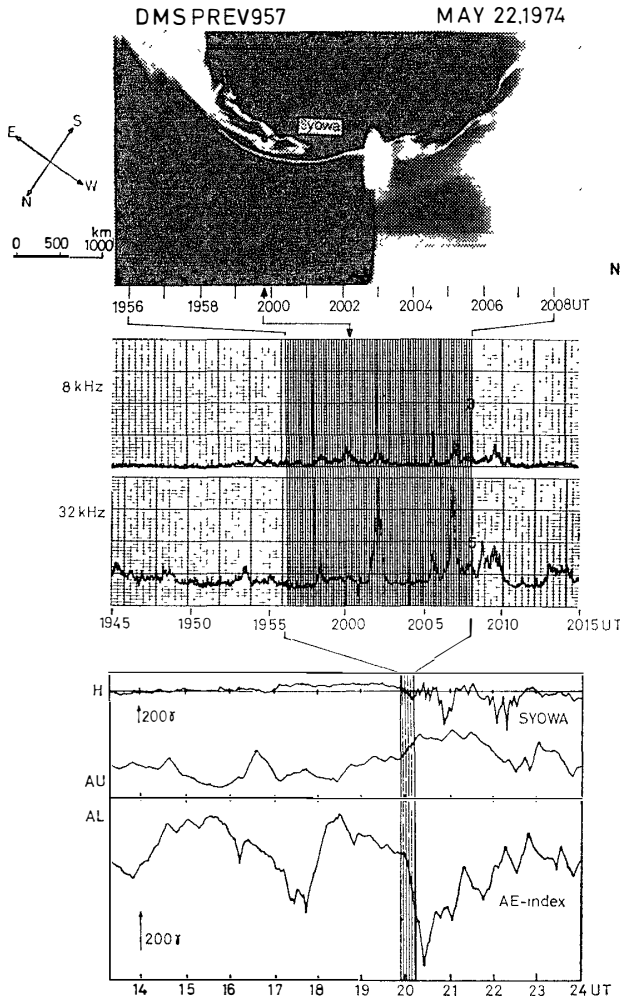


Fig. 76. The top panel shows the DMSP auroral photograph and the middle panel shows the intensity of auroral hiss at the 8 and 32 kHz bands. The bottom panel shows the AE index and the H-component magnetogram at Syowa Station.

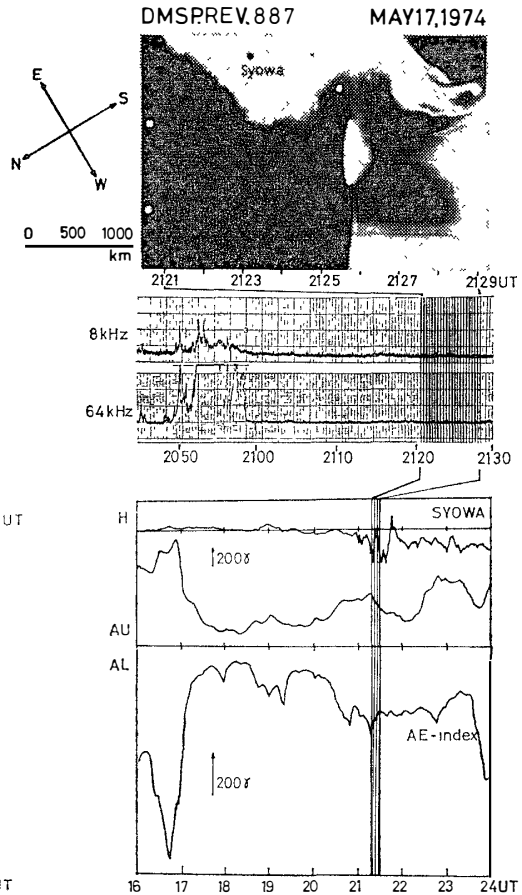


Fig. 77. The auroral photograph, AE index, VLF emissions at the 8 and 64 kHz bands and the H-component magnetogram at Syowa Station are shown. The format is the same as that in Fig. 76.

the records of VLF emission and the magnetic field variation obtained at Syowa Station. From 2016 UT to 2027 UT, a thin auroral arc was seen about 300 km south (poleward) of Syowa Station. Continuous hiss emissions with frequencies lower than 20 kHz were observed around 2030 UT. During this interval, a small positive change ( $\sim 50 \gamma$ ) of the magnetic horizontal component was observed at Syowa Station but the AE index shows an onset of an expansion phase. Fig. 79 also shows the auroral photograph and the VLF emission in the 8 and 32 kHz

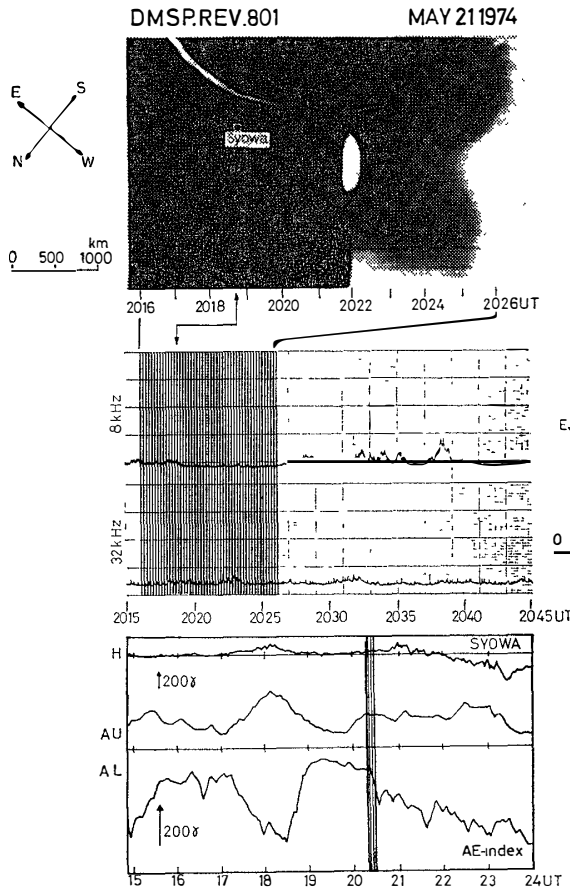


Fig. 78. The auroral photograph, AE index, VLF emissions and the H-component magnetogram obtained at Syowa Station. The notation is the same as that in Fig. 76.

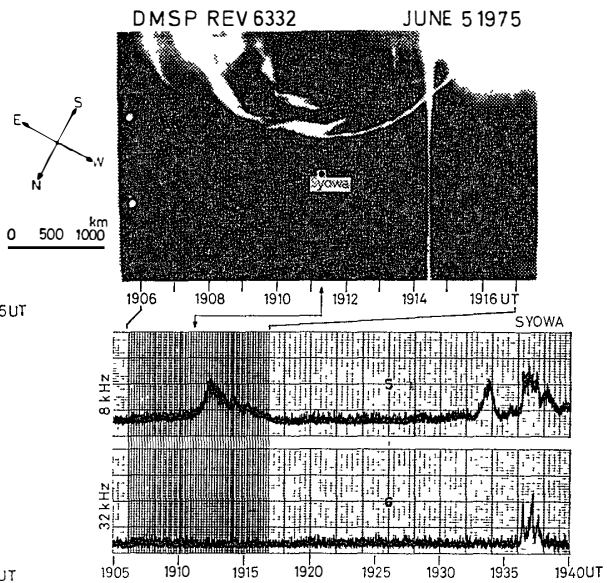


Fig. 79. The auroral photograph, the intensity of auroral hiss at the 8 and 32 kHz bands observed at Syowa Station.

bands. A bright auroral arc, with a westward traveling surge, was seen about 400 km south of Syowa Station. The strong hiss emission in the 8 kHz band that was observed around 1913 UT would be related to the nearest approach of the bright auroral arc to Syowa Station. An impulsive hiss with a high frequency component above 32 kHz was observed around 1936 UT. It may be an indication that the active aurora reached the zenith of Syowa Station, but we had no auroral data at the time.

The intensity of hiss emission is generally weaker when the auroral activity is far away from the observation site of VLF emission. When the aurora is located within about 400 km away from the station as shown in Figs. 78 and 79, the hiss emission can be observed. However, when the aurora is located 700 km or more away apart from Syowa Station, the auroral hiss is not observed in

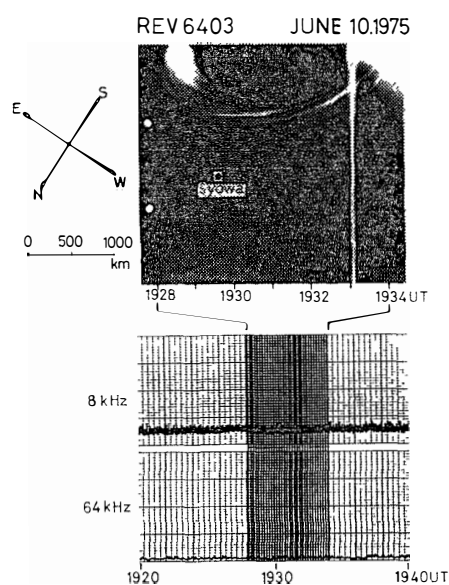


Fig. 80. The auroral photograph, the intensity of auroral hiss at the 8 and 64 kHz bands observed at Syowa Station.

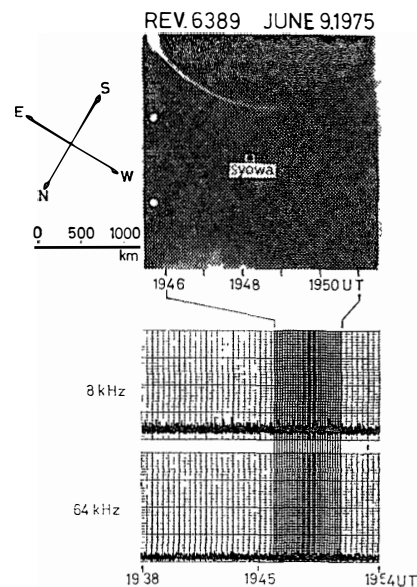


Fig. 81. The auroral photograph, the intensity of auroral hiss at the 8 and 64 kHz bands observed at Syowa Station.

relation to the bright aurora as shown in Figs. 80 and 81. The auroral photograph and the VLF emission at the 8 and 64 kHz bands are shown in Fig. 80. The bright multiple auroral arcs was seen about 700 km south of Syowa Station from the auroral photograph taken from 1928 UT to 1934 UT. In this time interval, however, no auroral hiss emissions at the 8 kHz and 64 kHz bands were recognized. A similar example is shown in Fig. 81. A thin auroral arc was seen here again at about 600 km south of Syowa Station from 1946 UT to 1951 UT and no enhancement of auroral hiss were recognized at both the 8 and 64 kHz bands. These examples suggest that auroral hiss emission, generally, is not observed when the aurora is located farther than 700 km poleward of the station. Similar results were obtained by AYUKAWA (private communication, 1978). According to his examinations of the relationships between the location of aurora and the hiss intensity when the auroral location is 500 km away from the station, the associated hiss intensity becomes very weak ( $\sim 50$  dB damping). SRIVASTAVA (1976) examined simultaneous hiss observations at College and Barter Island which are about 600 km apart and observed that auroral hiss emissions were not identical at these two stations. From these results, he suggested that the maximum propagation distance of hiss emission must be about 600 km.

### 6.3. Summary

The present analyses indicates that most of the auroral hiss emissions, including impulsive and continuous hiss emissions, are observed during the expansion

phase of a substorm in the midnight sector. Generally speaking, the impulsive hiss emission appears in the local auroral breakup associated with the initial brightening of aurora. It suggests that the impulsive hiss is generated in the region closer to the auroral precipitation that causes the local breakup. On the other hand, the continuous hiss emissions associated with the steady auroral arc are not observed in the local breakup of auroras. As AKASOFU (1968) proposed, most continuous hiss emissions are associated with the polar magnetic substorm in the midnight sector and thus these hiss emissions are one of the aspects of the VLF emission substorm in the evening sector. However there are some auroral hiss emissions which are not directly related to either local or global auroral breakup. Some of these emissions seem to occur in the growth phase as shown by KOKUBUN *et al.* (1972). Regarding the relationships between global auroral activities and auroral hiss phenomena, it can be said that the appearance of impulsive hiss relates to the active bright aurora observed near the zenith of the station and the continuous hiss emission relates to the steady poleward auroral arc. These results are consistent with the conclusion obtained from the all-sky photograph data described in Chapter 3. Furthermore, when the aurora is located more than 700 km from the station, hiss emissions are not observed at the station above the threshold level ( $\sim 10^{-16}$  W/m<sup>2</sup> Hz).

## 7. Summary and Discussion

In this chapter the important observational results are summarized, and the generation and propagation of auroral hiss emission are discussed on the basis of the observations.

### 7.1. Observation results

The auroral hiss emissions observed on the ground (Syowa and Mizuho Stations) are categorized into two types, the narrow-band continuous hiss and the wide-band impulsive hiss. The continuous hiss has a narrow-band frequency range with a center frequency of about 10 kHz and band-width of a few kHz. This kind of hiss generally has a long duration (longer than a few tens of minutes). On the other hand, the impulsive hiss has a wide frequency range with a center frequency of about 10 kHz and a band-width of a few tens of kHz. The duration of this emission is usually shorter than 10 minutes. Comparing these two types of hiss emission with the auroral type and activity, the continuous hiss emissions are usually found to occur associated with the steady auroral arc located near the poleward horizon. When the auroral arc is seen a few hundreds of km ( $\sim 300$  km) poleward of Syowa Station, strong continuous hiss emissions are frequently observed. The variations in intensity of the continuous hiss are occasionally found to be well correlated with the fluctuations in luminosity of the auroral arc. On the other hand, impulsive hiss emissions tend to be accompanied by a sudden brightening of the active aurora near the zenith, mostly at the onset of the auroral break-up. These relationships between the two types of hiss and the global auroral activity can be confirmed by the comparison of auroral data observed on the DMSP satellite and the ground data of hiss also. In addition it was also found that hiss emissions are usually not observed at Syowa Station when the aurora is located beyond about 700 km poleward of Syowa Station. The measurement of the arrival direction shows that the continuous hiss arrives from several hundreds of km equatorward of the related aurora, while the impulsive hiss sometimes arrives from the vicinity of the auroral location. A similar result was also obtained at Churchill in Canada by OGUTI *et al.* (private communica-

tion, 1977). The arrivals of hiss from the active auroral forms are much more frequently observed at Churchill than at Syowa Station. Most likely, this fact is due to the difference in the magnetic dip angle between Churchill and Syowa Station, as will be discussed later. A systematic local time, variation of the arrival direction is also an important feature of continuous hiss emissions. In the early evening (18 h–19 h), the arrival direction is the east and changes from the east to the west around 20 h–21 h. After 21 h, most of the hiss emission comes from the west. This local time variation of the arrival direction may indicate that the peak activity region of the continuous hiss is located around  $\sim 21$  h magnetic local time.

As to the propagation path from the generation region to the ground, the simultaneous data of VLF emissions observed on ISIS 2 and on the ground suggest an important fact, *i.e.*, that the auroral hiss emissions do not propagate along the magnetic field line from the satellite altitude ( $h \sim 1400$  km) to the ground but propagate along a non-ducted path. Another important result from the hiss at satellite altitudes is that hiss is generally observed on the high latitude side of the geomagnetic field lines passing through the most equatorward auroral arc, while saucer emissions are observed on the lower latitude side of these field lines. Although VLF hiss emissions are almost always observed on the satellite in a wide latitudinal region in the auroral zone ( $\sim 1000$  km), the corresponding auroral hiss is not always seen on the ground. This shows that a part of the VLF emissions observed on the satellite can propagate to the ground. Most of the auroral hiss emissions, both impulsive and continuous hiss, are observed during the expansion phase of a substorm in the midnight sector, which is also an important point. The impulsive hiss emissions frequently appear at the time of local auroral breakup and most of the continuous hiss emissions (which are observed in the evening region) are also seen associated with the expansion phase of a substorm in the midnight sector. These emissions, thus, are one of the indicators of substorm initiation in the midnight sector.

Two important problems arising are

1) What is the physical difference between the continuous hiss and the impulsive hiss? and

2) What propagation path is reasonable to explain the observation results?

We will discuss these problems in the following sections.

## 7.2. Generation mechanism of auroral hiss

Many trials have been carried out to explain auroral hiss in terms of incoherent Cerenkov radiation from the precipitating electrons (ELLIS, 1957; LIEMOHN, 1965; JØRGENSEN, 1968; LIM and LAASPERE, 1972; JAMES, 1973; TAYLOR and SHAWHAN, 1974; MAEDA, 1975; SWIFT and KAN, 1975; NODA and TAMAO, 1976). However, it is difficult to explain the observed power fluxes as high as  $10^{-11} \sim 10^{-12}$  W/m<sup>2</sup> Hz

at satellite altitudes (GURNETT, 1966; BARRINGTON *et al.*, 1971; GURNETT and FRANK, 1972; MOSIER and GURNETT, 1972) by the incoherent mechanism. Recently, MAGGS (1976) has shown that the wave amplification of incoherent whistler mode radiation by the convective instability caused by a beam of precipitating auroral electrons accounts for the observed power fluxes of VLF hiss. The power flux at an observer in the auroral arc is given by MAGGS (1976) as

$$\frac{d^2}{dk_{\parallel} d\omega} P(\omega, k_{\parallel}) = \int_{\text{obs}}^{\infty} E \cdot F \exp [2M(\omega, k_{\parallel}, s')] ds'$$

(This equation is already written in Chapter 1.)

The magnitude of the power flux is determined mostly by the ray path length and the amplification factor ( $M$ ). MAGGS (1976) calculated the amplification factor and obtained that it is larger than 8.5 for a strong beam of  $10^9$  electron/cm<sup>2</sup> · s · sr · keV, a drift Maxwellian velocity distribution and the length of the amplified ray path is 1000 km. This value of the amplification factor is enough to explain the observed hiss power flux. In the following, we will discuss the characteristics differences in two types of auroral hiss emissions in terms of the convective beam amplification theory. As continuous hiss and impulsive hiss emissions are observed associated with the different activities of aurora, the two types of emission are likely to correspond to auroral electrons with different spectra. The energy spectra of the precipitating electrons in auroral regions have been examined by many investigators using data from satellites and rockets (FRANK and ACKERSON, 1972; ARNOLDY and CHOY, 1973; REASONNER and CHAPPEL, 1973; ARNOLDY and CHOY, 1973; ARNOLDY *et al.*, 1974; WINNINGHAM *et al.*, 1975;

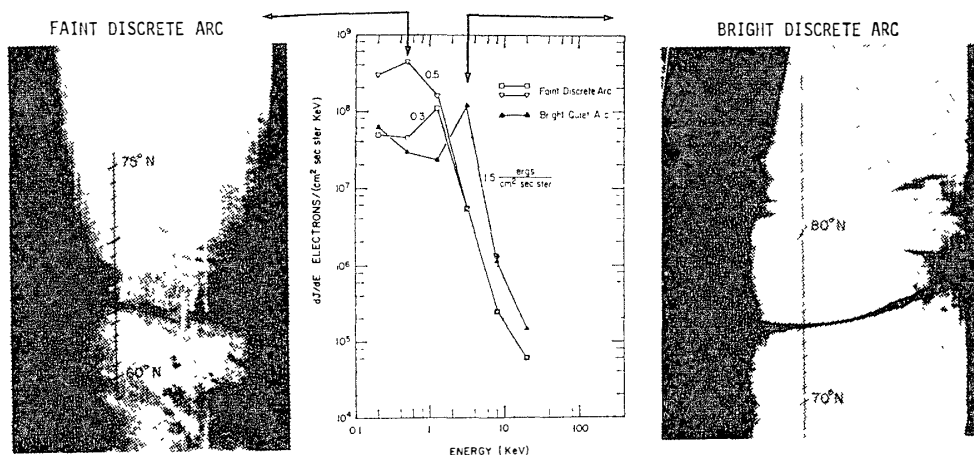


Fig. 82a. The center panel shows the schematic differential energy spectrum of the electron precipitation associated with two types of simple auroral forms observed on the DMSP satellite. The left and right panels show the faint discrete arc and the bright discrete arc respectively (after MENG, 1976).

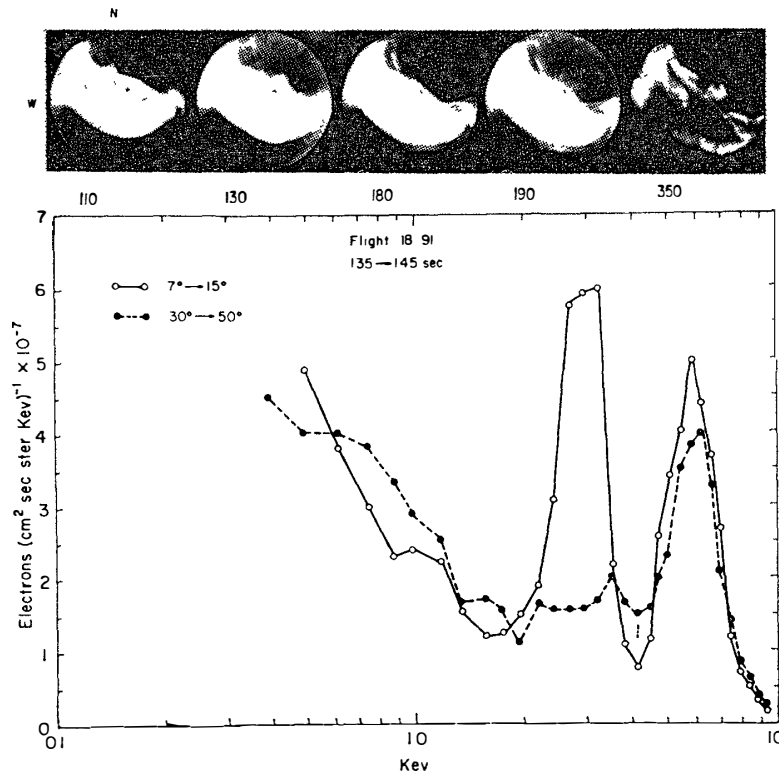
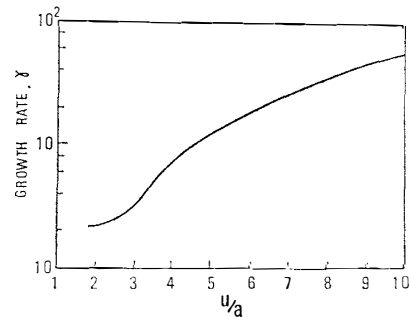


Fig. 82b. The top panel all-sky photos show the active aurora and the position of the rocket projected to the 100-km level. The bottom panel shows the pitch angle sorted electron spectra observed on the rocket in this interval (after ARNOLDY and CHOY, 1974).

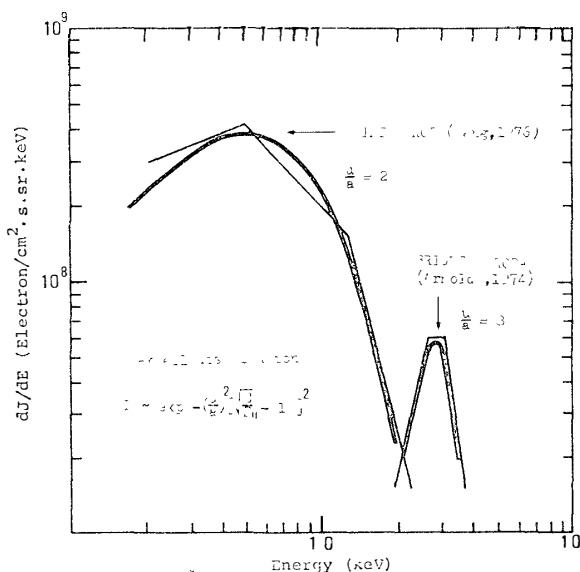
MENG, 1976; LUI *et al.*, 1977; MENG *et al.*, 1978). Especially MENG (1976), and ARNOLDY and CHOY (1974), examined in detail the precipitating electron spectra corresponding to several kinds of auroras. Figs. 82a and b show the differential energy spectra of the precipitating electrons associated with the faint and bright auroras observed by MENG (1976), and ARNOLDY and CHOY (1974). As seen in Figs. 82a and b precipitation in a faint discrete arc is characterized by a spectral peak near 0.5 or 1.2 keV with a differential flux between  $10^8$  and  $10^9$  electron/cm<sup>2</sup> s·sr·keV. Inside a bright aurora a distinct spectral peak near 3.2 keV is found with fluxes between  $10^7$  and  $10^8$  electron/cm<sup>2</sup>·s·sr·keV. MENG *et al.* (1978), also showed that the differential spectra near the surge are different from those in quiet arcs. The differential spectrum is highly variable and sometimes can be approximated by a power law extending from 0.2 keV to at least 20 keV. A spectral peak near 8 keV or higher energies was also observed occasionally on the flat background spectrum. ARNOLDY and CHOY (1974) also detected the electron fluxes associated with bright aurora and obtained a similar spectrum as reported by MENG (1976). Since they observed electron fluxes with an array of electrostatic analyzers with 50 point spectral samples from 0 to 15 keV, it is relevant to examine the differential energy spectrum in detail. Because the con-

Fig. 83. Peak growth rate  $\gamma$  at  $f=1043$  kHz in the whole  $\mu_{\parallel}$  range as a function of the ratio  $u/a$ . The drifting Maxwellian is assumed to be the beam distribution and  $\gamma$  is taken as unity when  $u/a=1.83$ . It is calculated for parameter values of the ambient medium at 300-km altitude (after YAMAMOTO, 1979).



tinuous hiss appears associated with a quiet auroral arc and the impulsive hiss occurs accompanied by a bright aurora, the precipitation of electrons which generate the continuous hiss may be characterized by soft electrons with a spectral peak from a few hundreds of eV to a few keV. On the other hand, the differential energy spectrum of electrons which is related to the impulsive hiss may be identified as harder precipitations with a spectral peak at a few keV or more. YAMAMOTO (1979) pointed out that two types of VLF hiss (continuous hiss and impulsive hiss) spectra observed on the ground can be accounted for by the difference in velocity of the electron beam. According to his calculation shown in Fig. 83, the growth rate increases as the ratio ( $u/a$ ) increases, where  $u$  is the beam velocity and  $a$  is the thermal velocity. Assuming the Maxwellian distribution, the value of ( $u/a$ ) corresponding to the differential energy spectrum observed on rockets and satellites can be calculated as shown in Fig. 84. The ratio of ( $u/a$ ) which is related to the faint auroral arc is about 2 and the ratio which is related to the bright aurora is about 8. As shown in Fig. 83, the growth rate of the wave in the electron beam corresponding to the bright aurora is much larger than that in the

Fig. 84. The precipitating electron beams are modeled as warm beams with drifting Maxwellian velocity distribution. For a faint auroral arc, the peak energy of the beam is 0.5 keV and the ratio of the beam velocity ( $u$ ) to the thermal velocity ( $a$ ) is 2. For a bright aurora, the peak energy of the beam velocity is 3.0 keV and the ratio of the beam velocity ( $u$ ) to the thermal velocity ( $a$ ) is 8.



faint aurora. On the other hand, the ratio of the beam density  $n_b$  to the cold electron density  $n_o$  also plays an important role in the wave amplification as given by MAGGS (1978) and YAMAMOTO (1979). When  $n_b$  is taken to be proportional to the magnetic field intensity  $B$ , the growth rate is written as

$$\gamma \propto (B/n_o) \times \gamma'(u/a) \quad (5)$$

and the group velocity is given by

$$V_g = 2C[(\omega_{He}\omega \cos \theta)^{1/2}/\omega_{pe}] \sim \left(\frac{B}{n_o}\right)^{1/2}. \quad (6)$$

Therefore, the amplification factor is given as

$$M \sim \left(\frac{\gamma}{V_g}\right) \times l \sim \left(\frac{B}{n_o}\right)^{1/2} \times l \times \gamma'\left(\frac{u}{a}\right) \quad (7)$$

where  $\gamma'(u/a)$  is the growth rate term due to the beam energy spectrum.

The amplification factor decreases with decrease in altitude ( $h < 1000$  km) due to a rapid increase in  $n_o$ , compared with the increase in  $B$ . Since the amplification factor rapidly decreases in altitudes lower than a few hundreds of km and the ray path length for amplification becomes short, hiss emissions are hardly generated by the coherent Cerenkov instability in altitudes lower than a few hundreds of km. However, some altitude dependence of generation can be expected, since the amplification factor depends upon not only the ray path length ( $l$ ) of the amplification and square root of the ratio of magnetic field intensity to cold electron density  $(B/n_o)^{1/2}$ , but also the  $(u/a)$  ratio of the beam. That is to say, when the electron beam has a large growth rate due to a high  $(u/a)$  ratio, considerable amplification of the wave can be achieved even at low altitudes. As mentioned previously, since impulsive hiss emissions are observed related to an electron beam with a high  $(u/a)$ . Hence it can be said that the impulsive hiss is possibly generated even at an altitude lower than that of the continuous hiss.

Generally the amplification factor becomes smaller if the background electron density ( $n_o$ ) around the generation region increases in summer. From VLF observations on the ISIS 2 satellite, the occurrence frequency of auroral hiss and saucer emissions are found to be smaller in summer. It may be possible to explain these seasonal variations of hiss occurrence by this theory. Hence, it is important to examine the seasonal variations of background electron density and to examine how the seasonal variations in the density relates to the occurrence of hiss emissions.

### 7.3. Characteristics of the propagation path

From the coordinated observation of VLF emissions between the satellite and the ground mentioned in the previous chapters, it was suggested that hiss emissions emerging from the duct at the altitude higher than the satellite level ( $h \sim 1400$  km)

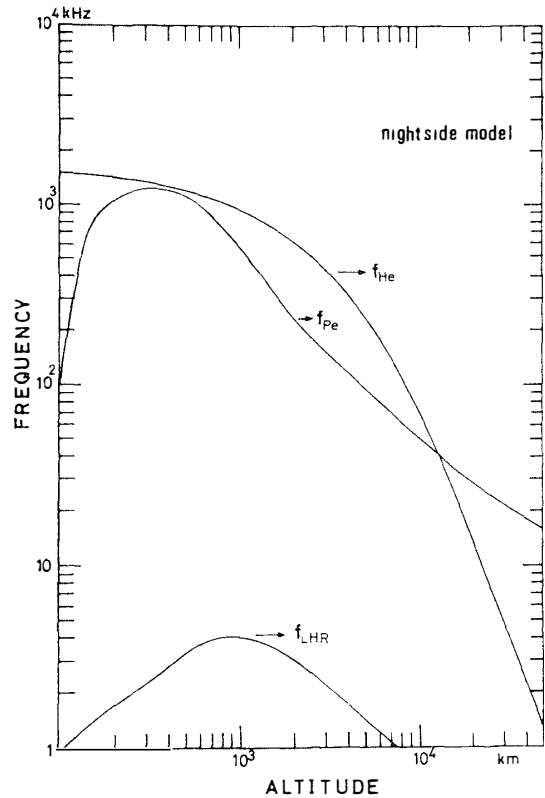


Fig. 85. The altitude dependence of the gyro-frequency of electrons,  $f_{He}$ . The electron plasma frequency,  $f_{pe}$  and the lower-hybrid frequency,  $f_{LHR}$ , in the magnetosphere along the  $70^\circ$  field line from the Earth's surface.

propagate down to the ionosphere in the non-ducted mode of propagation. The characteristics of the propagation path are examined by using the ray tracing technique (KIMURA, 1966). We employed the familiar diffusive equilibrium model (ANGERAMI and THOMAS, 1963) represented at a reference level of 600 km by an electron density of  $1 \times 10^4$  electron  $\text{cm}^{-3}$  and temperature of  $3000^\circ\text{K}$ . The electron density of this model is near the nightside electron density profile obtained from the ISIS 2 topside ionogram. A centered dipole field model was adopted for the magnetic field. Fig. 85 represents the magnetospheric model used here. In this calculation the ray tracing program developed by KIMURA and YAMAGISHI (private communication, 1977) was used. At first, we examined carefully the wave normal directions of the ray at the ionospheric level ( $h_i=200$  km) because the wave transmission through the lower ionosphere requires that the wave normal directions of the down-going rays must be in a small transmission cone (MAEDA and OYA, 1963; HELLIWELL, 1965). In order that a wave can be observed on the ground the horizontal component of the refractive index vector at the ionospheric level must be less than 1.

$$n \sin \alpha < 1 \quad (8)$$

where

$$n^2 = \frac{f_{pe}^2}{f(f_{He} \cos \theta - f)} \quad (9)$$

- $n$  : whistler mode refractive index  
 $\alpha$  : incident wave normal angle measured from the ionospheric vertical plane  
 $f_{pe}$  : electron plasma frequency  
 $f_{He}$  : electron gyro-frequency  
 $\theta$  : wave normal angle from the field line.

The width of the transmission cone varies with the plasma frequency, gyro frequency and the magnetic dip angle. Assuming the altitude of the ionosphere is 200 km, we calculated the transmission angle for several plasma frequencies and a wave-frequency of 8 kHz at the magnetic latitude of  $69^\circ$  (Syowa Station, dip  $\sim 65^\circ$ ). Results indicated that the transmission angles were  $11.3^\circ$ ,  $5.3^\circ$  and  $2.6^\circ$  corresponding to a plasma frequency of 0.5, 1.0 and 2.0 MHz with a constant gyrofrequency of 1.2 MHz. Note that the value of the transmission cone calculated by using Snell's law does not differ much (within a few percent) from the one derived from the full wave theory (NAGANO, private communication, 1978). Considering these conditions of the accessibility of the waves to the ground, we computed the ray paths from 3000 km altitude where the ducts would terminate (CERISIER, 1974). Note that there are other possibilities in that the waves depart from the duct at altitudes higher than 3000 km or the waves propagate near the ionospheric level ( $h \sim 200$  km) along the field line. We examined these possibilities in detail as described in the next section and obtained that this model explains well the relationships between the arrival direction of hiss and the locations of aurora described in Chapters 3, 4 and 5. The ray paths computed with different initial wave normal angles  $\theta_i$  (angle measured from the field line, positive in the clockwise direction and negative in the anticlockwise direction) at an interval of  $10^\circ$  around the exit point from the duct are shown in Fig. 86. The figure also shows the wave normal angles of the ray paths (measured from the ionospheric vertical plane) at 200 km altitude. The wave normal directions of the two ray paths indicated by 4 and 5 are almost vertical and lie in the transmission cone. Hence the corresponding waves would be observed on the ground. In these cases, the initial wave normal angles were  $-6^\circ$  and  $-16^\circ$  at the duct-exit point. Similar results were also obtained by SRIVASTAVA (1974) and SINGH *et al.* (1978). These results indicate that the transmission region of VLF waves is located on the low latitude side of the foot point of the field line where VLF waves depart from the duct. From our calculations, it is found that the distance between the region where the wave normal angle at the ionosphere is almost vertical and the foot point of the field line along which the duct terminates at 3000 km in altitude, is 300–400 km. The auroral particles precipitate along the field line and the hiss propagates along the non-ducted path through the ionosphere where the normal directions lie in a transmission cone. This result suggests that the duct of auroral hiss terminates at

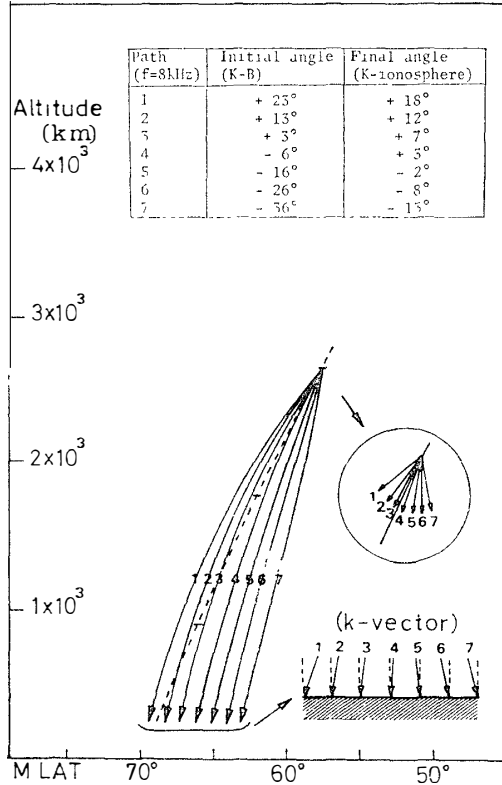


Fig. 86. Ray paths for the waves of 8.0 kHz at various initial wave normal angles starting at 3000 km and coming down to the final altitude near 200 km. The initial wave normal angles are measured from the field line and the final wave normal angles are measured from the ionospheric vertical plane ( $h \sim 200$  km). The final latitude is  $70.0^\circ$ .

about 3000 km in altitude and the wave propagation path is different from the auroral precipitating path below that level. From examination of the continuous hiss spectra observed on ISIS 2 and on the ground, similar hiss spectra are recognized at both the ISIS 2 altitude ( $h \sim 1400$  km) and on the ground, where the satellite is in the region linked to Syowa Station through the non-ducted propagation path "4" shown in Fig. 86. The calculated non-ducted propagation paths are also illustrated in Figs. 60, 63 and 66 in Chapter 5. These results confirm the previous conclusion that the duct of auroral hiss terminates at about 3000 km in altitude and after that the wave propagates along a non-ducted path through the ionosphere below 3000 km altitude. The result of the calculated ray paths also explains that the distance between the exit of hiss and the aurora at the ionospheric level depends on the magnetic dip angle. Namely, if the dip angle of a station is near  $90^\circ$ , the arrival direction tends to coincide nearly with the aurorally active region as seen at Churchill (dip  $\sim 83^\circ$ ). On the contrary, if the dip angle of a station is small, the arrival direction likely indicates the wave exit to be located hundreds of km equatorward of the auroral location as seen at Syowa Station (dip  $\sim 65^\circ$ ).

The arrival direction of the impulsive hiss associated with the bright aurora occasionally shows near the auroral location even at Syowa Station. A possibility is the effect of field-aligned irregularities that act as ducts closer than 3000 km to the

ionosphere during this time interval since the auroral precipitation is apt to produce field-aligned irregularities. The other possibility is the large-scale horizontal gradients of ionization existing in the ionosphere. For example, JAMES (1972) have reported the tilting of the wave normals due to the large-scale horizontal gradient of the ionization. SINGH and SINGH (1978) also has shown similar results due to the horizontal gradients of ionization at low latitudes during periods of magnetic disturbance. If such strong field-aligned irregularities or the large-scale horizontal gradient of ionization exist along the propagation path, the wave can propagate to the ground nearly along the field-line. Hence, in order to determine the propagation path in such a condition, it is necessary to know the field-aligned irregularities or the large scale horizontal gradient of ionization in the ionosphere.

#### 7.4. The generation region of auroral hiss

From the observations of VLF emission with the simultaneous observations of auroral particles (HOFFMAN and LAASPERE, 1972; GURNETT and FRANK, 1972), it was shown that the auroral hiss emissions are likely generated by the precipitating electrons with energies less than a few keV. Using the magnetospheric model shown in Fig. 85, we computed the resonance angle of the whistler mode wave excited by an electron beam with energy of 1 keV through the Cerenkov interaction. The well known Cerenkov condition is written as

$$n \cos \theta = C/V_{\parallel}, \quad (10)$$

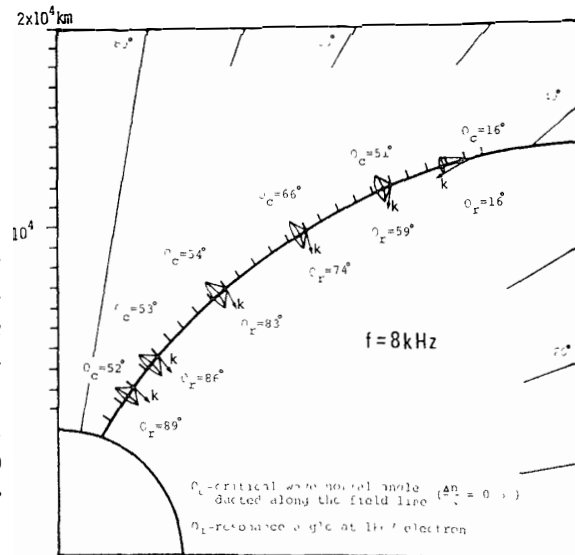
where

- $\theta$  : the angle between the wave vector ( $\mathbf{k}$ ) and magnetic field vector ( $\mathbf{B}$ )
- $n$  : the whistler mode refractive index
- $C$  : the light velocity
- $V_{\parallel}$  : the parallel velocity of the particle.

A wave frequency of 8 kHz was chosen for these computations. In Fig. 87 the resonance angle at heights 3000, 5000, 10000, 15000, 20000 and 24000 km are shown. As seen in the figure, the resonance cone of Cerenkov emission at 3000 km amounts to 89°. Similarly, it amounts to about 86°, 83°, 74°, 59° and 16° at 5000, 10000, 15000, 20000 and 24000 km in altitude respectively. On the other hand, there must be some irregularities along the field-line in order that the wave can propagate to the ground along the field-line. The theory of trapping of whistler mode signals has been studied in detail by SMITH and HELLIWELL (1960). Here we followed the treatment by SMITH and HELLIWELL (1960) which is based on ray tracing calculations and shows the initial wave normal angle,  $\theta_e$ , that permits the whistler mode signals to be trapped in a duct, with parameters such as frequency  $f$ , the gyrofrequency  $f_{He}$  and the enhancement factor ( $\Delta n/n$ ).

Trapping is, in principle, possible both in crests ( $f < f_{He}/2$ ) and troughs ( $f > f_{He}/2$ )

Fig. 87. The resonance angles ( $\theta_r$ ) of the whistler mode wave (at 8 kHz frequency) excited by an electron beam with energy of 1 keV through Cerenkov interaction at heights 3000, 5000, 10000, 15000, 20000 and 24000 km. The critical wave normal angles ( $\theta_c$ ) to be trapped along the field line are also shown.



and one can compute the initial wave normal angles for both types of irregularities. SMITH and HELLIWELL (1960) obtained that the enhancement factors are in the range of 0.1 to less than 0.02 for geomagnetic latitudes between  $50^\circ$  and  $70^\circ$ . From recent satellite observations, CERISIER (1974) reported that the local electron density fluctuations of the duct are about 10% in mid-latitudes and that the distances between adjacent ducts are about one hundred km.

The local electron density fluctuations along the auroral field line in high latitudes may be larger than that in mid-latitudes. We assume here the enhancement factor is 0.5 and calculate the initial wave normal angle to be trapped along the field line duct. The calculated results are shown in Fig. 87. The limited initial wave normal angles are estimated to be  $52^\circ$ ,  $53^\circ$ ,  $54^\circ$ ,  $66^\circ$ ,  $51^\circ$  and  $16^\circ$  at 3000, 5000, 10000, 15000, 20000 and 24000 km in altitudes, respectively. By comparing the resonance angles previously obtained from the Cerenkov emission and using these results, it can be shown that the resonance angle is larger than the critical initial wave normal angle to be trapped along the field line in altitude lower than 24000 km. Hence it can be said that waves radiated by a keV electron in an altitude lower than 24000 km cannot propagate in the magnetosphere along the field-line. On the contrary, waves radiated above 24000 km altitude can propagate along the field line. RAO *et al.* (1973) reported that if the enhancement factor is larger than 3 along the field line, waves with large wave normal angles ( $\theta_r \sim 80^\circ$ ) can also propagate along the field line. However, since it is difficult to consider such a large enhancement factor along the field line from the observations, it is concluded that the waves generated by 1 keV electrons at altitude below 24000 km cannot propagate along the field line in the magnetosphere.

Assuming the waves propagate through the magnetosphere along the non-

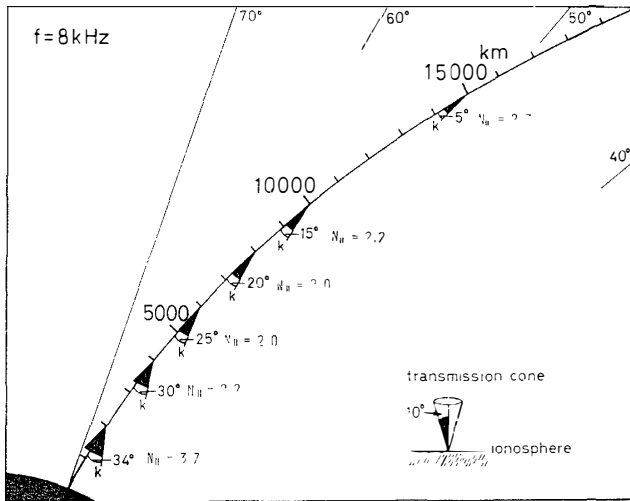


Fig. 88. The critical value of the initial wave normal angle at 8 kHz frequency that can be observed on the ground and lie in a transmission cone (within  $10.0^\circ$ ) at 200 km in altitude.

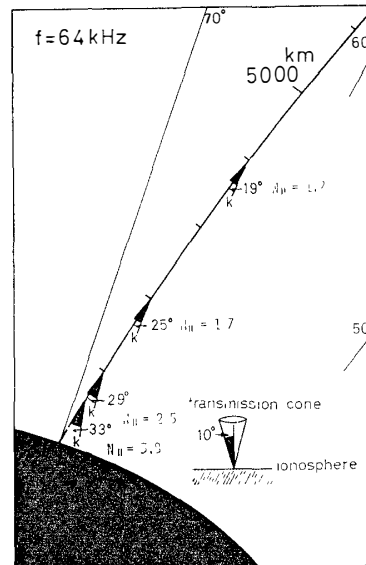


Fig. 89. The critical value of the initial wave normal angle at 64 kHz frequency that can be observed on the ground and lie in a transmission cone (within  $10.0^\circ$ ) at 200 km in altitude.

ducted path from altitudes lower than 24000 km, we next examine the initial wave normal angle of the waves necessary to penetrate the ionosphere. Since the wave normal directions of the downcoming rays in the ionosphere ( $h \sim 200$  km) must lie in a transmission cone, the initial wave normal angle at the duct exit point should be limited within a certain range. Assuming the maximum transmission angle to be  $10.0^\circ$  (the angle is obtained corresponding to a gyrofrequency of 1.2 MHz and a plasma frequency of 0.56 MHz at 200 km altitude), we calculated the ray path of the 8 kHz band from 2000, 4000, 6000, 8000, 10000 and 15000 km altitudes to 200 km. The same magnetospheric model shown in Fig. 85 is adopted here. Fig. 88 represents the value of the initial wave normal angle that can be observed on the ground and lies in a transmission cone at 200 km in altitude.

The initial wave normal angle that can be transferred to the ground is smaller than  $34^\circ$  at 2000 km,  $30^\circ$  at 4000 km,  $25^\circ$  at 6000 km,  $20^\circ$  at 8000 km,  $15^\circ$  at 10000 km and  $5^\circ$  at 15000 km in altitude. The calculation for the whistler mode wave of 64 kHz shows a similar result as shown in Fig. 89. In the range of the limited wave normal angle obtained at several heights, the maximum refractive index is obtained for a zero wave normal angle. Since the parallel component of the refractive index,  $n_{\parallel}(\theta=0^\circ)$  can be obtained from eq. (9) as

$$n_{\parallel}^2 = \frac{f_{pe}^2}{f(f_{He} - f)} \quad (11)$$

the particle energy which interacts with waves with zero wave normal angle can be calculated from eq. (11). We calculated the parallel refractive index of the whistler mode ( $n_{\parallel}$ ) for 8 kHz at heights of 2000, 4000, 6000, 8000, 10000 and 15000 km and for 64 kHz at heights of 6000, 1000, 2000, 4000 km in altitudes. The results are also shown in Figs. 88 and 89. They show that the parallel refractive index ( $n_{\parallel}$ ) is in the range from 1 to 4. As the parallel refractive indices, for example,  $n_{\parallel}=3, 5$  and 16 correspond to particle energies of 25 keV, 10 keV and 1 keV respectively, the parallel refractive index ( $n_{\parallel}$ ) of about 1~4 obtained above corresponds to a particle energy greater than 10 keV. That is to say, auroral hiss emissions cannot be observed on the ground unless the waves are generated by precipitating electrons with energies greater than 10 keV. Since a relation is seen between a precipitation with energy less than 10 keV and auroral hiss emissions, the auroral hiss emissions observed on the ground are hardly attributed to particles with energies greater than 10 keV. On the other hand, if the auroral hiss emissions are assumed to be generated by the precipitating particles with energies of 1 keV or less, the resonance angle of the wave becomes large around the altitude from 2000 to 15000 km as previously shown and such a wave cannot be transferred to the ionosphere and below.

Assuming that auroral hiss emissions are generated by electrons with energies of a few keV or less through the Cerenkov radiation, and assuming further that very intense electron density irregularities ( $\Delta n/n > 3$ ) do not exist along the magnetic field line, the auroral hiss at 8 kHz frequency, for example, which is generated around the altitude from a few thousands of km to twenty thousands of km, cannot propagate in the magnetosphere along the field-aligned duct, and hence cannot be transmitted through the ionosphere even if the wave propagates along the non-ducted path. If the consideration above is correct, it is concluded that the generation region of auroral hiss at 8 kHz observed on the ground is not located below 24000 km in altitude.

Thus the regions where the parallel refractive index ( $n_{\parallel}$ ) is larger than about 16 for 8 kHz can be examined, which corresponds to the resonance energy of Cerenkov radiation less than 1 keV. These regions are found in altitudes lower than 600 km where the plasma frequency is large and the altitude beyond 25000 km where the gyrofrequency is near to the wave frequency in our magnetospheric model. It can be considered that in these two regions the waves are generated by a few keV electrons with small initial wave normal angle and can propagate to the ground. However, according to the convective coherent instability theory suggested by MAGGS (1976), the amplification factor is small and the ray path of amplification is short at altitudes lower than 600 km. Hence, auroral hiss emissions are hardly generated around altitudes lower than 600 km. The hiss emissions observed on the

ground would be generated around the altitude where the wave frequency is near the gyrofrequency (or plasma frequency). From previous considerations, the generation region can be estimated directly from the magnetospheric model as shown in Fig. 85. For example, the auroral hiss at 8 kHz is probably generated around 25000 km in altitude where the gyrofrequency is a little higher (within about 10%) than 8 kHz frequency (where  $f \lesssim f_{He} < f_{pe}$ ), and the auroral hiss at 100 kHz frequency is probably generated around 6000 km in altitude where the plasma frequency is a little higher than 100 kHz frequency (where  $f \lesssim f_{pe} < f_{He}$ ). These results indicate that high frequency hiss occurs around the lower altitude more than low frequency hiss. This is consistent with the fact that impulsive hiss with high frequency components occurs at lower altitudes than continuous hiss as described previously. In Fig. 90 our conclusion is summarized. Generally, the generation region of auroral hiss varies with the frequency of hiss. For example, the continuous hiss at 8 kHz frequency would be generated around 25000 km altitude where the wave frequency (8 kHz)

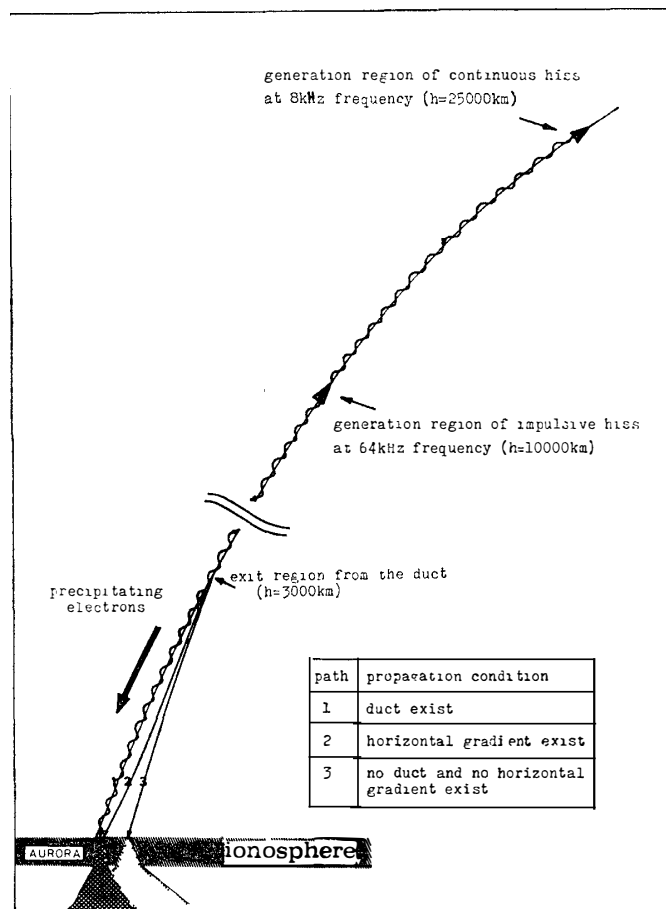


Fig. 90. Schematic diagram of a model for the generation and the propagation of the auroral hiss emissions.

is near the local gyrofrequency and the impulsive hiss at 64 kHz would be generated around 10000 km altitude where the wave frequency (64 kHz) is near the local plasma frequency. Probably the generation altitude of impulsive hiss at 8 kHz frequency is similar to that of continuous hiss at 8 kHz frequency. Auroral hiss emissions generated around such altitudes can propagate along the field-aligned duct because the waves radiate with a small wave normal angle as shown before. If the duct is terminated around 3000 km altitude the wave propagates through the ionosphere along the non-ducted path "3" in Fig. 90 if the intense field-aligned irregularities or the large-scale horizontal gradient does not exist. As discussed previously, if the intense field-aligned irregularities or the large-scale horizontal gradient exists, the wave can propagate near the field line (path 1 and 2 in Fig. 90). The generation region of auroral hiss estimated here is supported by several other experimental results. SIREN (1972, 1975) observed fast hissers with dispersive spectra at Byrd Station. He estimated the generation region of hisser to be about 25600 km altitude for 8.5 kHz using the value of the nose frequency. The generation region of hisser is a similar altitude to the one examined here. Furthermore, the intense radio emissions are known to escape outward from the earth's auroral regions in the frequency spectrum from about a few tens kHz to 500 kHz. (Called the auroral kilometric radiations (GURNETT, 1974)). The occurrence of auroral kilometric radiation is closely correlated with the auroral electrojet index,  $AE$  and with the occurrence of auroral arcs. Ray tracing and radio direction finding measurements indicate that the auroral kilometric radiation is generated along the auroral field-lines relatively close to the earth, at radial distances from about 2.5 to 5  $R_E$  (GREEN *et al.*, 1977). Therefore the generation region of auroral kilometric radiation is very similar to that of auroral hiss examined here. Recently observations of a D. C. electric field were carried out by MOZER *et al.* (1977). They reported that a strong D. C. potential (a few mV/m) exists along the auroral field-line and the peak potential region may be higher than around 8000 km altitude.

Both the auroral hiss and auroral kilometric radiation may be generated associated with the acceleration of auroral particles by these parallel electric fields.

## 8. Conclusions

MOROZUMI (1965), KOKUBUN *et al.* (1972) and TANAKA *et al.* (1976) showed that the auroral hiss observed on the ground can be categorized into two types: continuous hiss and impulsive hiss. However, the difference of spectra, intensity and duration between these two types of hiss and the characteristics of auroral type, luminosity and location related to these two types of hiss were not examined in detail in their studies. The characteristic differences between these two types of hiss were quantitatively confirmed in this paper using the VLF and aurora data observed at both Syowa and Mizuho Stations and using the arrival direction of auroral hiss at Syowa Station in Antarctica.

GURNETT (1966), JØRGENSEN (1968) and SRIVASTAVA (1976) compared the VLF emissions simultaneously observed on both the ground and satellite, but they did not obtain conclusive results about the relationships between the characteristics of hiss observed at the satellite altitude and on the ground. We compared some auroral hiss spectra observed on both ISIS 2 and the ground (Syowa Station) in detail and reasonably inferred the propagation path from the satellite to the ground. In order to explain these observation results, the generation mechanism and the propagation path were also examined, reaching a reasonable conclusion on the propagation path and the generation region of auroral hiss observed on the ground. Fig. 91 schematically shows the results of this paper. Continuous hiss associated with distinct auroral arcs is usually observed in the evening sector and impulsive hiss associated with active auroras is often observed near the midnight sector. Both types of hiss occurred frequently near the onset of a magnetospheric substorm. The impulsive hiss especially, occurred at the onset of local auroral break-up. On the other hand, continuous hiss is one of the indicators of substorm initiation in the midnight sector, that is noticeable in the evening sector. Continuous hiss emissions are observed in a wider region of latitude than those of impulsive hiss and are frequently observed associated with the brightening of an auroral arc located a few hundreds of km ( $\sim 300$  km) poleward of Syowa Station. On the other hand, impulsive hiss emissions usually occur accompanied by active bright aurora near the zenith. The intensity of both types of hiss increases with an increase in auroral

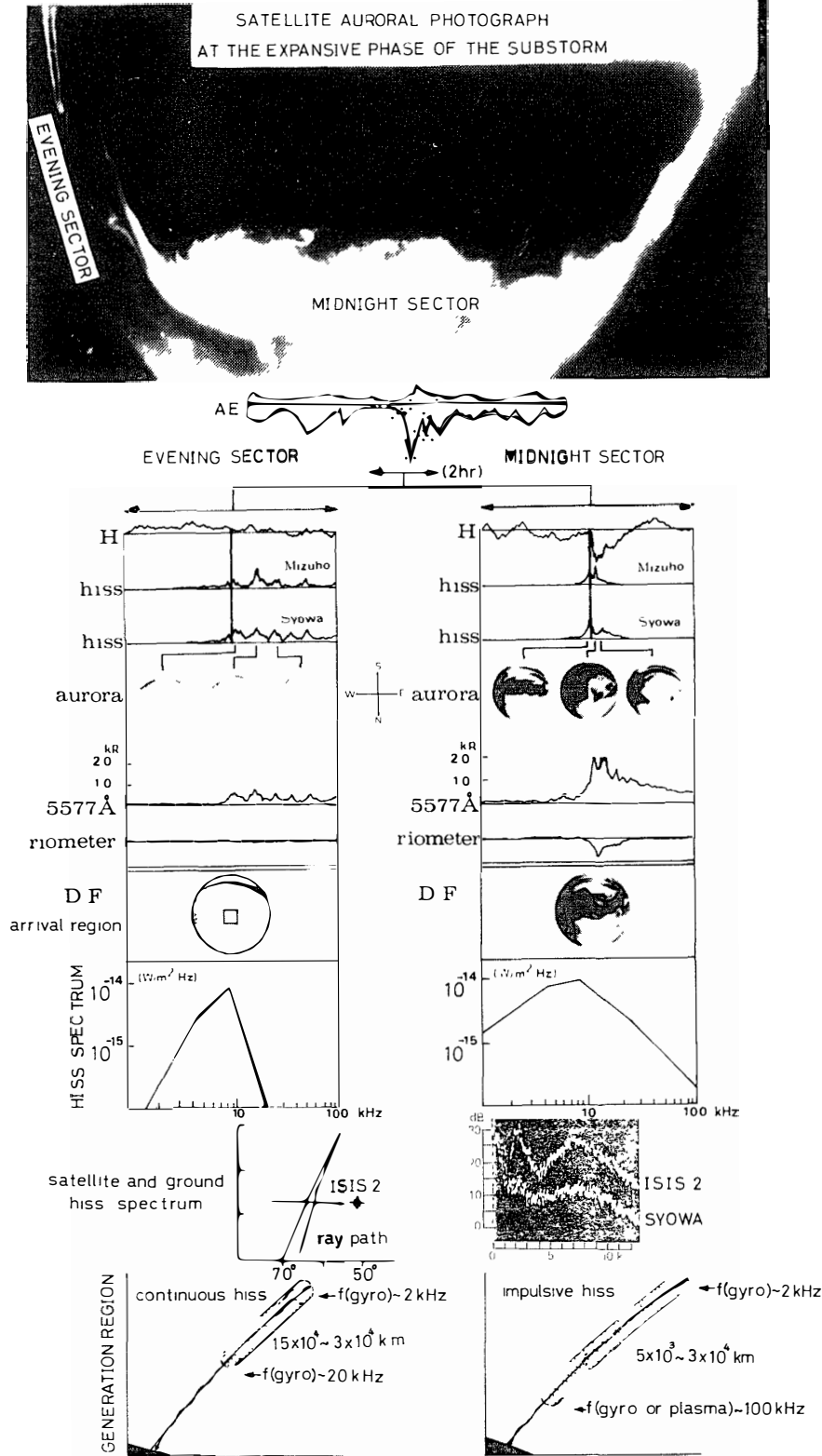


Fig. 91. The characteristics of two types of auroral hiss associated with the development of the magnetospheric substorm

luminosity. However, the intensity of impulsive hiss frequently decreases after the onset of auroral break-up, although the aurora is still highly luminous. This is understood to be due partly to ionospheric absorption. The good correlations observed between hiss intensity and auroral luminosity when the absorption is weak indicate that the auroral hiss emissions are mostly excited by the precipitating auroral electrons. According to recent observations of auroral particles by FRANK and ACKERSON (1972), ARNOLDY *et al.* (1974), MENG (1976) and MENG *et al.* (1978), continuous hiss emissions associated with the auroral arc seem to be generated by electrons precipitating with energies less than 1 keV and the impulsive hiss emissions associated with the bright aurora seem to be generated by precipitating electrons with energies higher than a few keV. Following the coherent Cerenkov instability as suggested by YAMAMOTO (1979), the difference in the energy spectra of the precipitating particles in excitation of the auroral hiss may lead to the differences in the generation region for these two types of hiss. Namely, when the beam energy of an electron is low ( $u/a$  is small), auroral hiss cannot be amplified enough except at high altitudes and will have a comparatively narrow and distinct frequency spectrum at ground levels. On the other hand, when the beam energy is high ( $u/a$  is large), auroral hiss with a broad band spectrum will be observed at ground levels since it can be sufficiently amplified even at low altitudes. According to the simultaneous VLF observations on the ground and the satellite, it is reasonably concluded that the continuous hiss emissions propagate along the non-ducted path. The conclusion that the continuous hiss propagates along the non-ducted path can also be supported by comparing the arrival direction of the hiss and the location of related aurora. The continuous hiss generally arrives from several hundreds of km equatorward of the associated aurora.

In order to explain this result, the propagation path was calculated by the ray tracing technique. Assuming that the wave duct terminates at 3000 km in altitude, it was shown that the propagation path of hiss that could penetrate the ionosphere downward must tend to become vertical rather than follow the magnetic field. This could explain why the arrival direction of continuous hiss observed at Syowa Station is usually some hundreds of km equatorward of related aurora. In contrast, the arrival direction of impulsive hiss is sometimes much nearer the auroral activity. In this case, the impulsive hiss likely propagates along the field-line lower than 3000 km on account of the strong field-aligned irregularities or the large-scale horizontal gradient of ionization along the propagation path.

Assuming that particles and waves are coupled in the Cerenkov condition and the waves are generated by an electron beam with the energy of a few keV or less, and further assuming the enhancement factor along the field-line duct to be smaller than 0.5, it was shown that the emissions cannot be trapped along the field-aligned irregularity in the generation region (except the wave frequency near to local gyrofrequency or plasma frequency). On the other hand, if the waves propagate

along the non-ducted path, the emission angle must be limited to a critical angle since the wave normal directions of the downcoming rays in the ionosphere ( $h \sim 200$  km) must lie in a transmission cone. When the wave frequency is far from the local gyro or plasma frequency at the generation region, the resonance angle becomes larger than the critical angle and hence such a wave cannot propagate to the ground. Therefore, it is concluded that only hiss emissions generated around the altitude where the wave frequency is near the local gyro or plasma frequency can propagate to the ground. Auroral hiss with 2 and 20 kHz frequencies, for example could be generated around  $3 \times 10^4$  and  $1.5 \times 10^4$  km in altitude respectively where the gyrofrequencies are a little higher than the wave frequencies. Auroral hiss at 100 kHz may be generated around  $5 \times 10^3$  km in altitude where the plasma frequency is a little higher than 100 kHz. Therefore, if the frequency of the continuous hiss is limited from 2 to 20 kHz, the range of the generation region can be estimated from  $1.5 \times 10^4$  to  $3 \times 10^4$  km. Similarly, if the frequency band of the impulsive hiss is assumed to be from 2 to 100 kHz, the range of the generation altitude can be estimated from  $5 \times 10^3$  to  $3 \times 10^4$  km. The source region estimated here is almost the same as that estimated from the nose frequency of the fast hissler (quite a different method) by SIREN (1975).

Assuming that the waves and the particles are coupled in the Cerenkov condition, and the energy of the electron beam is less than a few keV, and that no intense field-line duct exists, we estimated the generation region of auroral hiss observed on the ground. However, in order to determine the generation region of auroral hiss conclusively, it is necessary to know the electron spectrum of the precipitating particles in more detail and to know the background electron density irregularities along the field line for various cases. It may be also considered that there is a possibility that the waves can propagate to the ground in an evanescent mode even if the wave normal angle is larger than a transmission cone. Hence, it is very important to examine in detail the transmission conditions of waves around the ionosphere to estimate this effect. Although both the auroral hiss and the auroral kilometric radiation appear to originate from a common spatial region, distinctly different mechanisms are required to explain these two types of radiation since they are propagating in different plasma wave modes. It is also important for plasma physics to understand the generation mechanisms of the auroral hiss and the auroral kilometric radiation, because their mechanism may also be applied to the decameter wave from Jupiter and many radiations from radio stars. Recently WESCOTT *et al.* (1976a,b), MOZER *et al.* (1977) showed that auroral electrons are accelerated by parallel electric fields at altitude ranging from 5000 to 15000 km, in the same region where the auroral hiss and the auroral kilometric radiation seem to be produced. If these emissions are generated associated with the accelerated particles by parallel electric fields, the generation region of these emissions must be identical to the location of the parallel electric field. The region around a few earth radii in

altitude is one of the most important areas for future study.

### Acknowledgments

The author wishes to express his appreciation to Prof. T. OGUTI for his guidance and support during the course of this study. The author also deeply appreciates the many important suggestions and comments at various stages of this work from Drs. S. KOKUBUN and K. HAYASHI. He is grateful to Drs. T. TAMAQ, T. SATO and T. YAMAMOTO for valuable discussions about wave-particle interactions. Prof. N. FUKUSHIMA and the other members of Geophysical Research Laboratory, University of Tokyo kindly encouraged him to complete this study.

The author would like to thank Prof. T. NAGATA, Prof. T. HIRASAWA, Dr. H. FUKUNISHI, Dr. N. SATO, Mr. R. FUJII and other members of the National Institute of Polar Research for their help in initiating this study and in the data analysis. The author wishes to thank Drs. A. NISHIDA and K. TSURUDA for providing many useful comments. The author's appreciation is also expressed for the computer programs developed by Prof. I. KIMURA and Mr. H. YAMAGISHI in calculating the ray path. The program was ran at HITAC M-160 II computer installed at the National Institute of Polar Research.

None of these data used in this study would have been available except for the kind help of the 17th Japanese Antarctic Research Expedition members, especially Prof. T. YOSHINO, Dr. H. FUKUNISHI, Messrs. T. MATSUO, K. NIKKI, A. YAMAKOSHI, T. HANEDA, F. NISHIO, T. SASAKI and F. ITO. The author would also like to thank the 10, 11, 14, 15, 16 and 18th Japanese Antarctic Research Expedition members for giving him much valuable data, especially Messrs. M. AYUKAWA, F. OMI, M. KUWASHIMA, N. IWAGAMI and T. TOYA.

The author is indebted to Dr. R. E. BARRINGTON, CRC, ISIS Working Group and NASA for their kind support of the telemetry of ISIS-VLF data at Syowa Station, Antarctica. DMSP data were provided by the USAF Air Weather Service, Global Weather Central, through the World Data Center A at Boulder. The author's thanks are also due to the organization for supplying DMSP auroral photograph data.

The author thanks Misses Y. SHINDO, T. NAKAJIMA and Mrs. S. BABA for their kind help in typing this paper. Finally it is a pleasure for the author to thank his parents and his wife Michiko for their support and patience.

This research was supported in part by the Geophysics Research Laboratory, University of Tokyo, and in part by the National Institute of Polar Research.

## References

- AKASOFU, S.-I. (1968): Polar and Magnetospheric Substorms. Dordrecht, D. Reidel, 140–154 (Astrophys. Space Sci. Lib., 11).
- ANGERAMI, J. J. and THOMAS, J. O. (1963): The distribution of ions in the earth's exosphere. Tech. Rep., Stanford University No. 3412–3.
- ANDERSON, R. R. and GURNETT, D. A. (1973): Plasma wave observations near the plasmopause with the S<sup>3</sup>-A Satellite. *J. Geophys. Res.*, **78**, 4756–4764.
- ARNOLDY, R. L. and CHOY, L. W. (1973): Auroral electrons of energy less than 1 keV observed at rocket altitudes. *J. Geophys. Res.*, **78**, 2187–2200.
- ARNOLDY, R. L., LEWIS, P. B. and ISSACSON, P. O. (1974): Field-aligned auroral electron fluxes. *J. Geophys. Res.*, **79**, 4208–4221.
- BARRINGTON, R. E., HARTZ, T. R. and HARVEY, R. W. (1971): Diurnal distribution of ELF, VLF and LF noise at high latitudes as observed by Alouette 2. *J. Geophys. Res.*, **76**, 5278–5291.
- BULLOUGH, K., HUGHES, A. R. W. and KAISER, T. R. (1969): VLF observations on Ariel 3. *Proc. R. Soc. London, Ser. A*, **311**, 563–569.
- BURTIS, W. J. and HELLIWELL, R. A. (1969): Banded chorus—A new type of VLF radiation observed in the magnetosphere by OGO 1 and OGO 3. *J. Geophys. Res.*, **74**, 3002–3010.
- BURTIS, W. J. and HELLIWELL, R. A. (1975): Magnetospheric chorus; Amplitude and growth rate. *J. Geophys. Res.*, **80**, 3265–3270.
- BURTON, E. T. and BOARDMAN, E. M. (1933): Audio-frequency atmospheric. *Proc. IRE*, **21** (10), 1476–1494.
- BURTON, R. K. and HOLZER, R. E. (1974): The origin and propagation of chorus in the outer magnetosphere. *J. Geophys. Res.*, **79**, 1014–1023.
- CERISIER, J. C. (1974): Ducted and partly ducted propagation of VLF waves through the magnetosphere. *J. Atoms. Terr. Phys.*, **36**, 1442–1467.
- DOWDEN, R. L. (1959): Low frequency (100 kC./S.) radio noise from the aurora. *Nature*, **184**, 803.
- DOWDEN, R. L. (1960): Geomagnetic noise at 230 kC./S. *Nature*, **187**, 677–678.
- DOWDEN, R. L. (1962): Theory of generation of exospheric VLF noise (hiss). *J. Geophys. Res.*, **67**, 2223–2230.
- DUNCKEL, N. and HELLIWELL, R. A. (1969): Whistler-mode emissions on the OGO 1 satellite. *J. Geophys. Res.*, **74**, 6371–6385.
- EIDMAN, V. I. (1958): The radiation from an electron moving in a magnetoactive plasma. *Sov. Phys. JETP*, **34**, 91–95.
- ELLIS, G. R. A. (1957): Low frequency radio emission from auroras. *J. Geophys. Res.*, **10**, 302–306.
- ELLIS, G. R. A. (1959): Low frequency electromagnetic radiation associated with magnetic disturbances. *Planet. Space Sci.*, **1**, 253–258.
- ELLIS, G. R. A. (1960): Geomagnetic disturbances and 5 kilocycles per second electromagnetic radiation. *J. Geophys. Res.*, **65**, 1705–1710.
- ELLIS, G. R. A. (1961): Spaced observations of the low frequency radiation from the earth's upper atmosphere. *J. Geophys. Res.*, **66**, 19–23.
- ENGLISH, H. W. and HUGHES, A. R. W. (1974): An attempt to explain satellite observations of high latitude VLF hiss in terms of generation by incoherent Cerenkov radiation. *Space Res.*, **14**, 359–367.
- EVANS, D. S. (1968): The observations of a near monoenergetic flux of auroral electrons. *J. Geophys. Res.*, **73**, 2315–2323.
- FRANK, L. A. and ACKERSON, K. L. (1972): Local-time survey of plasma at low altitudes over the auroral zones. *J. Geophys. Res.*, **77**, 4116–4127.

- FRANKEL, M. S. (1973): LF radio noise from the earth's magnetosphere. *Radio Sci.*, **8**, 991–1005.
- FREDRICKS, R. W. and SCARF, F. L. (1973): Recent studies of magnetospheric electric field emissions above the electron gyrofrequency. *J. Geophys. Res.*, **78**, 310–314.
- GALLET, R. M. and HELLIWELL, R. A. (1959): Origin of very low frequency emissions. *J. Res. Nat. Bur. Stand.*, **63D**, 21–27.
- GREEN, J. L., GURNETT, D. A. and SHAWHAN, S. D. (1977): The angular distribution of auroral kilometric radiation. *J. Geophys. Res.*, **82**, 1825–1838.
- GURNETT, D. A. (1966): A satellite study of VLF hiss. *J. Geophys. Res.*, **71**, 5599–5615.
- GURNETT, D. A. (1974): The earth as a radio source: Terrestrial kilometric radiation. *J. Geophys. Res.*, **79**, 4227–4238.
- GURNETT, D. A. (1975): The earth as a radio source: The nonthermal continuum. *J. Geophys. Res.*, **80**, 2751–2763.
- GURNETT, D. A. (1978): Electromagnetic plasma wave emissions from the auroral field lines. *J. Geomagn. Geoelectr.*, **30**, 257–272.
- GURNETT, D. A. and FRANK, L. A. (1972): VLF hiss and related plasma observations in the polar magnetosphere. *J. Geophys. Res.*, **77**, 172–190.
- HARANG, L. (1968): VLF-emissions observed at stations close to the auroral zone and at stations on lower latitudes. *J. Geophys. Res.*, **30**, 1143–1159.
- HARANG, L. (1969): Burst of VLF-emission simultaneous with sharp dip of absorption and SC in geomagnetic H. *Planet. Space Sci.*, **17**, 1565–1572.
- HARANG, L. and HAUGE, K. N. (1965): Radio wave emissions in the VLF-band observed near the auroral zone -II. The physical properties of the emissions. *J. Atmos. Terr. Phys.*, **27**, 499–512.
- HARANG, L. and LARSEN, R. (1965): Radio wave emissions in the VLF-band observed near the auroral zone—I. Occurrence of emissions during disturbances. *J. Atmos. Terr. Phys.*, **27**, 481–497.
- HARANG, L., LARSEN, R. and SKOGTVEDT, J. (1965): The distribution of intensities in VLF-emissions. *J. Geophys. Res.*, **27**, 1147–1150.
- HARTZ, T. R. (1970): Low frequency noise emissions and their significance for energetic particle procession. *The Polar Ionosphere and Magnetospheric Processes*, ed. by G. SKOULI. New York, Gordon and Breach.
- HAYAKAWA, M., TANAKA, Y. and OHTSU, J. (1975): The morphologies of low-latitude and auroral VLF 'hiss'. *J. Atmos. Terr. Phys.*, **37**, 517–529.
- HAYASHI, K., KOKUBUN, S. and OGUTI, T. (1968): Polar chorus emission and worldwide geomagnetic variations. *Rep. Ionos. Space Res. Jpn.*, **25**, 369–382.
- HAYASHI, K. and KOKUBUN, S. (1971): VLF emissions during post breakup phase of polar substorm. *Rep. Ionos. Space Res. Jpn.*, **25**, 369–382.
- HELLIWELL, R. A. (1965): *Whistlers and Related Ionospheric Phenomena*. Stanford Univ., Stanford Press, 23–82.
- HIRASAWA, T. and NAGATA, T. (1972): Constitution of polar substorm and associated phenomena in the southern polar region. *JARE Sci. Rep., Ser. A*, **10**, 76p.
- HOFFMAN, R. A. (1969): Low-energy electron precipitation at high latitude. *J. Geophys. Res.*, **74**, 2425–2432.
- HOFFMAN, R. A. and BERKO, F. E. (1971): Primary electron influx to day-side auroral oval. *J. Geophys. Res.*, **76**, 2967–2976.
- HOFFMAN, R. A. and LAASPERE, T. (1972): Comparison of very-low-frequency auroral hiss with precipitating low-energy electrons by the use of simultaneous data from two OGO-4 experiments. *J. Geophys. Res.*, **77**, 640–650.

- HOLZER, R. E., FARLEY, T. A. and BURTON, R. K. (1974): A correlated study of ELF waves and electron precipitation on OGO 6. *J. Geophys. Res.*, **79**, 1007–1013.
- HUGHES, A. R. W., KAISER, T. R. and BULLOUGH, K. (1971): The frequency of occurrence of VLF radio emissions at high latitudes. *Space Res.*, **11**, 1323–1330.
- IJIMA, T. and NAGATA, T. (1972): Signatures for substorm development of the growth phase. *Planet. Space Sci.*, **20**, 1095–1112.
- JAMES, H. G. (1972): Refraction of whistler-mode waves by large-scale gradients in the middle-latitude ionosphere. *Ann. Geophys.*, **28**, 301–339.
- JAMES, H. G. (1973): Whistler-mode hiss at low and medium frequencies in the dayside-cusp ionosphere. *J. Geophys. Res.*, **78**, 4578–4599.
- JAMES, H. G. (1976): VLF saucers. *J. Geophys. Res.*, **81**, 501–513.
- JIRICEVK, F. and TRISKA, P. (1976): Lower hybrid resonance associated phenomena observed with the Intercosmos 10 satellite. *Space Res.*, **16**, 567–573.
- JØRGENSEN, T. S. (1966): Morphology of VLF hiss zone and their correlation with particle precipitation events. *J. Geophys. Res.*, **71**, 1367–1375.
- JØRGENSEN, T. S. (1968): Interpretation of auroral hiss measured on OGO 2 and at Byrd Station in terms of incoherent Cerenkov radiation. *J. Geophys. Res.*, **73**, 1055–1069.
- JØRGENSEN, T. S. and UNGSTRUP, E. (1962): Direct observation of correlation between aurora and hiss in Greenland. *Nature*, **194**, 462–463.
- KAISER, T. R. (1972): VLF phenomena. *Earth's Magnetospheric Processes*, ed. by B. M. MCCORMAC. Dordrecht, D. Reidel, 340–350.
- KAMIDE, Y. and WINNINGHAM, T. D. (1977): A statistical study of the instantaneous nightside auroral oval: the equatorward boundary of electron precipitation as observed by the ISIS 1 and 2 satellites. *J. Geophys. Res.*, **82**, 5573–5588.
- KENNEL, C. F. and PETSCHER, H. E. (1966): Limit on stably trapped particle fluxes. *J. Geophys. Res.*, **71**, 1–28.
- KENNEL, C. F., SCARF, F. L., FREDRICKS, R. W., MEGEHEE, J. H. and CORONITI, F. V. (1970): VLF electric field observations in the magnetosphere. *J. Geophys. Res.*, **75**, 6136–6151.
- KIMURA, I. (1966): Effects of ions on whistler-mode ray tracing. *Radio Sci.*, **1**, 269–283.
- KOKUBUN, S., HAYASHI, K. and OGUTI, T. (1969): VLF emission study at Syowa Station, Antarctica: Polar chorus emission and worldwide geomagnetic variation. *JARE Sci. Rep.*, Ser. A, **6**, 34p.
- KOKUBUN, S., MAKITA, K. and HIRASAWA, T. (1972): VLF-LF hiss during polar substorm. *Rep. Ionos. Space Res. Jpn.*, **26**, 138–148.
- LAASPERE, T. and JOHNSON, W. C. (1973): Additional results from an OGO 6 experiment concerning ionospheric electric and electromagnetic fields in the range 20 Hz to 500 kHz. *J. Geophys. Res.*, **78**, 2926–2944.
- LAASPERE, T. and HOFFMAN, R. A. (1976): New results on the correlation between low-energy electrons and auroral hiss. *J. Geophys. Res.*, **81**, 524–530.
- LAASPERE, T., JOHNSON, W. C. and SEMPREBON, L. C. (1971): Observations of auroral hiss, LHR noise and other phenomena in the frequency range 20 Hz–540 kHz on OGO 6. *J. Geophys. Res.*, **76**, 4477–4493.
- LIEMOHN, H. B. (1965): Radiation from electrons in magnetoplasma. *Radio Sci.*, **69D**(5), 741–766.
- LIM, T. L. and LAASPERE, T. (1972): An evaluation of the intensity of Cerenkov radiation from auroral electrons with energies down to 100 eV. *J. Geophys. Res.*, **77**, 4145–4157.
- LUI, A. T. Y., VENKATESAN, D., ANGER, C. D., AKASOFU, S.-I., HEIKKILA, W. J., WINNINGHAM, J. D. and BURROWS, J. R. (1977): Simultaneous observations of particle precipitations and auroral emissions by the ISIS satellite in the 19–24 MLT sector. *J. Geophys. Res.*,

- 82**, 2210–2226.
- MAEDA, K. (1975): A calculation of auroral hiss with improved models for geoplasma and magnetic field. *Planet. Space Sci.*, **23**, 843–865.
- MAEDA, K. and OYA, H. (1963): Penetration of VLF radio waves through the ionosphere. *J. Geomagn. Geoelectr.*, **14**, 151–171.
- MAGGS, J. E. (1976): Coherent generation of VLF hiss. *J. Geophys. Res.*, **81**, 1707–1724.
- MAGGS, J. E. (1978): Electrostatic noise generated by auroral electron beam. *J. Geophys. Res.*, **83**, 3173–3188.
- MANSFIELD, V. N. (1967): Radiation from a charged particle spiraling in a cold magnetoplasma. *Astrophys. J.*, **147**, 672–680.
- MARTIN, L. H., HELLIWELL, R. A. and MARKS, K. R. (1960): Association between auroral and very low-frequency hiss observed at Byrd Station, Antarctica. *Nature*, **187**, 751–753.
- MCDIARMID, I. B., BURROWS, J. R. and BUDZINSKI, E. E. (1975): Average characteristics of magnetospheric electrons (150 eV to 200 keV) at 1400 km. *J. Geophys. Res.*, **80**, 73–79.
- MC EWEN, D. J. and BARRINGTON, R. E. (1976): Some characteristics of the lower hybrid resonance noise bands observed by the Alouette 1 satellite. *Can. J. Phys.*, **45**, 13–20.
- MCKENZIE, J. F. (1967): Radiation from a test particle in a plasma. *Phys. Fluids*, **10**, 2680–2694.
- MCILWAIN, C. E. (1961): Coordinates for mapping the distribution of magnetically trapped particles. *J. Geophys. Res.*, **66**, 3681–3691.
- MCPHERRON, R. L. (1973): Satellite studies of magnetospheric substorms on August 15, 1968. *J. Geophys. Res.*, **66**, 3681–3691.
- MENG, C. (1976): Simultaneous observations of low-energy electron precipitation and optical auroral arcs in the evening sector by the DMSP 32 satellite. *J. Geophys. Res.*, **81**, 2771–2785.
- MENG, C. I., SNYDER, A. L. and KROEL, H. W. (1978): Observations of auroral westward traveling surges and electron precipitations. *J. Geophys. Res.*, **83**, 575–585.
- MOROZUMI, H. M. (1962): A study of aurora australis in connection with an association between VLF hiss and auroral arcs and bands observed at south geographical pole 1960. *State Univ. Iowa, SUI* **62**.
- MOROZUMI, H. M. (1965): Diurnal variation of auroral zone geophysical disturbances. *Rep. Ionos. Space Res. Jpn.*, **19**, 286–299.
- MOROZUMI, H. M. and HELLIWELL, R. A. (1966): A correlating study of the diurnal variation of upper atmospheric phenomena in the southern auroral zone. *Sci. Rep. Radiosci. Lab., Stanford Univ.*, **2**.
- MORSE, F. A., NELSON, D. F., ROGERS, E. H. and SAVAGE, R. C. (1973): Low-energy electrons and auroral forms (abstract). *EOS; Trans., Am. Geophys. Union*, **54**, 404.
- MOSIER, S. R. and GURNETT, D. A. (1969): VLF measurements of the Poynting flux along the geomagnetic field with the Injun 5 satellite. *J. Geophys. Res.*, **74**, 5675–5687.
- MOSIER, S. R. (1971): Poynting flux studies of hiss with the Injun 5 satellite. *J. Geophys. Res.*, **76**, 1713–1728.
- MOSIER, S. R. and GURNETT, D. A. (1972): Observed correlations between aurora and VLF emissions. *J. Geophys. Res.*, **77**, 1137–1145.
- MOZER, F. S., CARLSON, C. W., HUDSON, M. K., TORBERT, R. B., PARADY, B., YATTEAU, J. and KELLEY, M. C. (1977): Observations of paired electrostatic shocks in the polar magnetosphere. *Phys. Rev. Lett.*, **38**, 292–295.
- NAGATA, T., YOSHINO, T., HIRASAWA, T. and FUKUNISHI, H. (1976a): Substorm observations by sounding rockets and by reception of polar-orbiting satellite data. *Mem. Natl Inst. Polar Res., Spec. Issue*, **6**, 1–14.

- NAGATA, T., HIRASAWA, T., AYUKAWA, M. and FUKUNISHI, H. (1976b): Multipoint ground observations around Syowa Station, Antarctica by means of unmanned and automatic observations. *Mem. Natl Inst Polar Res., Spec. Issue*, **6**, 44–51.
- NISHIDA, A. and NAGAYAMA, N. (1973): Synoptic survey for the neutral line in the magnetotail during the substorm expansion phase. *J. Geophys. Res.*, **78**, 3782–3798.
- NODA, A. and TAMAO, T. (1976): The model dependence of differential power spectra of incoherent Cerenkov radiation. *J. Geophys. Res.*, **81**, 287–290.
- OGUTI, T. (1974): Identification of hiss emitting auroral activity. *Rep. Ionos. Space Res. Jpn.*, **28**, 124–128.
- OGUTI, T. (1975): Hiss emitting auroral activity. *J. Atmos. Terr. Phys.*, **37**, 761–768.
- ONDOH, T. (1963): The ionospheric absorption of the VLF emissions at the auroral zone. *J. Geomagn. Geoelectr.*, **15**, 90–108.
- PIKE, C. P. and WHALEN, J. A. (1974): Satellite observations of auroral substorms. *J. Geophys. Res.*, **79**, 985–1000.
- RAO, M., DIKSHIT, S. K. and TANTRY, B. A. P. (1973): Incoherent Cerenkov radiation in the magnetosphere and the ground observations of VLF hiss, *J. Geophys. Res.*, **78**, 191–196.
- REASONER, D. L. and CHAPPELL, C. R. (1973): Twin payload observations of incident and back-scattered auroral electrons. *J. Geophys. Res.*, **78**, 2176–2186.
- RODRIGUEZ, P. and GURNETT, D. A. (1975): Electrostatic and electromagnetic turbulence associated with the earth's bow shock. *J. Geophys. Res.*, **80**, 19–31.
- ROSENBERG, T. J. (1968): Correlated bursts of VLF hiss, auroral high and X-rays. *Planet. Space Sci.*, **16**, 1419–1421.
- SATO, N., HAYASHI, K., KOKUBUN, S., OGUTI, T. and FUKUNISHI, H. (1974): Relationships between quasi-periodic VLF emission and geomagnetic pulsation. *J. Atmos. Terr. Phys.*, **36**, 1515–1526.
- SATO, N. and HAYASHI, K. (1976): Kyokkô-tai ni okeru ELF hôsha no tôrai hôkô kansoku (Direction finding of ELF emissions in auroral zone). *Nankyoku Shiryô (Antarct. Rec.)*, **55**, 1–19.
- SINGH, D. P. and SINGH, B. (1978): Propagation characteristics of ground observed VLF waves after emerging from the ducts in the ionosphere. *Ann. Geophys.*, **34**, 113–118.
- SINGH, D. P., JAIN, S. K. and SINGH, B. (1978): Propagation characteristics of VLF hiss observed at low latitude ground stations. *Ann. Geophys.*, **34**, 37–45.
- SIREN, J. C. (1972): Dispersive auroral hiss. *Nature Phys. Sci.*, **238**, 118–119.
- SIREN, J. C. (1975): Fast hissers in substorms. *J. Geophys. Res.*, **80**, 93–97.
- SMITH, R. L. and HELLIWELL, R. A. (1960): A theory of trapping of whistlers in field-aligned columns of enhanced ionization. *J. Geophys. Res.*, **65**, 815–823.
- SMITH, E. J., HOLZER, R. E. and RUSSELL, C. T. (1969): Magnetic emissions in the magnetosheath at frequencies near 100 Hz. *J. Geophys. Res.*, **74**, 3027–3036.
- SRIVASTAVA, R. N. (1974): Propagation of VLF emissions in the magnetosphere and the ionosphere. *Planet. Space Sci.*, **22**, 1545–1564.
- SRIVASTAVA, R. N. (1976): VLF hiss, visual aurora and geomagnetic activity. *Planet Space Sci.*, **25**, 375–379.
- STRINGER, T. E. (1963): Low-frequency waves in an unbounded plasma. *Plasma Phys.*, **5**, 89–107.
- SWIFT, P. W. and KAN, J. R. (1975): A theory of auroral hiss and implications on the origin of auroral electrons. *J. Geophys. Res.*, **80**, 985–992.
- TANAKA, Y. (1972): VLF hiss observed at Syowa Station, Antarctica. I—Observation of VLF hiss. II—Occurrence and polarization of VLF hiss during disturbances. *Proc. Res. Inst. Atmos., Nagoya Univ.*, **19**, 33–94.

- TANAKA, Y., HAYAKAWA, M. and NISHINO, M. (1976): Study of auroral VLF hiss observed at Syowa Station, Antarctica. Mem. Natl Inst. Polar Res., Ser. A, **13**, 58p.
- TAYLOR, W. W. L. and GURNETT, D. A. (1968): Morphology of VLF emissions observed with the Injun 3 satellite. J. Geophys. Res., **73**, 5615–5626.
- TAYLOR, W. W. L. and SHAWHAN, S. D. (1974): A test of incoherent Cerenkov radiation for VLF hiss and other magnetospheric emissions. J. Geophys. Res., **79**, 105–117.
- THORNE, R. M. (1973): Plasmaspheric hiss. J. Geophys. Res., **78**, 1581–1596.
- TRULSEN, J. and FEJER, J. A. (1970): Radiation from a charged particle in a magnetoplasma. J. Plasma Phys., **4**, 825–841.
- TSURUDA, K. and HAYASHI, K. (1975): Direction finding technique for elliptically polarized VLF electromagnetic waves and its application to the low latitude whistlers. J. Atmos. Terr. Phys., **37**, 1193–1202.
- TSURUTANI, B. T. and SMITH, E. J. (1974): Postmidnight chorus; A substorm phenomena. J. Geophys. Res., **79**, 118–127.
- TSURUTANI, B. T. and SMITH, E. J. (1977): Two types of magnetospheric ELF chorus and their substorm dependences. J. Geophys. Res., **82**, 5112–5128.
- UNGSTRUP, E. (1959): Observations of 'whistlers' and VLF phenomena at Godhavn, Greenland. Nature, **184**, 806.
- UNGSTRUP, E. (1966): Association between VLF emissions and flickering aurora. J. Geophys. Res., **71**, 2395–2396.
- UNGSTRUP, E. and JACKROTT, I. M. (1963): Observations of chorus below 1500 cycles per second at Godhavn, Greenland, from July 1959 to December 1961. J. Geophys. Res., **68**, 2141–2146.
- VERSHININ, E. F. (1970): About the intensity of the hiss near the inner boundary of the plasmapause and about the bursts of hiss with drifting frequency. Ann. Geophys., **26**, 703–707.
- WESCOTT, E. M., STENBACK-NIELSON, H. C., DAVIS, T. N. and PEEK, H. M. (1976a): The skylab barium plasma injection experiments 1. Convection observations. J. Geophys. Res., **81**, 4487–4494.
- WESCOTT, E. M., STENBACK-NIELSEN, H. C., HALLINAN, T. J., DAVIS, T. N. and PEEK, H. M. (1976b): The skylab barium plasma injection experiments 2. Evidence for a double layer. J. Geophys. Res., **81**, 4495–4502.
- WINNINGHAM, J. D., YASUHARA, F., AKASOFU, S. -I. and HEIKKILA, W. J. (1975): The latitudinal morphology of 10 eV to 10 keV electron fluxes during magnetically quiet and disturbed times in the 2100–0300 MLT sector. J. Geophys. Res., **80**, 3148–3171.
- YAMAMOTO, T. (1976): Nonlinear wave-particle interactions in the magnetosphere. Ph. D. Thesis, University of Tokyo.
- YAMAMOTO, T. (1979): On the amplification of VLF hiss. Planet. Space Sci., **27**, 273–284.

(Manuscript received May 28, 1979)

### APPENDIX A. NOTATIONS (1)

Notations used in eq. (1) are as follows

$$\begin{aligned}
 \beta_{\perp} &= v_{\perp}/c & \beta_{\parallel} &= v_{\parallel}/c & \mu_{1,2}^2 &= [-B_n \pm (B_n^2 - 4C_n \varepsilon_1)^{1/2}]/2\varepsilon_1 \\
 B_n &= (c/v_{\parallel})^2(\varepsilon_3 - \varepsilon_1) + \varepsilon_2^2 & \cos \theta &= 1/\beta_{\parallel} \mu & T_{11} &= \varepsilon_1 \varepsilon_3 - \varepsilon_1 \mu^2 \sin^2 \theta - \varepsilon_3 \mu^2 \cos^2 \theta \\
 & - \varepsilon_1^2 - \varepsilon_1 \varepsilon_3 & & & T_{13} &= \varepsilon_2 \mu^2 \sin \theta \cos \theta \\
 C_n &= (c/v_{\parallel})^2(\varepsilon_1^2 - \varepsilon_2^2 - \varepsilon_1 \varepsilon_3) & & & T_{33} &= \varepsilon_1^2 - \varepsilon_2^2 - \varepsilon_1 \mu^2 + (\mu^4 - \varepsilon_1 \mu^2) \cos^2 \theta \\
 & + \varepsilon_3(\varepsilon_1^2 - \varepsilon_2^2) & & & L_0 &= (f/f_{He}) \beta_{\perp} \mu \sin \theta.
 \end{aligned}$$

In these expressions  $q$  is the charge of the electron,  $v_{\perp}$  is the transverse velocity of the particle,  $\varepsilon_1$ ,  $\varepsilon_2$  and  $\varepsilon_3$  are the dielectric tensor elements with the ions included,  $\theta$  is the wave normal angle relative to the earth's magnetic field  $J_0$  and  $J_1$  are the Bessel functions of first kind and zeroth- and first order, respectively, and  $L_0$  is the argument of the Bessel functions.

### APPENDIX B. NOTATIONS (2)

Notations used in eq. (4) are as follows

$$\begin{aligned}
 R &= \left(\frac{\Pi_{-}}{\Omega_{-}}\right)^2 & z &= \left(\frac{\omega}{\Omega_{-}}\right)^2 & \mu &= \frac{kc}{\omega} \\
 A &= \mu^2(1-Z) - 1 + Z - R + (1-Z)\delta R/Z \\
 S &= R + (1-Z)(1-\delta R/Z) \\
 G &= S \sin^2 \theta + (1-Z)\{1 - (1+\delta)R/Z\} \cos^2 \theta \\
 N &= -Z + R(\delta + \cos^2 \theta)/Z \\
 C_1 &= A - 2(\mu^2 - Z) \\
 C_2 &= R\{-(R/Z)^2 - (Z - \delta R/Z)(A+R)/Z - (S+R)(\mu^2/Z - 1)\}
 \end{aligned}$$

where  $c$  is the speed of light and  $\delta$  the electron to ion mass ratio.

### APPENDIX C. DIRECTION FINDING SYSTEM

According to TSURUDA and HAYASHI (1975), in free space, from Maxwell equations, the vertical electric field  $E_z$  and two horizontal magnetic field  $H_x$  and  $H_y$  of a plane monochromatic wave are related to the two horizontal wave numbers  $n_x$  and  $n_y$  as

$$E_z = -n_x H_y + n_y H_x. \quad (\text{A-1})$$

The coordinate system used here is shown in Fig. A-1.

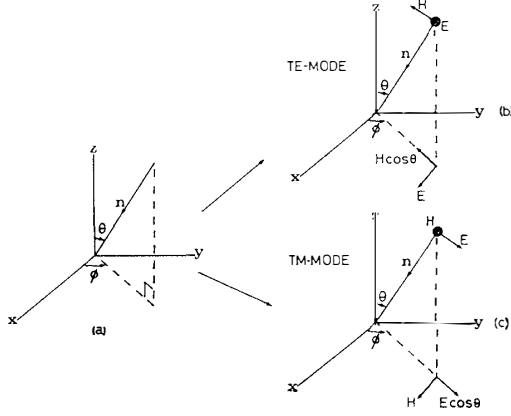


Fig. A-1. Coordinate system.  $n$  is the incident wave number,  $\theta$  is the incident elevation angle measured from zenith and  $\phi$  is the incident azimuthal angle measured from the north. TM-mode is transverse electric component and TE-mode is transverse magnetic component.

$n_x$  and  $n_y$  can be written as

$$n_x = \sin \theta \cos \phi \quad (\text{A-2})$$

$$n_y = \sin \theta \sin \phi. \quad (\text{A-3})$$

In order to find the incident wave direction (zenithal angle  $\theta$  and azimuthal angle  $\phi$ ), we must know the values of  $n_x$  and  $n_y$  on the basis of the observed VLF emission intensities ( $E_z$ ,  $H_x$ ,  $H_y$ ).

Generally the incident elliptically polarized wave is separated into two linear polarized waves. Fig. A-1 shows the wave characteristics of the linearly polarized TM wave and the TE wave with respect to the coordinate system. The horizontal magnetic fields  $H_x$ ,  $H_y$  and the vertical electric field  $E_z$  are written by the linear combinations of TE and TM mode as

$$H_x = H_{TM} \sin \phi \cos \omega t - H_{TE} \cos \theta \cos \phi \cos (\omega t + \alpha) \quad (\text{A-4})$$

$$H_y = -H_{TM} \cos \phi \cos \omega t - H_{TE} \cos \theta \sin \phi \cos (\omega t + \alpha) \quad (\text{A-5})$$

$$E_z = -E_{TM} \sin \theta \cos \omega t \quad (\text{A-6})$$

where  $\omega$  is the angular frequency of the TM mode.  $\alpha$  is the phase lag of TE behind TM mode.

$(\tilde{H}_x, \tilde{H}_y, \tilde{E}_z)$  advanced in phase by 90 degree from  $(H_x, H_y, E_z)$  are written as

$$\tilde{H}_x = -H_{TM} \sin \phi \sin \omega t + H_{TE} \cos \theta \cos \phi \sin (\omega t + \alpha) \quad (\text{A-7})$$

$$\tilde{H}_y = H_{TM} \cos \phi \sin \omega t + H_{TE} \cos \theta \sin \phi \sin (\omega t + \alpha) \quad (\text{A-8})$$

$$\tilde{E}_z = E_{TM} \sin \theta \sin \omega t. \quad (\text{A-9})$$

Then the following quantities can be obtained using eqs. (A-4)–(A-9).

$$[E_z, H_x] = E_z \tilde{H}_x - \tilde{E}_z H_x = E_{TM} H_{TE} \sin \theta \cos \theta \cos \phi \sin \alpha \quad (\text{A-10})$$

$$[E_z, H_y] = E_z \tilde{H}_y - \tilde{E}_z H_y = E_{TM} H_{TE} \sin \theta \cos \theta \sin \phi \sin \alpha \quad (\text{A-11})$$

$$[H_x, H_y] = H_x \tilde{H}_y - \tilde{H}_x H_y = H_{TM} H_{TE} \cos \theta \sin \alpha. \quad (\text{A-12})$$

From eqs. (A-2), (A-3), (A-10), (A-11) and (A-12),  $n_x$  and  $n_y$  can be written as

$$\frac{[E_z, H_x]}{[H_x, H_y]} = \sin \theta \cos \phi = n_x \quad (\text{A-13})$$

$$\frac{[E_z, H_y]}{[H_x, H_y]} = \sin \theta \sin \phi = n_y. \quad (\text{A-14})$$

So the incident wave direction angle  $\theta$  and  $\phi$  are obtained as follows

$$\sin^2 \theta = n_x^2 + n_y^2 \quad (\text{A-15})$$

$$\tan \phi = n_y / n_x. \quad (\text{A-16})$$

Generally, for monochromatic waves, wave amplitude  $A_r$  and  $B_r$  can be written as

$$A_r = A_{r0} \cos \omega t \quad (\text{A-17})$$

$$B_r = B_{r0} \cos (\omega t + \alpha) \quad (\text{A-18})$$

then

$$[A_r, B_r] = A_r \tilde{B}_r - \tilde{A}_r B_r = A_{r0} B_{r0} \sin \alpha. \quad (\text{A-19})$$

This is equal to the D.C. part ( $\omega=0$ ) of  $A_r \tilde{B}_r$ , namely

$$[A_r, B_r] = (A_r \tilde{B}_r)_{\omega=0}. \quad (\text{A-20})$$

Therefore eqs. (A-13) and (A-14) are written as

$$n_x = \frac{(E_z, \tilde{H}_x)}{(H_x, \tilde{H}_y)} \quad (\text{A-21})$$

$$n_y = \frac{(E_z, \tilde{H}_y)}{(H_x, \tilde{H}_y)}. \quad (\text{A-22})$$

A direction finding analyzer operates these configurations. The block diagram of the direction analyzer is shown in Fig. A-2. The center frequency of the band pass filter is variable from 0.5–20 kHz. For auroral hiss emissions, we fixed the center frequency around 8 kHz.

The most important point in finding the arrival direction is the equalization of response of the three antennas because the calculation of the arrival direction is sensitive both to relative amplitude and phase of the  $E_z$ ,  $H_x$  and  $H_y$  fields. In order to equalize the response, we inserted equalizer networks between each antenna and preamplifier. Fig. A-3 shows the equalizer networks. The  $E_z$ -com-

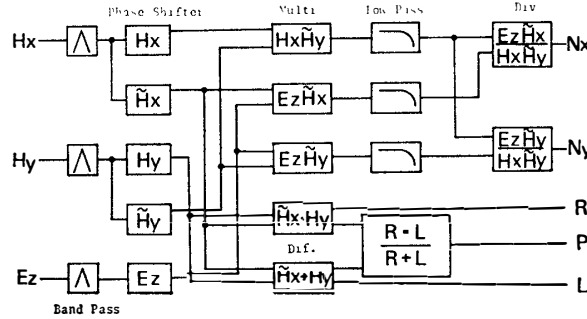


Fig. A-2. VLF direction analyzer. Two horizontal components of wave number ( $n_x$  and  $n_y$ ) and polarization ( $P, R, L$ ) are obtained in this system.

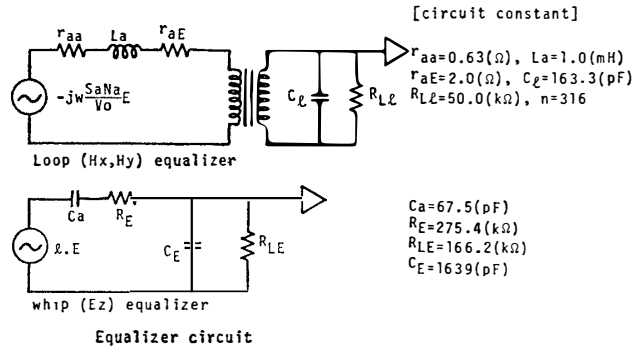


Fig. A-3. Equalizing networks for  $H_x, H_y$  and  $E_z$  antennas.

ponent was received by a vertical antenna which was simulated by a series circuit of capacitance  $C_a$  and voltage source  $l \cdot E$  where  $l$  is the antenna height and  $E$  is the electric field of the input wave. The  $H_x$  and  $H_y$  components were received by two loop antennas in the vertical plane whose normals are directed toward the N-S and the E-W direction. The loop antenna was simulated as a series network of antenna impedance  $L_a$  and resistance  $\gamma_{aa}$  and voltage source  $-j\omega(S_a N_a / v_0)E$ , where  $S_a$  is the area of the  $N_a$ -turn loop antenna and  $v_0$  is the light velocity in m/s.

The response of the vertical antenna equalizer  $Y_E(\omega)$  is given as

$$Y_E(\omega) = \frac{j\omega C_a R_{LE}}{1 + j\omega\{(C_a + C_E)R_{LE} + C_a R_E\} - \omega^2 C_a C_E R_{LE} R_E} \quad (A-23)$$

and that of the loop antenna  $Y_l(\omega)$  is

$$Y_l(\omega) = \frac{-j\omega n \frac{R'_{Li}}{\gamma_a + R'_{Li}} \frac{S_a N_a}{v_0 l}}{1 + j\omega \frac{C'_l R'_{Li} \gamma_a + L_a}{\gamma_a + R'_{Li}} - \omega^2 \frac{C'_l R'_{Li} L_a}{\gamma_a + R'_{Li}}} \quad (A-24)$$

where  $\gamma_a = \gamma_{aa} + \gamma_{aE}$ ,  $R'_{Li} = R_{LE} / n^2$ ,  $C'_l = n^2 C_l$ .

Since  $Y_E(\omega)$  must be equal to  $Y_l(\omega)$ , we obtain the following equations

$$C_a R_{LE} = \frac{n R'_{Ll} S_a N_a}{v_0 (\gamma_a + R_{Ll}) l} = \frac{1}{\omega_0} \quad (\text{A-25})$$

$$(C_a + C_E) R_{LE} + C_a R_E = \frac{C'_i R'_{Ll} \gamma_a + C_a}{\gamma_a + R'_{Ll}} = \frac{1}{\omega_1} \quad (\text{A-26})$$

$$C_a R_{LE} C_E R_L = \frac{C'_i L_a R'_{Ll}}{\gamma_a + R'_{Ll}} = \frac{1}{\omega_2^2} \quad (\text{A-27})$$

using these angular frequency  $\omega_0$ ,  $\omega_1$  and  $\omega_2$ , the response function can be written as:

$$Y(\omega) = \frac{\frac{\omega}{\omega_0}}{1 + j \frac{\omega}{\omega_1} - \frac{\omega^2}{\omega_2^2}} \quad (\text{A-28})$$

The maximum value of  $|Y(\omega)|$  is  $\omega_1/\omega_0$  at  $\omega_2$  and the frequencies  $\omega_L$  and  $\omega_H$  at where the  $|Y(\omega)|$  are 3 db less than the maximum value are expressed as:

$$\omega_L = \frac{\omega_2}{2} \left[ \left( \frac{\omega_2^2}{\omega_1^2} + 4 \right)^{1/2} - \frac{\omega_2}{\omega_1} \right] \quad (\text{A-29})$$

$$\omega_H = \frac{\omega_2}{2} \left[ \left( \frac{\omega_2^2}{\omega_1^2} + 4 \right)^{1/2} + \frac{\omega_2}{\omega_1} \right] \quad (\text{A-30})$$

The parameters of the equalizer networks used here are also shown in Fig. A-3. From the choice of parameters we get  $f_L(\omega_L/2\pi) \sim 485$  (Hz) and  $f_H(\omega_H/2\pi) \sim 20.0$  kHz. The response of equalizer networks was measured by feeding the signal through dummy antennas. The results are shown in Figs. A-4a and b. A good agreement of the amplitude and phase response among the  $E_z$ ,  $H_x$  and  $H_y$  equalizer networks was attained over the frequency range from 1.0 to 20 kHz. SATO and HAYASHI

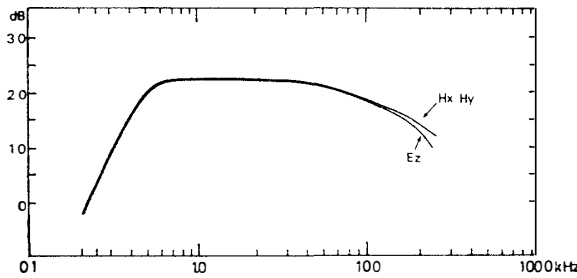


Fig. A-4a. Amplitude response of equalizing network and dummy antenna.

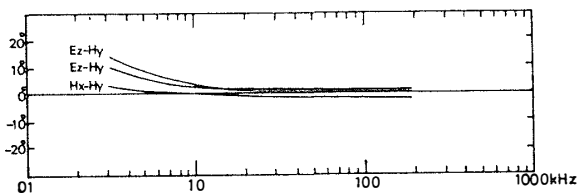


Fig. A-4b. Phase difference amount  $H_x$ ,  $H_y$  and  $E_z$  due to the equalizing network and dummy antenna.

(1976) estimated the error of the direction finding systems due to the phase differences among the three components. Following their results, even if a phase difference exists among the three components if it is less than a few degrees, the error of the arrival is small (less than a few degrees) for the wave whose incident angle is less than  $60^\circ$  and the polarization of the wave at least larger than 0.25. Since the phase difference among the three systems is within three degrees in our antenna-equalizer networks, the computed results are reliable to a few degrees for a wave with a polarization larger than 0.25.

When the VLF emission signal is weak, an error comes from the analog multiplier also. In our system, the gain in the amplifier was adjusted so that the output signal intensity was stronger than one volt pp for the moderate auroral hiss emissions ( $\sim 10^{-15}$  W/m<sup>2</sup> Hz at 8 kHz) by monitoring the intensity of the wave signal at the input terminal of the analog multiplier. The automatic gain control system was operated for weak VLF emissions.

In order to check the analog multiplier, a dummy signal was fed into the direction analyzer. Fig. A-5 shows the X-Y cathode ray display on oscilloscopes of  $n_x$  and  $n_y$  of calibration signals with various  $\theta$  and  $\phi$ . The errors in the direction analyzer are very small (within a few degrees) for incident angle  $\theta$  less than  $45^\circ$ .

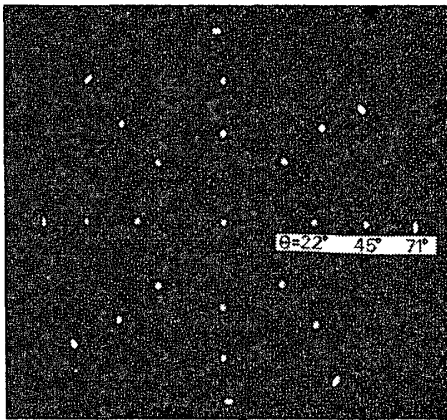
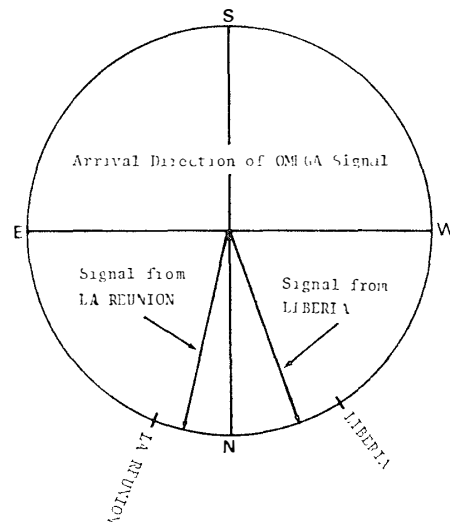


Fig. A-5. Calibration of direction analyzer. The X-Y cathode ray display on oscilloscopes on  $n_x$  and  $n_y$  calibration when  $\theta$  and  $\phi$  are changed.

Another problem was the poor grounding conditions of the circuits. At Syowa Station, the vertical whip antenna was seriously affected by the poor grounding. A radial counterpoise for the grounding of the whip antenna resulted in some improvement but it was not enough to reject the artificial electromagnetic noise (dynamo noise, etc.) around the station. A grounding cable into the sea water from the whip antenna was found effective in reducing the artificial noise in order to keep the high quality of VLF records.

We observed the omega signals ( $f=10.3, 11.3$  and  $13.6$  kHz) in order to calibrate the direction finding system. The omega signal is usually believed to be linearly polarized because of its wave guide propagation mode. If the omega signal is linear-



*Fig. A-6. The locations of La Reunion and Liberia and the arrival directions of omega signals from these stations.*

ly polarized, this system cannot calculate its arrival direction. However, the omega signal actually had some right-hand polarization and the arrival direction could be determined by this system. Omega signals from La Reunion and Liberia were received at Syowa Station. Fig. A-6 shows the arrival directions of these waves. The differences in the azimuthal angle ( $\phi$ ) between the geometry of these stations and arrival directions of the signals were less than  $10^\circ$ .

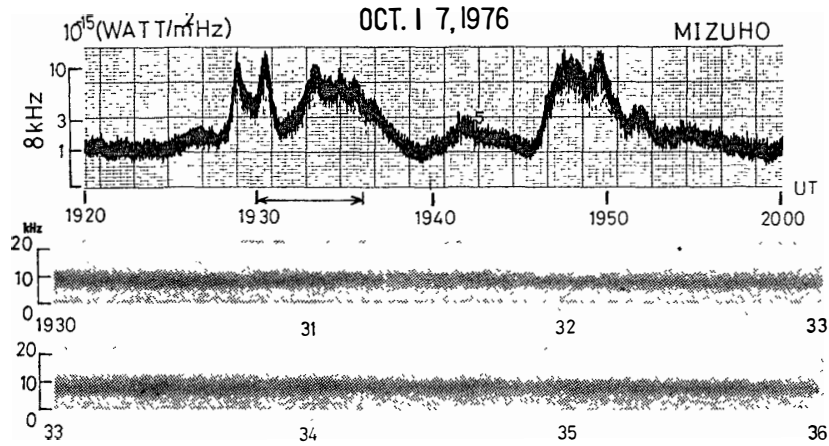


Fig. A-7. The top panel shows the intensity of auroral hiss at the 8 kHz band and the bottom panel shows the frequency-time spectra observed at Syowa Station.

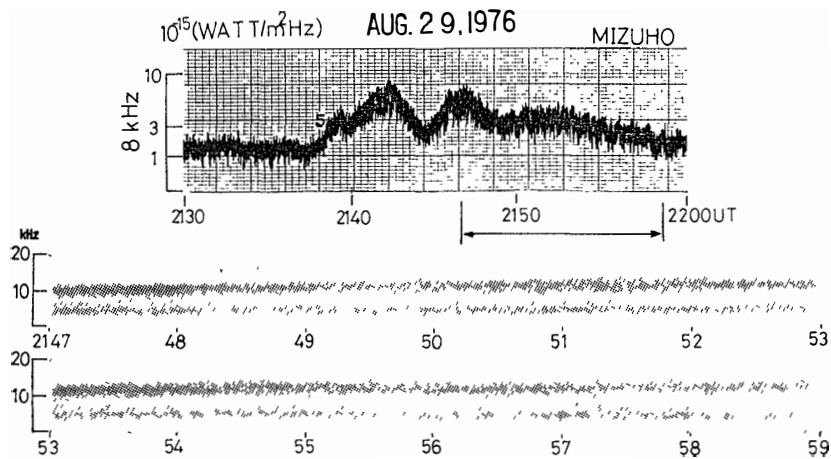


Fig. A-8. The intensity of auroral hiss at the 8 kHz band and the frequency-time spectra observed at Syowa Station. The notation is the same as in Fig. A-7.

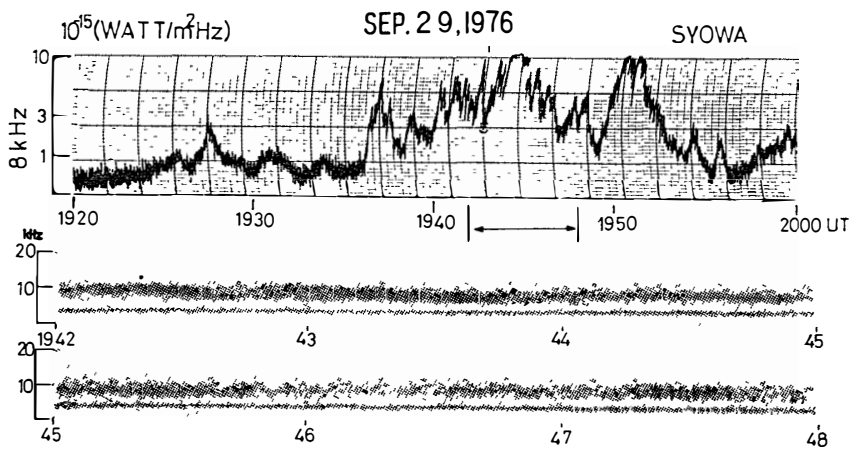


Fig. A-9. The intensity of auroral hiss at the 8 kHz band and the frequency-time spectra observed at Syowa Station.

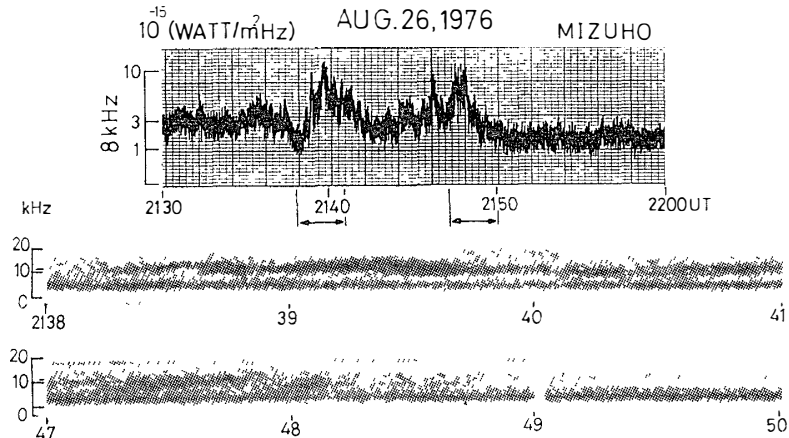


Fig. A-10. The intensity of auroral hiss at the 8 kHz band and the frequency-time spectra observed at Syowa Station.

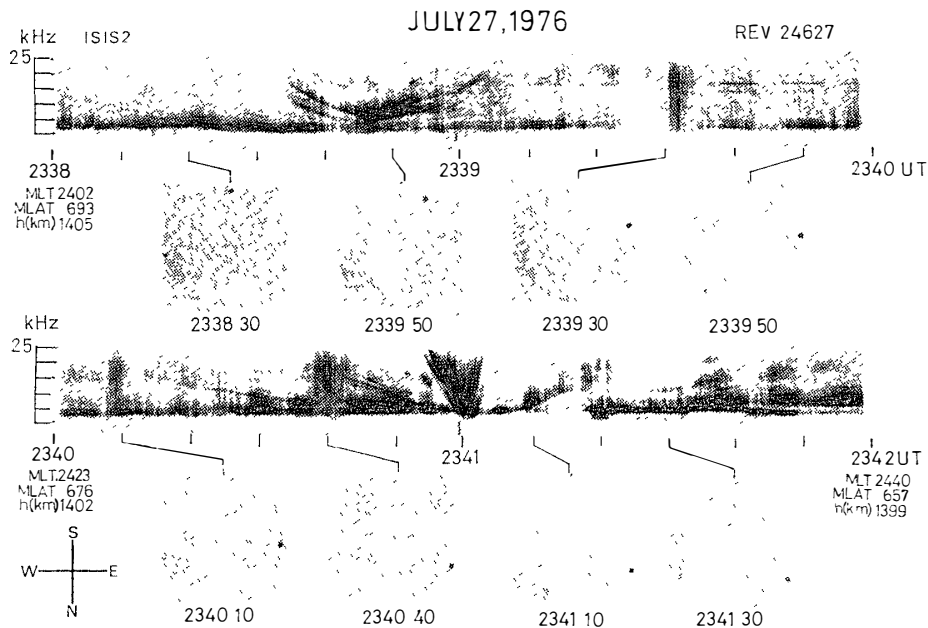


Fig. A-11. All-sky camera photographs at Syowa Station and VLF frequency-time spectra observed on ISIS 2. A faint auroral arc was observed at the northern horizon of Syowa Station. Hiss emissions were not observed on the ground. Multiple saucer emissions were observed at 2339:45 UT and 2341:00 UT. Auroras related to the saucer emissions at 2339:45 UT were not observed in the all-sky photographs, whereas the intense saucer emissions at 2341:00 UT were observed just after the satellite passed over the field lines through the faint auroral arc.

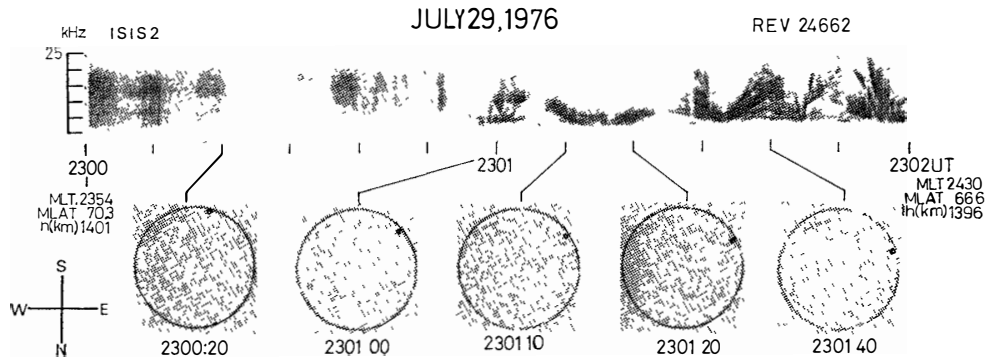


Fig. A-12. All-sky camera photographs at Syowa Station and VLF frequency-time spectrum observed on ISIS 2. A faint auroral arc was observed at the southern horizon of Syowa Station. Hiss emissions were not observed on the ground. Multiple saucer emissions were observed just after the satellite passed over near the faint arc at 2301:00 UT. The latitudinal width of each saucer emission was around a few tens of kilometers.

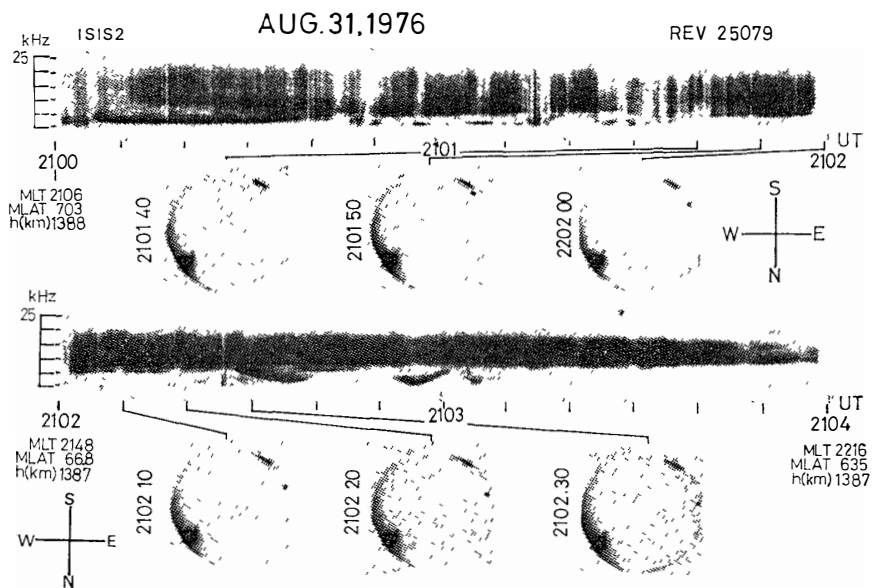


Fig. A-13. All-sky camera photographs at Syowa Station and VLF frequency-time spectra observed on ISIS 2. An auroral arc was observed at the southern horizon of Syowa Station. The moon was seen at the western horizon of Syowa Station. Weak auroral hiss emissions were observed on the ground. The lower cutoff frequency of emissions changed from a few kHz to 10 kHz. Saucer emissions were observed just after the satellite passed over the field lines threading the weak auroral arc at 2102:30 UT.

## VLF-LF Hiss Emissions Associated with Aurora

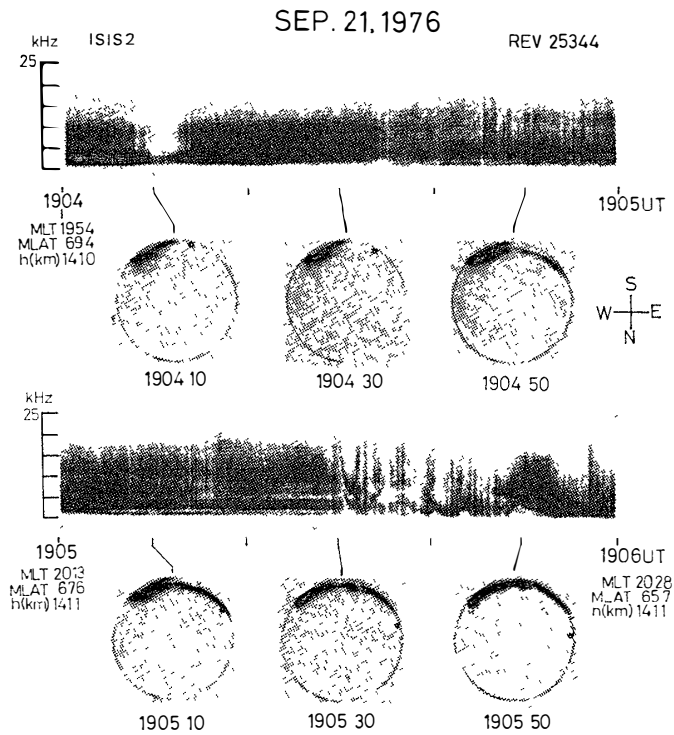


Fig. A-14. All-sky camera photographs at Syowa Station and VLF frequency-time spectra observed on ISIS 2. A bright auroral arc was observed at the southern horizon of Syowa Station. Hiss emissions were not observed on the ground until 1908:00 UT. Wide-band VLF emissions were continuously observed on ISIS 2. The saucer emissions were observed just after the satellite passed over the field lines through the bright aurora arc at 1905:30 UT.